Measurement of Lifetimes of Bottom Hadrons in Z Decays

D I S S E R T A T I O N

zur Erlangung des akademischen Grades

im Fach Physik

eingereicht an der

von

geboren am 8. Mai 1970 in Weimar

Gutachter: Prof. Dr. Thomas Hebbeker
Prof. Dr. Klaus Winter
Prof. Dr. Walter Schmidt-Parzefall

Tag der mundlichen Prufung: 27. Marz 1998

Zusammenfassung

Das Thema dieser Arbeit ist die Messung der Lebensdauern von Bottom-Hadronen. Die Lebensdauermessung bezieht sich auf ein Gemisch von Bottom-Hadronen wie es in Zerfällen des Z-Bosons auftritt. Es enthält geladene B-Mesonen B^+, neutrale Mesonen B^0 und B_s und B-Baryonen Λ_b.

Die Lebensdauer, welche von der Größenordnung 1 ps ist, wurde mit einer Driftkammer und einem hochauflösenden Silizium-Streifen-Detektor gemessen. Die Werte der B-Lebensdauern wurden aus einer Anpassung an die Zerfallsverteilung von $\sim 200\,000$ Bottom-Hadronen gewonnen.

Als Ergebnis der Messung wurde die mittlere Lebensdauer aller Bottom-Hadronen aus Z Zerfällen,

$$\tau_b = (1554 \pm 7 \pm 17)\ \text{fs}\ ,$$

das Verhältnis der Lebensdauern von geladenen und neutralen B-Hadronen in Z-Zerfällen,

$$\tau(B^+)/\tau(B^0) = 1.11 \pm 0.07 \pm 0.03\ ,$$

und eine obere Grenze für die Differenz der Zerfallsraten der CP-Eigenzustände des neutralen B_s Mesons,

$$(\Delta\Gamma/\Gamma)_{B_s} < 0.5 \qquad (95\%\ \text{C.L.})\ ,$$

bestimmt.

In der Fehlerangabe für τ_b und $\tau(B^+)/\tau(B^0)$ enthält der erste Fehler die statistischen und der zweite die systematischen Unsicherheiten. Im Verhältnis $\tau(B^+)/\tau(B^0)$ bezieht sich $\tau(B^0)$ auf die mittlere Lebensdauer aller neutralen B-Hadronen.

Aus diesen Messungen läßt sich die Amplitude für schwache Wechselwirkungen angeben, mit der ein Bottom-Quark in ein Charm-Quark bzw. ein Top-Quark in ein Down-Quark umgewandelt wird. Diese Amplituden sind fundamentale Naturkonstanten der schwachen Wechselwirkung. Sie werden beschrieben im Rahmen der Theorie von Cabibbo, Kobayashi und Maskawa, welche einen Teil des Standardmodells der elektroschwachen Wechselwirkung bildet.

Die obigen Resultate für τ_b und $\Delta\Gamma/\Gamma$ erlauben unter Hinzunahme anderer Messungen eine Bestimmung des Cabibbo-Kobayashi-Maskawa Matrixelementes $|V_{cb}|$ und die Angabe einer unteren Grenze für das Verhältnis $|V_{td}\,/\,V_{ts}|$. Das Resultat ist:

$$|V_{cb}| = (41.0 \pm 1.0\,(\text{exp}) \pm 1.4\,(\text{theo})) \times 10^{-3}\ ,$$

und

$$|V_{td}/V_{ts}| > 0.1 \qquad (95\%\ \text{C.L.})\ .$$

Im Resultat für $|V_{cb}|$ gibt der erste Fehler die experimentelle Unsicherheit, der zweite die theoretische Unsicherheit an. Die Grenze für $|V_{td}\,/\,V_{ts}|$ ist der erste Wert einer experimentellen unteren Grenze.

Diese Untersuchung wurde im Rahmen des L3-Experimentes am Europäischen Forschungszentrum CERN in Genf (Schweiz) durchgeführt.

Abstract

This thesis describes a measurement of lifetimes of bottom hadrons. The measurement uses a mixture of bottom hadrons as it is produced in decays of Z bosons. It contains charged B mesons B^+, neutral mesons B^0 and B_s and B baryons Λ_b.

The lifetime, which is of the order 1 ps, was measured with a drift chamber and a high-precision silicon-strip detector. The values of the B lifetimes were obtained from a fit to the decay distribution of $\sim 200\,000$ bottom hadrons.

The results of the measurement are the average lifetime of bottom hadrons in Z decays,

$$\tau_b = (1554 \pm 7 \pm 17)\ \text{fs}\ ,$$

the ratio of lifetimes of charged and neutral B hadrons in Z decays,

$$\tau(B^+)/\tau(B^0) = 1.11 \pm 0.07 \pm 0.03\ ,$$

and an upper limit on the rate difference between the CP eigenstates of the neutral B_s meson of

$$(\Delta\Gamma/\Gamma)_{B_s} < 0.5 \qquad (95\%\ \text{C.L.})\ .$$

The first error of τ_b and $\tau(B^+)/\tau(B^0)$ describes the statistical and the second error the systematic uncertainty inherent in the measurements. The value of the ratio $\tau(B^+)/\tau(B^0)$ is given with respect to the average lifetime of all neutral B hadrons in Z decays.

The above measurements determine the amplitudes of weak interactions that transform bottom quarks into charm quarks and top quarks into down quarks, respectively. These amplitudes are fundamental parameters of the weak interaction. They are described within the framework of the Cabibbo-Kobayashi-Maskawa quark mixing matrix which is part of the standard model of electroweak interactions.

The results for τ_b and $\Delta\Gamma/\Gamma$ allow, together with other measurements, the determination of the value of the Cabibbo-Kobayashi-Maskawa matrix element $|V_{cb}|$ and of a lower limit on the ratio $|V_{td}\,/\,V_{ts}|$. The result is:

$$|V_{cb}| = (41.0 \pm 1.0\,(\text{exp}) \pm 1.4\,(\text{theo})) \times 10^{-3}\ ,$$

and

$$|V_{td}/V_{ts}| > 0.1 \qquad (95\%\ \text{C.L.})\ .$$

In the result for $|V_{cb}|$ the first error denotes the experimental uncertainty and the second error the theoretical uncertainty. The limit on $|V_{td}\,/\,V_{ts}|$ is the first experimental lower limit value.

These investigations were carried out within the frame of the L3 experiment at the European Laboratory for Particle Physics CERN in Geneva (Switzerland).

Contents

1 Introduction **1**

1.1 Motivation 1

1.2 The Standard Model 3

1.2.1 The elektroweak interaction 3

1.2.2 The strong interaction 5

1.3 History of the bottom quark discovery 6

1.4 The process $e^+e^- \to b\overline{b}$ at the Z resonance 7

1.5 Bottom hadron production from Z decays 11

2 Cabibbo-Kobayashi-Maskawa quark mixing matrix **12**

2.1 Matrix element $|V_{cb}|$ 17

2.1.1 Inclusive semileptonic width $\Gamma(B \to X_c\, l\, \nu)$ of b hadrons . . 17

2.1.2 Exclusive semileptonic decays 20

2.2 Matrix elements $|V_{ub}|$, $|V_{td}|$ and $|V_{ts}|$ 22

2.2.1 Rare b hadron decays 22

2.2.2 Observation of $B^0 - \overline{B}^0$ and search for $B_s - \overline{B}_s$ oscillations . 25

2.2.3 Lifetime differences of neutral B mesons 34

2.2.4 Possible scenarios for values of $|V_{ub}|$ and $|V_{td}|$ 40

3 The L3 detector at LEP **44**

3.1 The LEP e^+e^- storage ring 44

3.1.1 The LEP accelerator system 45

3.1.2 Luminosity 47

3.2 The L3 detector 48

3.2.1 The silicon microvertex detector 50

3.2.2 The time expansion chamber 54

3.2.3 The z chamber 56

3.2.4 Outer detector components 56
3.2.5 Trigger system 58
3.2.6 Event simulation 59

4 Measurement of the b hadron production and decay location 60
4.1 Hadronic event selection 60
4.2 Charged particle trajectory 62
4.3 Common vertex of several tracks 63
4.4 Track resolution near the e^- beam location 64
4.4.1 Impact parameter resolution 64
4.4.2 z_0 resolution 68
4.5 Beam position measurement 69
4.5.1 Central beam spot position 69
4.5.2 Beam spot dimension 69
4.6 Track quality selection 70
4.6.1 Antiselection of tracks from identified K^0_S and Λ decays . . . 71
4.7 Reconstruction of Z decays into $b\overline{b}$ 73

5 Average b hadron lifetime 79
5.1 Principle of measurement 79
5.2 Monte Carlo simulation of bottom hadrons 80
5.2.1 Bottom quark fragmentation 81
5.2.2 Simulation of b hadron decays 82
5.2.3 Determination of model parameters 83
5.3 Decay length method 85
5.4 Impact parameter method 87
5.5 Systematic uncertainties and cross checks 89
5.5.1 Detector uncertainties 90
5.5.2 Uncertainties from modeling of heavy quarks 90
5.5.3 Cross checks 93
5.6 Combination of decay length and impact parameter results 95

6 Bottom hadron identification 98
6.1 Charge measurement in inclusive b decays 99

7 Lifetimes of neutral and charged b hadrons and $\Delta\Gamma$ of B_s mesons 104
7.1 The free parameters in the fit . . . 104
7.2 Fit results . . . 105
7.2.1 Three-parameter fit . . . 105
7.2.2 LEP constrained five-parameter fit . . . 109
7.3 Systematic uncertainties . . . 113
7.4 Discussion of the fit results . . . 115
7.4.1 The lifetime ratio $\tau(B^+)/\tau(B^0)$ . . . 115
7.4.2 The upper limit on $\Delta\Gamma/\Gamma$ . . . 116

8 Determination of the $|V_{cb}|$ value 117
8.1 The $|V_{cb}|$ value . . . 117
8.1.1 Measurement of τ_b . . . 117
8.1.2 Measurement of $\mathcal{B}(B \to X_c\, l\, \nu)$ . . . 119
8.1.3 Result . . . 122
8.2 Comparison with the $|V_{cb}|$ determination from the decay $B \to D^*\, l\, \bar{\nu}$ 122

9 Lower bound on the value of $|V_{td}\,/\,V_{ts}|$ 124
9.1 Determination of the value of $|V_{td}\,/\,V_{ts}|$ . . . 124
9.1.1 Result . . . 125
9.1.2 Upper bound on the value of ΔM_{B_s} . . . 125

10 Summary and conclusions 126
10.1 Status of the CKM matrix elements . . . 126
10.1.1 What can we learn from magnitudes? . . . 126
10.2 The issue of this thesis . . . 129
10.2.1 A brief look into the future . . . 130

A Correlation of fit variables 133

Chapter 1

Introduction

1.1 Motivation

The basic aim of elementary particle physics is to discover the building blocks of matter and to understand the interactions between them. The ideas in this field have come a long way since the ancient times when nature was believed to be composed of air, water, earth and fire. The concept of the atom as an elementary and indivisible constituent of the macroscopic world was first introduced by the Greek philosophers. The essential innovation attributed to modern science, developing since the Middle Ages, was the importance of the experiment as a guide to establish the truth of our ideas. In consequence it has lead to today's view of "big science": an experiment is performed by a team of a few hundred scientists and technicians, and the microscopes used for the observation of the smallest units of matter exceed the dimensions of an apartment house.

Today's understanding of the fundamental constituents of matter is based on the existence of two kinds of point-like particles - the fermions and bosons. All matter is composed of fermions of which there are two distinct classes, quarks and leptons, and the interactions between them are mediated by bosons. We can distinguish four classes of interactions: electromagnetic, weak, strong and gravitational, which differ in strength and range. Glashow, Salam and Weinberg [1] realized that the electromagnetic and the weak interactions can be unified in the framework of a local gauge invariant field theory, termed the Standard Model of electroweak interactions (SM). The subsequent discovery of the predicted intermediate vector bosons, $W^{\pm}$ and Z at CERN [1] [2] in 1983, was a triumph for the Standard Model. The Large Electron Positron collider (LEP) and the Stanford Linear Collider (SLC) were commissioned at CERN and SLAC [2], respectively, to further study the properties of the weak neutral and charged currents mediated by these bosons. LEP, operational since 1989, has collected $\sim$ 15 million annihilations of electrons and positrons at center-of-mass energies in the vicinity of the

[1] European Laboratory for Particle Physics, Geneva, Switzerland
[2] Stanford Linear Accelerator Center, California, USA

Z resonance and was upgraded in 1995 to operate above the W pair production threshold.

The symmetry between the electromagnetic and the weak force also manifests itself as a symmetry between the particles on which they act. Particles that cannot be distinguished by the weak force are arranged in families, so-called weak isospin doublets. One family is composed of a quark and a lepton doublet. All matter which exists on earth in the form of gas, liquid or solid state is composed of quarks (up and down) and leptons (electron and neutrino) of one family. One of the great achievements of modern particle laboratories, as for instance CERN and SLAC, was the observation, that, in addition to the fermions of this family, other novel fermion families exist. These new particles obey the same laws of nature as electrons, protons and neutrons, the main difference being that they are not stable and decay rapidly (on time scales of 1 μs until 10^{-7} μs) into "particles of our world". If we are able to produce new forms of matter by enormous concentration of energy in a small volume at our laboratories it implies that this matter was also present in the universe subsequent to the big bang. The LEP energy corresponds to a temperature of 10^{15} K which was the average temperature of the universe 10^{-10} s (=100 ps) after the big bang. In its relation to cosmology the LEP collider is a "time machine" that brings us close to the big bang. Particle physics can be understood as the physics of the early universe.

The question arises why different fermion families are realized in nature and how many of them exist. At present three fermion families have been observed and we also have strong evidence that these are all the families that exist. But it is neither understood why replicae of the "constituents of our world" exist nor has the "magic number three" found any explanation. There is one hint for the solution of this puzzle. It is possible that the number of three fermion families is related to the observed violation of the symmetry between matter and antimatter. However, at present, no experimental evidence can support this hypothesis.

Quark families do not exist separately from each other, but do undergo transitions. This phenomenon can be described in the Standard Model, but it is still a mystery why it occurs. The so called Cabibbo-Kobayashi-Maskawa (CKM) matrix elements [3] account for these quark transitions between different families and describe the coupling strengths between quarks. This thesis is dedicated to a measurement of matrix elements of quark transitions, in particular those involving quarks of the third family. The information about CKM matrix elements is obtained from a study of decays of bottom hadrons - the down quarks of the third family. The bottom quark is the most massive quark accessible at LEP. The average lifetime of bottom quarks is of the order of 1 ps (=10^{-12} s) and its measurement requires precision apparatus. A study of the b quark decay distribution at LEP allows the determination of the CKM matrix element $|V_{cb}|$ (coupling between charm and bottom quark) and in principle, if the measurement is precise enough, also the matrix elements $|V_{ts}|$ (coupling between top and strange quark) and $|V_{td}|$ (coupling between top and down quark) can be evaluated. The current experimental and theoretical accuracy allows the determination of $|V_{cb}|$ with an uncertainty of 5%.

In contrast, the ratio $|V_{td}\,/\,V_{ts}|$ has never been measured, so far. It is the aim of this thesis to perform a precision measurement of the $|V_{cb}|$ element and to attempt a measurement of the ratio $|V_{td}\,/\,V_{ts}|$.

The sensitivity to the matrix element $|V_{cb}|$ arises from its relation to the average b hadron lifetime, whereas the matrix elements $|V_{td}|$ and $|V_{ts}|$ are related to the $B^0 - \overline{B}^0$, $B_s - \overline{B}_s$ oscillation phenomenon. Oscillations between particles and antiparticles, as for instance that of neutral bottom mesons, are a consequence of quark mixing in the weak interaction. The flavour-changing quark transitions yield two distinct mass eigenstates of neutral B mesons which differ in their masses and lifetimes but are built from the same quark constituents. Interference between these two mass eigenstates causes an initial pure flavour state to change its flavour composition as a function of time. This oscillation behaviour has been studied in detail in the neutral kaon system. Since 1987 it has been observed that also the bottom quantum number is oscillating in time [4]. The oscillation phenomenon has two complementary manifestations: the flavour eigenstates oscillate with a frequency ω into one another and the mass eigenstates decay with two distinct decay times Γ_1, Γ_2. The oscillation frequency ω as well as the lifetime difference $\Delta\Gamma = \Gamma_1 - \Gamma_2$ of neutral mesons are correlated to the relevant CKM matrix elements, in case of B mesons $|V_{td}|$ and $|V_{ts}|$. The approach of this thesis is a measurement of the lifetime difference $\Delta\Gamma$, which would complete the existing measurements of ω.

1.2 The Standard Model

1.2.1 The elektroweak interaction

The Standard Model of *electroweak* interaction (SM) is based on a SU(2) $\times$ U(1) gauge group. The gauge group of the unified electroweak interaction is formed as a direct product of the SU(2) group of the weak isospin and a U(1) group for the description of the electric charge. The *fundamental fermions*, i.e. the quarks and leptons, as well as the transmitters of the force, the so-called *gauge bosons*, are irreducible representations of this gauge symmetry group. There are three families of fundamental fermions, each containing an up-type quark, a down-type quark, a charged lepton and a neutrino, as listed in table 1.1. Each fermion is characterized by a specific *flavour*. Forces between the fermions are mediated by the exchange of gauge bosons. The SM contains four of them: the photon and the massive Z and $W^{\pm}$ bosons. The SU(2) $\times$ U(1) symmetry is spontaneously broken by the ground state due to the presence of a third kind of particle, the scalar *Higgs boson*. The Higgs boson is attributed to be responsible for the masses of the fermions and gauge bosons. It has not been observed yet and the understanding of this mechanism remains one of the most fundamental problems facing particle physicists. The values of the masses of fermions and gauge bosons are listed in table 1.2.

fermions	family 1	2	3	Q/e
quarks	u	c	t	2/3
	d	s	b	-1/3
leptons	e	μ	τ	-1
	ν_e	ν_μ	ν_τ	0
gauge bosons	γ			0
	Z			0
	$W^\pm$			$\pm$ 1

Table 1.1: The three known families of elementary fermions, the electroweak gauge bosons that act as their force carriers, and their respective charges.

		mass
quarks	u	$\sim$ 300 MeV
	d	$\sim$ 300 MeV
	c	(1.5 $\pm$ 0.2) GeV
	s	$\sim$ 500 MeV
	t	(175 $\pm$ 6) GeV
	b	(4.9 $\pm$ 0.2) GeV
leptons	e	0.511 MeV
	ν_e	$\sim$ 0?
	μ	105.6 MeV
	ν_μ	$\sim$ 0?
	τ	1.777 GeV
	ν_τ	$\sim$ 0?
gauge bosons	γ	0
	Z	91.19 GeV
	$W^\pm$	(80.33 $\pm$ 0.15) GeV

Table 1.2: The masses of elementary fermions and electroweak gauge bosons [5].

In the SM the coupling strength between fermions and gauge bosons is related to a few fundamental parameters. These are the fermion electric charge Q_f, the weak isospin I_f, the electroweak mixing angle θ_W and the parameters of the so-called Cabibbo-Kobayashi-Maskawa matrix. The transition matrix elements between fermions are expressed in terms of *currents*, i.e. terms bilinear in the fermion fields. The currents couple to the boson fields γ, Z and $W^\pm$. The currents that couple to the neutral gauge bosons γ and Z are termed *neutral currents*, those that couple to the charged $W^\pm$ bosons *charged currents*.

In the SM the Lagrangian of the neutral current interaction is given by:

$$\mathcal{L}_{int}^{NC} = \sum_i \bar{f}_i \left(e\,\gamma^\mu\,Q_f\,A_\mu + \frac{e}{\sin\theta_W\cos\theta_W}\,\gamma^\mu\,(I_{3f}\,(1-\gamma_5) - 2\,Q_f\sin^2\theta_W)\,Z_\mu \right) f_i \tag{1.1}$$

Here γ^μ are the Dirac matrices and $(1-\gamma_5)/2$ is the projection operator to left-handed states. I_{3f} denotes the third component of the weak isospin. The unification of electromagnetic and weak interactions is visible in a combined description involving the photon field A_μ and the Z boson field Z_μ. Often used variables are also the vector and axial-vector coupling constants g_V and g_A. They denote the Z coupling constants proportional to γ^μ and $\gamma^\mu\,\gamma_5$, respectively:

$$\begin{aligned} g_V &= I_{3f} - 2\,Q_f\sin^2\theta_W\ , \\ g_A &= I_{3f}\ . \end{aligned} \tag{1.2}$$

In the following sections a measurement of g_V and g_A will be discussed as an example of an experimental proof of relation (1.2). The neutral current is flavour-conserving, i.e. a fermion can never change its flavour in a neutral current reaction. However the charged current contains flavour-changing transitions. As it was shown by Kobayashi and Maskawa [3] the Lagrangian of the charged current interaction has the form:

$$\mathcal{L}_{int}^{CC} = \frac{e}{\sqrt{2}\sin\theta_W}\ \sum_{i,j}(\bar{u}')^i\ \gamma^\mu(1-\gamma_5)\ W_\mu^+\ (V_{CKM})_{ij}\ (d')^j\ + \text{h.c.}\ . \tag{1.3}$$

Here V_{CKM} denotes the so-called Cabibbo-Kobayashi-Maskawa matrix. The elements of this matrix describe the coupling strengths between charge 2/3 quarks $u' = (u, c, t)$ and charge -1/3 quarks $d' = (d, s, b)$. The determination of these elements is the main topic of this thesis. Chapter 2 contains a detailed discussion of charged current interactions.

It can be shown [6] that non-trivial combinations of vector and axial-vector couplings violate the parity symmetry. This is the case of couplings to the Z and $W^\pm$ bosons. The weak interaction is not invariant under the parity transformation P. On the contrary, couplings to the photon involve only vector currents and conserve parity.

1.2.2 The strong interaction

Only the quarks take part in the strong interaction. They are confined to bound states, called hadrons, which are composed of a quark-antiquark pair (mesons) or of a quark-triplet (baryons):

$$\begin{aligned} \text{mesons} &\sim q\bar{q} \\ \text{baryons} &\sim qqq\ . \end{aligned}$$

In the theory of strong interactions, Quantum Chromo Dynamics (QCD), the quarks carry a *colour* charge, that is independent of the quark flavour. There are

three different colours for quarks and antiquarks, respectively. In this way mesons and baryons can be composed as colourless objects. The theory of QCD is based on a gauge group SU(3) of colour. This gauge group has eight gauge bosons called gluons. QCD is a non-abelian gauge theory, i.e. the gluons themselves carry a colour charge and therefore interact with each other. The strong interaction has the property that the effective coupling strength decreases with increasing energy scale Q^2. The limits of $Q^2 \to \infty$ and $Q^2 \to 0$ are known as *asymptotic freedom* and *confinement*, respectively. The consequence is that the applicability of QCD is energy-dependent. QCD has been very successful in the calculation of interactions at high energies, for instance in deep-inelastic scattering of electrons on protons. However, below a characteristic energy scale of $\Lambda_{QCD} \sim 200$ MeV, calculations in QCD diverge. This region of non-perturbative QCD still leaves many questions open. The description of hadron decays belongs to this difficult region. Analytic calculations in this region may be possible in special cases, such as for hadrons containing heavy quarks with masses $\gg \Lambda_{QCD}$, where the Heavy Quark Effective Theory can be used [7], as will be discussed later.

Mesons and baryons are classified according to their flavour composition, the spin and the angular momentum of the quarks. The large hadronic spectrum of the Particle Data Tables [5] can be successfully reproduced by this ordering scheme. In this thesis properties of the ground states of bottom hadrons are studied:

	B_u^+	B_d^0	B_s^0	Λ_b
abbreviation	B^+	B^0	B_s	Λ_b
quark content	$(\bar{b}u)$	$(\bar{b}d)$	$(\bar{b}s)$	(bud)
spectroscopic notation J^P	0^-	0^-	0^-	$\frac{1}{2}^+$

Table 1.3: Bottom hadron ground states. The flavour content and the spectroscopic notations are shown. The lowest lying b mesons are characterized by a zero value for the spin and for the angular momentum of the quark system. In case of the Λ_b baryon the diquark-system ud has a spin of zero. Note that the values for the total angular momentum J and the parity P are expectations from the quark model, none of them have actually been measured. The abbreviations shown in the second line will be used throughout this thesis.

1.3 History of the bottom quark discovery

The first experimental evidence for a fifth quark came in 1977 with the observation of a narrow resonance $\Upsilon(1S)$ and its first excited state $\Upsilon(2S)$ by the CFS Collaboration [8] in the process $p + nucleus \to \mu^+\mu^- + X$ at Fermilab. The $\Upsilon(1S)$ resonance at ~ 9.5 GeV in the invariant mass spectrum of μ-pairs has been tentatively interpreted as a bound state $|b\overline{b}\rangle$ of a new heavy quark in analogy to the discovery of the J/Ψ [9] in 1974. This interpretation was favoured by the discovery of the

third charged lepton, the τ [10], in 1975 and the postulation of a third quark family by Kobayashi and Maskawa [3] in 1973 in order to incorporate CP violation (an asymmetry between matter and antimatter) into the electroweak SM framework. However, a full identification of a new heavy quark requires a measurement of its electric charge and appropriate couplings to the $W^{\pm}$ and Z bosons.

The results of the CFS Collaboration were subsequently confirmed studying e^+e^- annihilations [11, 12] leading to observations of further Υ states ($\Upsilon(2S)$, $\Upsilon(3S)$, $\Upsilon(4S)$). The $\Upsilon(4S)$, at a center-of-mass energy at 10.58 GeV [12], is much broader than the previous three states, indicating that the threshold for the production of pairs of B mesons had been crossed (fig. 1.1). Within the framework of the SM the bottom quark production can be understood as a transformation of the energy of e^+e^- annihilations into the creation of new massive fermions. The Υ resonance is produced in a single-photon annihilation of an e^+e^- pair, illustrated in the Feynman diagram fig. 1.2. The coupling of the b quark to the intermediate photon is determined by its electric charge. A measurement of the Υ partial width into e^+e^- pairs $\Gamma_{ee}(\Upsilon(1S))= 1.3 \pm 0.3$ keV [11, 12] favoured the assignment of charge -1/3 for the new quark.

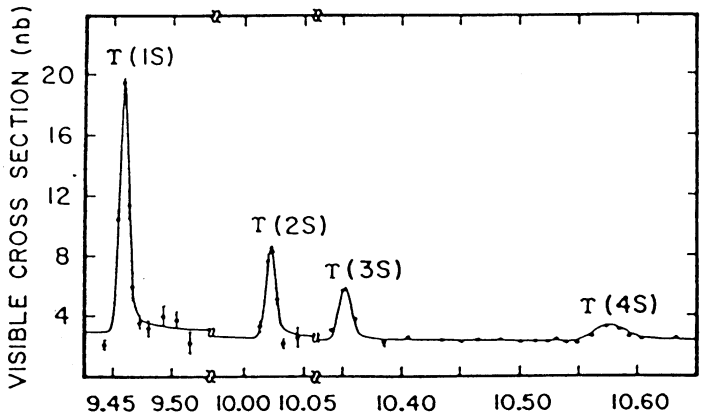

Figure 1.1: The e^+e^- total cross section for Υ production measured by the CLEO Collaboration [12].

1.4 The process $e^+e^- \to b\bar{b}$ at the Z resonance

Measurements at e^+e^- colliders of higher energies (PEP, PETRA, KEK, LEP and SLC) could establish the weak-isospin doublet character of the b quark by a measurement of its vector and axial-vector couplings to the Z boson. The processes at the e^+e^- storage rings LEP and SLC, operating at the Z resonance, are dominated by e^+e^- annihilations into Z bosons (fig. 1.2), whereas the previous colliders PEP, PETRA and KEK are mainly sensitive to e^+e^- annihilations into photons and the γ-Z interference term.

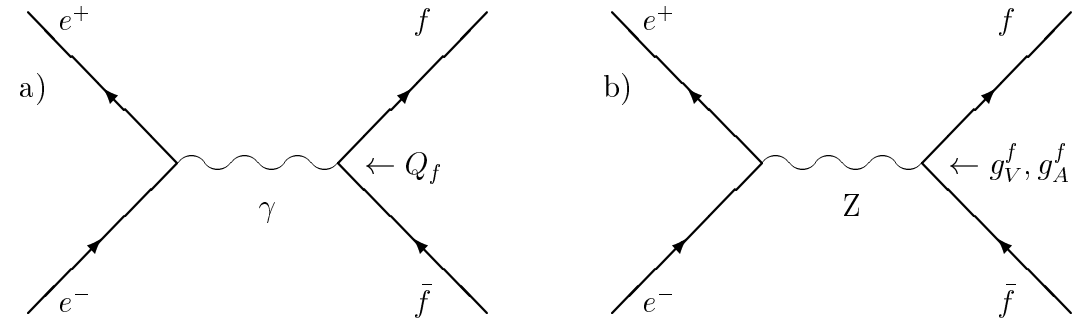

Figure 1.2: Fermion production via e^+e^- annihilation a) into photons and b) into Z bosons.

The partial decay width of the Z boson into fermions $f\overline{f}$ is:

$$\Gamma(Z \to f\overline{f}) = \frac{G_F \mathrm{M}_Z^3}{6\sqrt{2}\pi} \left(f_V \, g_V^2 + f_A \, g_A^2 \right) N_C^f (1 + \delta_{QED})(1 + \delta_{QCD}) \; . \tag{1.4}$$

Here g_V and g_A are the previously defined vector and axial-vector coupling constants. Several corrections need to be taken into account in formula (1.4). For leptons only Quantum Electrodynamic (QED) corrections δ_{QED} have to be applied, while for quarks equation (1.4) also contains a factor $N_C^f = 3$ due to colour and corrections δ_{QCD} due to Quantum Chromodynamics (QCD). The factors $f_V, f_A \sim 1$ account for fermion mass effects, which are small. Weak radiative corrections are incorporated by replacing $g_{V,A}$ by the effective couplings $\bar{g}_{V,A}$ at the Z-pole. There is an additional top-mass dependence for the partial decay width $Z \to b\overline{b}$. The SM prediction for bottom quarks is $\Gamma(Z \to b\overline{b}) = 375.9 \pm 0.2$ MeV [5]. An often used variable, $R_b = \Gamma_{b\overline{b}}/\Gamma_{\mathrm{had}}$, describes the partial width into bottom quarks normalized to the total hadronic decay width Γ_{had}, the SM value lies at $R_b = 0.2156 \pm 0.0001$ [5].

Two independent observables are needed for the determination of g_V and g_A. The second variable used is the forward-backward asymmetry of b quarks, A_{fb}, derived from the differential cross section:

$$\frac{d\sigma}{d\cos\theta} \propto \left(1 + \cos^2\theta + \frac{8}{3} A_{fb} \, \cos\theta \right) \; , \tag{1.5}$$

where the angle θ denotes the polar angle of the b quark with respect to the direction of the e^- beam. The term $(1 + \cos^2\theta)$ reflects the spin 1 intermediate state of the Z boson and the spin 1/2 of the bottom quarks. The asymmetry A_{fb} is correlated to $g_{V,A}^e$ of the electron initial state and $g_{V,A}^f$ of the final fermion state via:

$$A_{fb} = \frac{3 \, g_V^e \, g_A^e \, g_V^f \, g_A^f}{({g_V^e}^2 + {g_A^e}^2)({g_V^f}^2 + {g_A^f}^2)} \; . \tag{1.6}$$

The L3 measurements of R_b and A_{fb} [13] were interpreted in terms of $g_{V,A}^b$ of b quarks, giving four pairs of values for the coupling constants, where the electron

couplings $g^e_{V,A}$ were taken from the L3 measurements in the lepton sector [14] with the signs assumed to be that of the SM.

What can we conclude for the b quark couplings relative to that of the electron? First, the vector couplings cannot be distinguished from the axial-vector couplings, because they enter symmetrically into the equations for R_b and A_{fb}. Second, the signs of g^b_V and g^b_A cannot be measured separately, but the sign of the product $g^b_V g^b_A$ is defined by the A_{fb} measurement. This leads finally to a fourfold ambiguity, illustrated in fig. 1.3.

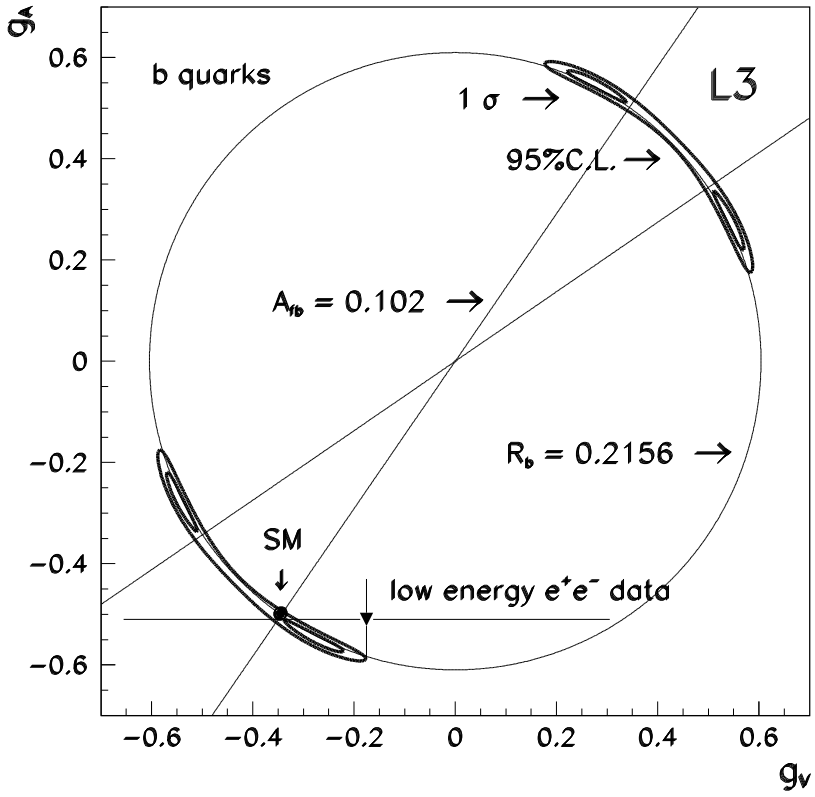

Figure 1.3: Vector and axial-vector couplings of the Z boson to bottom quarks measured by the L3 Collaboration [13]. The four regions show the experimentally allowed values in the g_V, g_A plane at 1σ and 95% confidence level. The SM point indicates the expected couplings g_V, g_A for b quarks using the weak mixing angle θ_W measured by L3 in the lepton sector [14]. The circle and straight lines show contour lines of constant R_b and A_{fb}, respectively, according to the SM expectation. Results from low energy e^+e^- experiments at PEP, PETRA and KEK are also shown which select a unique solution of g_V, g_A values [15].

The ambiguity can be resolved by including e^+e^- data from PETRA, PEP and KEK, where the asymmetry A_{fb} is dominated by the γ-Z interference term, proportional to $Q_e\, g_A^e\, Q_b\, g_A^b$. The sign of the axial coupling g_A^b is thus determined with respect to the reference definition of the electron. The limits obtained in [15] select a unique solution of the L3 values for g_V^b and g_A^b:

$$\begin{aligned} g_V^b &= -0.27^{+0.05}_{-0.07} \\ g_A^b &= -0.55^{+0.04}_{-0.03} \,. \end{aligned} \tag{1.7}$$

The measurement of $g_{V,A}^b$ can be compared with the SM expectation, that the vector and axial-vector couplings of all fermions are determined by a single parameter, the weak mixing angle θ_W, according to equation (1.2). The axial-vector coupling g_A^b is compatible with the SM value -0.5 and the vector coupling g_V^b compares well with the expectation -0.3459 $\pm$ 0.0015 derived from L3 measurements in the lepton sector [14]. The negative sign of g_A^b identifies the b quark as the bottom state of a weak isospin doublet.

We conclude, the weak-isospin doublet nature of the b quark has been experimentally established and the weak mixing angle θ_W derived from b quark measurements is in agreement with independent θ_W measurements using leptons. By implication, the other member of the isospin-doublet, namely the top quark, must exist! The long awaited observation of the the top quark, has been successful in 1995 at the world's highest-energy proton collider, the Tevatron at Fermilab [16]. The LEP data also allow a prediction of the top-mass due to the virtual presence of the top quark in higher-order processes. The combined LEP result $m_t = 171 \pm 8\ ^{+17}_{-19}$ GeV [17], where the central value refers to a Higgs-mass of 300 GeV and the second error shows the variation with the Higgs-mass in the range from 60 GeV to 1000 GeV, is in excellent agreement with direct top-mass measurements $m_t = 175 \pm 6$ GeV [18] reported by the CDF and D0 Collaborations.

It should also be mentioned here that the charged current couplings of b quarks to the $W^{\pm}$ boson have been measured, but not with the same precision as the neutral current couplings. Measurements of the b coupling constants to the W boson rely on the assumption that b hadron decays, in particular their semileptonic decays, can be modeled by the QCD-improved quark model decay $b \to c\, l\, \nu$. Observables sensitive to the chiral structure of the $b \to c$ charged current in semileptonic b decays are the momentum spectra of the charged leptons and neutrinos [19]. The V-A structure of the leptonic current (which was confirmed in τ and μ decays) has been exploited here as an analyzer of the polarization of the virtual W. Experimental analysis at the Υ resonance [20] and at LEP [21] shows strong evidence for the V-A form of the $b \to c$ current and rules out a (V+A)$\times$(V-A) structure for the b quark decay.

1.5 Bottom hadron production from Z decays

The Z resonance provides an abundant production of b flavoured hadrons through decays of the Z into $b\overline{b}$ pairs. The evolution of the primordial $b\overline{b}$ quark system into the final hadron system as observed in the detector, is qualitatively described by QCD but quantitatively complicated by the fact that QCD does not allow for perturbative expansions at momentum transfers of the order the confinement scale $\Lambda_{QCD} \sim 200$ MeV and below. In the first phase if the quarks are separated by less than ~ 1 fm they behave like asymptotically free particles, which is observable in the back-to-back two jet structure of e^+e^- events. In the following phase the quarks radiate hard gluons, that in turn radiate themselves, and lead to distinct three and four jet topologies. This stage can be treated perturbatively in QCD. At lower energies, the confinement of quarks and gluons into colour singlets leads to the formation of hadrons. This last stage, called fragmentation process, cannot be calculated exactly and must be treated using simplified models.

At the Z resonance a mixture of b hadrons is produced containing B^+, B^0, B_s mesons, Λ_b baryons and their excited states. A meson is formed when an original b quark from a Z decay combines with an u, d or s quark created in the fragmentation process. A baryon is produced if a di-quark is generated in the fragmentation. The relative production fractions of B^+, B^0, B_s, Λ_b hadrons stand in the following approximate ratios:

$$B^+ : B^0 : B_s : \Lambda_b = 4 : 4 : 1 : 1 \; . \tag{1.8}$$

It is still possibile to assume a rather simple relation like (1.8) which is in agreement with the measured values that have a resolution of not better than 20% for the B_s and Λ_b fractions [5]. The values of eq. (1.8) are the fractions of weakly decaying b hadrons. These are the ground states of the b hadrons. They are either produced as the primary fragmentation hadrons or originate from a decay of excited b hadrons. Excited b hadrons are hadrons of spin one, called B^* hadrons, or hadrons with a non-vanishing angular momentum of the quark constituents, denoted as B^{**} hadrons. The decays from excited b hadrons to the ground states proceed via the strong or the electromagnetic interaction.

The production fractions of b flavour states can be related to the masses of the b partner quarks. The probability of a $q\overline{q}$ pair to be generated in the fragmentation depends on its mass. The production of heavy quarks in the fragmentation is strongly suppressed. The total fraction of b baryons amounts to $\sim 10\%$. It is much smaller than the b meson fraction due to the suppression of di-quark pair production. As in the case of b mesons there exist several flavours of ground states of b baryons. However the Λ_b baryon is the most abundant one. It is followed by the Ξ_b^- baryon (quark content: bds) and the Ξ_b^0 baryon (bus) which have a total production fraction of $\sim 1\%$. In this thesis all kinds of b baryons are summarized under the notation Λ_b.

A detailed description of the fragmentation process is given in chapter 5.

Chapter 2

Cabibbo-Kobayashi-Maskawa quark mixing matrix

This section will first introduce the ideas leading to the Cabibbo-Kobayashi-Maskawa (CKM) mixing matrix which relates the quark mass eigenstates to those of the weak interaction. The way the information on the CKM matrix elements is obtained experimentally is the main subject addressed here. Particular interest is given to matrix elements involving quarks of the third family: the top and bottom quark. The relationship between the b hadron decay width, in particular the semileptonic width, and the CKM matrix element $|V_{cb}|$ will be outlined. The theoretical methods of Quantum Chromodynamics (QCD) to describe heavy flavour decays will be discussed briefly. Recent developments to measure the matrix elements $|V_{ub}|$, $|V_{td}|$, $|V_{ts}|$ will be presented, which are one goal of present experiments (as for instance CLEO-II and the LEP experiments) and future facilities (as CLEO-III, HERA-B, BABAR, BELLE and LHC-B). Precision studies of $B^0 - \overline{B}^0$ and $B_s - \overline{B}_s$ oscillations allow the determination of top quark transition amplitudes. A discussion of the observation of $B^0 - \overline{B}^0$ and the search for $B_s - \overline{B}_s$ oscillations, entering into the possibilities and consequences of an observation of lifetime differences of neutral B mesons, will conclude this chapter.

The elements of the Cabibbo-Kobayashi-Maskawa matrix are fundamental parameters of charge-changing weak interactions. Both leptons and quarks undergo charge-changing weak transitions. The patterns, however, appear to be radically different. At present (and this may change in the near future) each charged lepton is considered to transform into its own neutrino and vice versa the neutrino can transform back to the charged lepton, but the transitions never get out of one lepton family, as illustrated in fig. 2.1a. On the other hand, the quarks participate in a rich pattern of charge-changing currents. Transitions between quarks are not limited to one family but rather connect different families with each other (fig. 2.1b).

The first evidence for family-changing weak transitions was found in beta-decays of strange particles, as for instance $K^+ \to l^+ \nu$. These strangeness-changing decays appeared to have an amplitude of about 1/4 as big as strangeness-conserving

u $\rightarrow$ d transitions in beta-decays of nuclei [22]. On the other hand it was noted that the u $\rightarrow$ d transition strength is approximately equal to that of lepton transitions e $\rightarrow$ ν_e and $\mu \rightarrow \nu_\mu$. A solution to the "strangeness-puzzle" was given in 1963 by Cabibbo [3], who proposed a hadronic weak current with the same normalization as the leptonic one by introducing a mixing angle θ between strangeness-conserving ($\Delta S = 0$) and -changing ($\Delta S = 1$) transitions:

$$J_\mu^{Hadronic} = J_\mu^{\Delta S=0} \cos\theta + J_\mu^{\Delta S=1} \sin\theta \; . \tag{2.1}$$

The strangeness-changing transitions have been used to determine $\sin\theta \sim 1/4$, leading to only a slight departure of $\cos\theta$ from 1. The Cabibbo mixing scheme, originally formulated in terms of hadronic currents, was, after the existence of quarks has been accepted, transformed to a mixing between quarks. So far as only three quarks take part in the quark transitions also neutral strangeness-changing currents would be allowed. However, it has been observed that strangeness-changing transitions are strongly suppressed in neutral currents, as for instance stringent limits restrict the decay $K^0 \rightarrow \mu^+\mu^-$. This led to the prediction of the charm quark [23] in 1964 to banish neutral strangeness-changing currents, because the transitions involving the charm quark remove offending strangeness-changing terms.

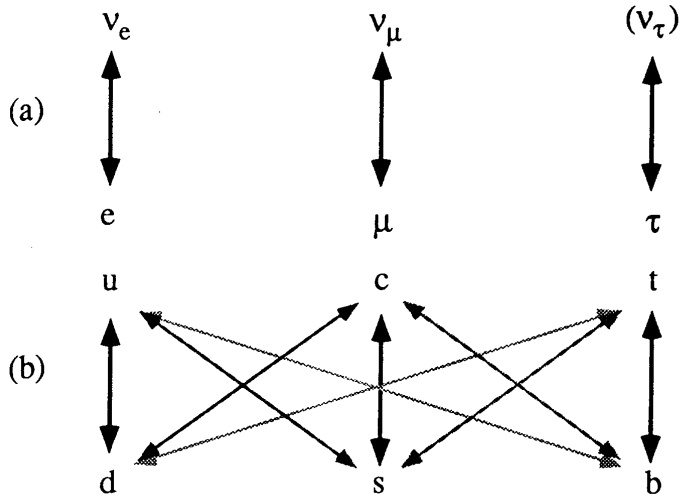

Figure 2.1: Patterns of charge-changing weak transitions among (a) leptons and (b) quarks. Direct evidence for ν_τ does not yet exist. In (b) the strongest transitions correspond to the darkest lines.

Kobayashi and Maskawa [3] have generalized the four-quark pattern to six quarks long before the τ lepton and the third quark family (t,b), and even the c quark, were observed. Only the τ-neutrino has not yet been detected directly. The balance in the number of quark and lepton doublets played a deep role in the construction of a selfconsistent and renormalizable gauge theory of electroweak interactions [24].

The Cabibbo-Kobayashi-Maskawa mixing matrix of equation (1.3) is given by:

$$V_{CKM} = \begin{pmatrix} V_{ud} & V_{us} & V_{ub} \\ V_{cd} & V_{cs} & V_{cb} \\ V_{td} & V_{ts} & V_{tb} \end{pmatrix} . \tag{2.2}$$

V_{CKM} is a 3×3 unitary matrix.

The values of individual matrix elements can in principle all be determined from weak decays of the relevant quarks, or, in some cases, from deep inelastic neutrino scattering and the oscillation strength of neutral B mesons. Table 2.1 summarizes the approximate strength of charge-changing weak transitions and their source of information. For detailed information the reader is referred to the excellent reviews in [5, 25].

Relative amplitude	Transition	Source of information (example)
~ 1	$u \leftrightarrow d$	Nuclear β-decay
~ 1	$c \leftrightarrow s$	Charm particle decays
~ 0.22	$u \leftrightarrow s$	Strange particle decays
~ 0.22	$c \leftrightarrow d$	Neutrino production of charm
~ 0.04	$c \leftrightarrow b$	Bottom particle decays
~ 0.04	$t \leftrightarrow s$	Rare penguin B decays ($b \rightarrow s$)
~ 1	$t \leftrightarrow b$	Top quark decays
~ 0.003	$u \leftrightarrow b$	Charmless B decays ($b \rightarrow u$)
~ 0.01	$t \leftrightarrow d$	$B^0 - \overline{B}^0$ oscillation

Table 2.1: Relative strengths of charge-changing weak transitions.

A table similar to 2.1 for the transitions between leptons does not exist at present. The absence of a mixing matrix in the lepton sector is related to the zero mass of neutrinos. In the limit of degenerate neutrino masses (for example zero mass) a lepton family mixing becomes physical meaningless. However the assumption of zero neutrino mass is not protected by a fundamental gauge symmetry and it might be that we are close to the discovery of non-vanishing neutrino masses by one of the recent neutrino oscillation experiments [26]. An observation of neutrino oscillations would confirm the existence of family mixing among leptons.

The tendency of neutrinos to have small or even zero masses was also used to derive the number of fermion families. A first indication for a new fermion family is expected to arise from neutrinos which could be pair produced in Z decays in the LEP experiments. This would influence the shape of the Z resonance. The LEP experiments derived $N_\nu = 2.989 \pm 0.012$ [17] from the invisible Z decay width, which is extracted from the Breit-Wigner relation between the width and the height of the Z resonance curve. Due to the balance in the number of lepton and quark families we can exclude a quark doublet of a fourth family, even with masses not accessible at present accelerators.

Now the number of free parameters in the mixing matrix V for three quark families will be evaluated. As already mentioned, V is a 3×3 unitary matrix. An arbitrary complex 3×3 matrix has 18 real parameters, but unitarity ($V^+V = 1$) provides nine constraints, so only nine real parameters remain. Five of these parameters can be removed by appropriate redefinitions of the relative phases of six quarks. The number of remaining parameters is then four. Of these, three, namely the number of independent rotations correspond to angles while the last one represents a phase. It was the necessary presence of this phase that served as the prime motivation of Kobayashi and Maskawa for the introduction of a third quark doublet. In the four-quark case there is only one angle and no phase, corresponding to the case of Cabibbo mixing.

The phase in the six-quark pattern provides a potential source of CP violation, i.e. a difference in the dynamical behaviour of particles and antiparticles. It is obvious that the symmetry between particles and antiparticles is broken, because our universe consists mainly of matter and only barely of antimatter. The notation CP stands for the discrete operations of the charge conjugation C, transforming particles into antiparticles, and the parity transformation P, switching the orientation of the particle spin relative to its flight direction. In the absence of any interaction an asymmetry between particles and antiparticles would appear as a violation of the C symmetry, making the free motion of particles different from antiparticles. However, a dynamical difference between matter and antimatter has to be defined as a violation of the CP symmetry, because the weak interaction does not respect the P symmetry [27]. The weak interaction can distinguish between the mirror images of a particle: that one of positive helicity behaves different than that of negative helicity, i.e. the spin has a preferred direction relative to the flight direction of the particle. It has been observed that the polarization of particles is opposite to that of antiparticles. This observation alone makes no distinction between matter and antimatter. On the contrary, it is necessary to compare particles and antiparticles of the same helicity. The question is if antimatter could be defined as matter of the opposite charge and opposite helicity or if there is real need for a new quantum number to characterize antimatter. To summarize, matter behaves identically to antimatter if the laws of nature are invariant under the product of C and P, the CP transformation.

How is CP violation correlated with quark mixing? Any process that is determined by a single quark transition occurs with a probability proportional to the square of the respective matrix element. This is independent of whether particles or antiparticles are involved in the process. If, however, two possibilities exist to transform a given initial state into a final state, and if both paths are determined by different quark transitions, then in addition to the sum of the squares of the matrix elements an interference term participates in the process that depends on the relative phase between the matrix elements. This interference term has the opposite sign for particles and antiparticles and causes a difference in the total rate of a process involving matter and its CP mirror process involving antimatter.

At present CP-violating effects were only observed in decays of neutral kaons [28].

Because of the absence of other hints the origin of CP violation is still a mystery. It is not even known if CP violation is a property of the weak interaction or rather caused by a superweak so far unknown force [29] because only tiny effects were observed. According to our present knowledge about the magnitude of CKM elements substantial CP asymmetries are expected in decays of bottom hadrons. Several future experiments (HERA-B, BABAR, BELLE, the run-II period at CDF and LHC-B) will be devoted to shed light on the mystery of CP violation by a measurement of these CP asymmetries.

Nevertheless it is interesting to study the three angles occuring in the CKM matrix. It was observed that these angles satisfy a hierarchy in the sense that transitions between the first and second quark family are much stronger than those between the second and third family but the latter ones are still stronger than those from the first to the third family. The angles differ approximately by one order of magnitude (see tab. 2.1). A crucial role in the discovery of this hierarchy was played by the first measurement of the b lifetime in 1983 by the MARK-II and MAC Collaborations [30] at SLAC. The average b lifetime was believed to be much shorter than the time resolution achieved at that time. Its measurement came completely unexpected and was interpreted as a strong suppression of the relevant matrix element $|V_{cb}|$ relative to the known matrix element $|V_{us}|$.

A parametrization of the CKM matrix reflecting the observed hierarchy is the one by Wolfenstein [31]:

$$V \approx \begin{pmatrix} 1-\lambda^2/2 & \lambda & A\lambda^3(\rho - i\eta) \\ -\lambda & 1-\lambda^2/2 & A\lambda^2 \\ A\lambda^3(1-\rho-i\eta) & -A\lambda^2 & 1 \end{pmatrix} . \tag{2.3}$$

Transitions between the first and second family appear at the order $\lambda = \sin\theta_{Cabibbo}$ whereas transitions between the second and third family occur at the order λ^2 and transitions between the first and third family are suppressed by a factor λ^3. The parameters A and ρ control the fine-tuning of the three angles and η represents the complex phase responsible for CP violation. Today the best measured parameter of the CKM matrix is λ followed by A, ρ and η, in order of decreasing accuracy. In the following we consider the parameter λ to be known (see references [5, 25]) and discuss the determination of A, ρ and η in more detail. Existing knowledge from recent measurements and theoretical approaches as well as proposals for future measurements will be reviewed.

It should be mentioned that the parametrization (2.3) is not exactly unitary. It was derived from a expansion in powers of λ where higher order terms above λ^3 were neglected. The observed hierarchy, which cannot be understood from first principles, is the underlying feature of this parametrization. An exact parametrization contains at least five elements with the complex phase η. However, as a consequence of the hierarchy all except two can be neglected in the Wolfenstein parametrization, so that η appears only in transitions from the first to the third family. Processes which are dominated by transitions between the first and third family, as for instance $B^0 - \overline{B}^0$ oscillations, are expected to have larger CP-violation effects [32]

than those observed in the neutral kaon system. But one should keep in mind that this prediction is based on purely empirical arguments. A deeper understanding of the hierarchy of CKM elements remains a challenge for the physics beyond the SM.

2.1 Matrix element $|V_{cb}|$

The measurement of $|V_{cb}|$ constituted the first evidence for family changing transitions involving quarks of the third family. The magnitude of $|V_{cb}|$ determines the parameter A in the Wolfenstein parametrization of the CKM matrix. There are several ways to measure $|V_{cb}|$. First, the average b hadron lifetime is interpreted in terms of the matrix element $|V_{cb}|$ and second, the rate of exclusive semileptonic b decays can be used to determine $|V_{cb}|$. As for many other CKM elements, a reliable theoretical description is needed to extract the $|V_{cb}|$ element with high accuracy. In case of b hadron decays promising theoretical techniques exist to reduce the model dependence in the $|V_{cb}|$ determination.

2.1.1 Inclusive semileptonic width $\Gamma(B \to X_c\, l\, \nu)$ of b hadrons

The description of weak b hadron decays will start with the spectator model, where differences between the decaying b hadron and the b quark are neglected and will be complemented by the modern treatment of strong interaction effects in b hadron decays, based on first principles of QCD.

Spectator model of semileptonic b decays

The spectator model of b hadron decays is based on the approximation that the b quark decays as a free particle, thereby neglecting all effects due to the accompanying light antiquark in b mesons and the diquark system in b baryons (fig. 2.2). Within this picture the charged-current weak decay of a b hadron can be treated as the muon decay, correcting for the mass of the b quark and the $b \to c$ transition strength:

$$\begin{aligned} \Gamma(b \to c\, e\, \bar{\nu}_e) &= \Gamma(\mu \to \nu_\mu e\, \bar{\nu}_e)\, |V_{cb}|^2 \left(\frac{m_b}{m_\mu}\right)^5 \\ &= \frac{G_F^2 m_b^5}{192\pi^3}\, |V_{cb}|^2 \qquad (l = e, \mu)\ . \end{aligned} \tag{2.4}$$

It is known that the dominant decays of b quarks involve charmed quarks in the final state, so that $|V_{cb}| \gg |V_{ub}|$, but in principle a similar expression for eq. (2.4) would relate $\Gamma(b \to u\, l\, \bar{\nu})$ with $|V_{ub}|$. The non-leptonic decay rate of b hadrons also can be calculated within the spectator model, in which case a factor $N_C = 3$ enters

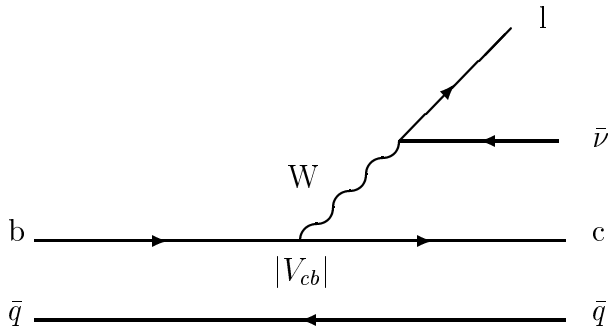

Figure 2.2: Spectator model diagram for b meson decays.

in eq. (2.4) due to colour. However the model is not expected to be as precise as in the case of semileptonic decays due to possible gluon exchange between final state quarks. It is necessary to take into account the masses of the final state fermions, so far neglected in eq. (2.4). The charm-quark mass m_c significantly reduces the available phase space, which is expressed by a phase-space factor f^{PS}. This factor depends on the ratio between the c and b quark mass:

$$f^{PS} = f^{PS}\left(\frac{m_c}{m_b}\right) \tag{2.5}$$

and evaluates to [33]:

$$f^{PS}(\epsilon) = 1 - 8\epsilon^2 + 8\epsilon^6 - \epsilon^8 - 24\epsilon^4 ln\epsilon \quad , \quad \epsilon = \frac{m_c}{m_b} \, . \tag{2.6}$$

For a reasonable choice of the quark masses [34],

$$\begin{aligned} m_b &\approx 4.8 \text{ GeV} \\ m_b - m_c &\approx 3.5 \text{ GeV} \, , \end{aligned} \tag{2.7}$$

the phase space correction factor amounts to f^{PS}=0.585, making the b lifetime almost a factor of two longer than that of a decay to massless fermions.

QCD model of semileptonic b hadron decays

The strong interaction effects in weak decays of heavy hadrons can be treated with QCD methods which were developed along two main directions, 'symmetry based' and 'dynamical'. Today a consistent well-defined theory is available combining the two counterparts: global heavy quark symmetry, on the one hand, and asymptotic freedom, on the other. The general idea of separating the two domains and applying different theoretical tools to them was formulated long ago by Wilson, whereas the heavy quark symmetry was first observed and developed by Isgur and Wise. The physical picture underlying the heavy quark symmetry is the following [7].

In a bound state such as a meson or baryon, the typical momenta exchanged between the constituents are of order the confinement scale Λ_{QCD}. Hadrons can be understood as a cloud of strongly interacting quarks, antiquarks and gluons. However, a typical property of heavy hadrons is the fact that $1/m_b \ll 1/\Lambda_{QCD}$, i.e. the Compton wavelength of the heavy quark is much smaller than the size of the hadron. As the portion of the volume that the b quark occupies inside the hadron is of order $(\Lambda_{QCD}/m_b)^3$ the accompanying quarks and gluons behave like spectators and their effects are small. This is a new global symmetry! The heavy quark is nothing but a static source of a colour field for the other constituents. The light hadron constituents only experience this colour field and decouple from the flavour and spin of the heavy quark.

Heavy quark symmetry is an approximate symmetry due to the finite b quark mass and corrections are calculated in powers of Λ_{QCD}/m_b. The way the expansion in powers of Λ_{QCD}/m_b is carried out is the Operator Product Expansion (OPE) [35], where bound-state effects of b hadrons can be accounted for in a systematic way.

The central result obtained by application of OPE to the inclusive decay width of b hadrons is the absence of $1/m_b$ corrections, the leading power corrections start with terms $1/m_b^2$. The theoretical expression for the inclusive semileptonic width has been evaluated in [34] including the α_s and leading nonperturbative corrections. It can be translated into a relation between the average lifetime τ_b, the semileptonic branching ratio $\mathcal{B}(B \to X_c\, l\, \nu)$ and $|V_{cb}|$ [34]:

$$|V_{cb}| = 0.0408 \left(\frac{\mathcal{B}(B \to X_c\, l\, \nu)}{0.105}\right)^{1/2} \left(\frac{1.6 \text{ ps}}{\tau_b}\right)^{1/2} . \tag{2.8}$$

The theoretical uncertainties in extracting $|V_{cb}|$ from eq. (2.8) are still a contentious issue [34, 36]. Several sources of systematic uncertainties may be distinguished: uncertainties in the phase space, i.e. the quark masses, uncertainties from higher-order perturbative corrections, and uncertainties in the values of the hadronic parameters contained in the non-perturbative corrections. The biggest uncertainty arises from our limited knowledge of the quark masses. The b quark mass has been determined from a study of the excitation states of the Υ system. At first sight it might seem that the fifth power of m_b in eq. (2.4) strongly magnifies the uncertainty in m_b. However the precise value of m_b is not too important since the $b \to c$ width depends to a large extent on the difference $m_b - m_c$ rather than on m_b itself [34]. The quark mass difference $m_b - m_c$ can be measured by fitting the endpoint lepton spectrum of b decays at the $\Upsilon(4S)$ resonance. Independently the heavy quark symmetry relates $m_b - m_c$ to the mass difference between heavy mesons via:

$$m_b - m_c = \frac{M_B + 3M_{B^*}}{4} - \frac{M_D + 3M_{D^*}}{4} + \mu^2 \left(\frac{1}{2m_c} - \frac{1}{2m_b}\right) , \tag{2.9}$$

where μ^2 characterizes an energy scale related to the average momentum of the b quark inside a B hadron at rest. The scale μ^2 has been obtained from QCD sum

rule calculations, but also could be extracted from data. A dedicated analysis of the lepton spectra will determine μ^2 with a better accuracy - so that the biggest theoretical uncertainty for $|V_{cb}|$ can be improved by measurements in the near future. The present uncertainties in the quark masses lead to a 3% uncertainty in $|V_{cb}|$ [34].

The appropriate definition of quark masses is the major source of controversy about extraction of $|V_{cb}|$ from the inclusive width. If $\Gamma(B \to X_c\, l\, \nu)$ is calculated in terms of the pole mass (mass of a free quark observed from infinity), on which the heavy quark theory was originally based, there are significant higher-order perturbative corrections of the order $\sim 10\%$ [36]. The solution of the problem is to avoid the use of unphysical quantities like the mass of a free quark. It cannot be determined from experiment and also the theoretical expressions are not well-behaved when parametrized in them. The mass that can be extracted from experiment with, in principle, unlimited accuracy is the short-distance running mass. If the inclusive width is expressed in terms of the short-distance mass, the higher-order corrections are small and well-behaved. In reference [34] an uncertainty of 2% in $|V_{cb}|$ is assigned as a conservative estimate of higher-order effects.

The uncertainties from non-perturbative corrections were estimated to be small ($\sim 0.5\%$). The quoted uncertainty of 3% from phase space in reference [34] already includes the uncertainty from Λ_{QCD}/m_b power corrections. Therefore, the numerical analysis implies that already at present the theoretical uncertainty in the value of $|V_{cb}|$ from the semileptonic inclusive width does not exceed 5%. The determination of the value for $|V_{cb}|$ from measurements of the semileptonic branching ratio $\mathcal{B}(B \to X_c\, l\, \nu)$ and the average lifetime τ_b according eq. 2.8 will be presented in chapter 8.

2.1.2 Exclusive semileptonic decays

One important consequence of the heavy quark symmetry is that all hadronic form factors in semileptonic decays of the type $B \to D^*\, l\, \bar{\nu}$ and $B \to D\, l\, \bar{\nu}$ are related to a single universal form factor, the Isgur-Wise function $\mathcal{F}(q^2)$, and the normalization of this function at maximum momentum transfer q^2 is fixed: $\mathcal{F}(q^2_{max}) = 1$ (corresponds to zero recoil of the $D^{(*)}$ meson in the B rest frame). The reason for that behaviour can easily be understood: The configuration of light constituents in a hadron containing a single heavy quark with velocity v and spin s does not change if this quark is replaced by another heavy quark with different flavour or spin s', but with the same velocity v. Therefore a measurement of the zero recoil rate $d\Gamma/dq\,(q^2 = q^2_{max})$ in decays $B \to D^*\, l\, \bar{\nu}$ or $B \to D\, l\, \bar{\nu}$ offers an alternative method for the determination of $|V_{cb}|$.

The advantage of small theoretical uncertainty in hadronic matrix elements has been obtained for the price of statistics. The phase space is strongly reduced in the region of maximum momentum transfer and converges to zero for $q^2 \to q^2_{max}$. The strategy for the $|V_{cb}|$ determination is to extract the product

$|V_{cb}|\mathcal{F}(q^2_{max})$ from a measurement of the differential decay rate $d\Gamma/dq$ and to extrapolate it to $q^2 \to q^2_{max}$. The relation $\mathcal{F}(q^2_{max}) = 1$ holds only in the infinite mass limit, for finite masses $m_{b,c}$ it acquires corrections. The power corrections enter at the level of $1/m^2_{b,c}$, as in the case of the inclusive method. Various calculations [34,36] have been performed to evaluate $\mathcal{F}(q^2_{max})$ in order to turn the exclusive measurements into a precise determination of $|V_{cb}|$. The accuracy in $|V_{cb}|$ already reaches that of the inclusive method, the results derived from measurements at the Υ resonance [37] and at LEP [38] will be discussed in chapter 8.

It is instructive to compare the inclusive method of the semileptonic decay rate with that of the exclusive approach of zero recoil rates. The zero recoil rate of exclusive decays has the conceptual advantage that, apart from the form factor itself, the measured rate is given in terms of the masses of real B and $D^{(*)}$ mesons, whereas the inclusive width is based on quark masses. On the other hand, with respect to the non-perturbative power corrections, the inclusive semileptonic width has a twofold theoretical advantage over the exclusive predictions: First, the expansion parameter is bigger in case of the exclusive rate, namely $1/m_c$, rather than $1/m_b$ as for the inclusive width. The predictions of the form factors at zero recoil are only valid for transitions between heavy quarks ($b \to c$), whereas the inclusive width is meaningful even in the limit of a light final quark (i.e. for the $b \to u$ transition). Similarly, the $|V_{cb}|$ determination from the inclusive semileptonic width with a c quark in the final state, $|V_{ub}|$ can be determined from the total $b \to u$ semileptonic width by a measurement of the branching ratio $\mathcal{B}(B \to X_u\, l\, \nu)$ (see discussion in next section). The second advantage of the inclusive decay rate concerns the fact that the sum over many hadronic channels eliminates bound-state effects related to the properties of individual hadrons. This property is termed "quark-hadron duality" in the literature. In case of the exclusive rate, long-distance effects in the form of wavefunction overlap may arise, which are difficult to control and depend rather arbitrarily on details of the wavefunction. This problem introduces a more significant model-dependence to the $|V_{cb}|$ determination from the exclusive rate. We can conclude that the dominant theoretical uncertainty in the inclusive approach is the uncertainty in the phase space, whereas the accuracy of the exclusive predictions is limited by uncertainties in the non-perturbative corrections.

From the experimental point of view the uncertainties of both methods originate from different sources as well. The inclusive approach is preferred because of statistical accuracy, whereas the exclusive one is not competitive. The systematic uncertainties of the inclusive width arise from systematic effects in the measurement of the semileptonic branching ratio and of the b lifetime. The main error sources in these measurements are uncertainties in the lepton identification efficiency on one side and uncertainties in the decay time of the charm hadron decay subsequent to the b decay on the other. In case of the exclusive rate it is important to have a good knowledge about the efficiency in the reconstruction of the exclusive channel. The error is dominated by uncertainties in branching ratios and detector efficiencies. To summarize, the methods to determine $|V_{cb}|$ are complementary to each other, both from the experimental technique as from the theoretical ansatz.

The accuracy obtained with both methods is of comparable order and the agreement in the $|V_{cb}|$ values constitutes an important test of our understanding of weak decays of b flavoured hadrons. This discussion will be continued in chapter 8.

2.2 Matrix elements $|V_{ub}|$, $|V_{td}|$ and $|V_{ts}|$

The values of the remaining CKM matrix elements involving quarks of the third family, $|V_{ub}|$, $|V_{td}|$ and $|V_{ts}|$, can all be determined from measurements of branching ratios of rare b hadron decays or transition amplitudes between b hadrons. In particular, the flavour changing neutral current (FCNC) transitions of b hadrons are sensitive to the top quark couplings $|V_{td}|$ and $|V_{ts}|$, which are difficult to measure otherwise. In this section the experimental status of the search for rare b hadron decays and $B^0 - \overline{B}^0$, $B_s - \overline{B}_s$ oscillations is reviewed and complemented by a quantitative analysis in terms of quark transition amplitudes.

2.2.1 Rare b hadron decays

All b hadron decays that do not occur through the usual $b \to c$ transition are called rare b decays. The simplest diagram for a rare b decay is obtained by replacing the $b \to c$ transition by a Cabibbo suppressed $b \to u$ transition, as shown in fig. 2.3a. These decays probe the small CKM matrix element $|V_{ub}|$, the magnitude of which sets bounds on the combination $\rho^2 + \eta^2$ in the Wolfenstein parametrization of the CKM matrix. Measurements of the magnitude of $|V_{ub}|$ have been obtained from inclusive and exclusive semileptonic b decays.

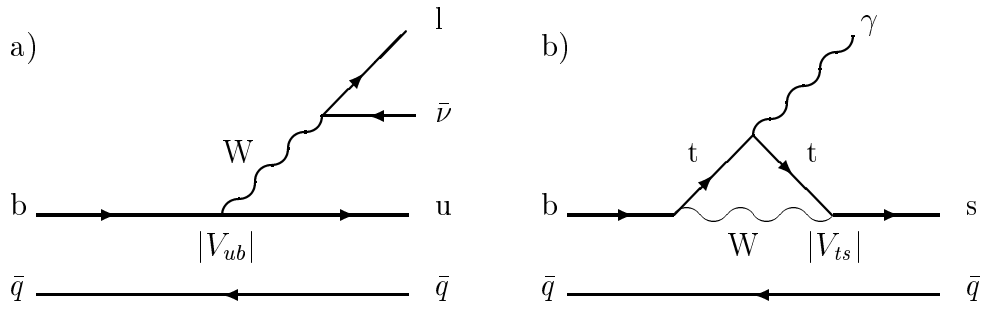

Figure 2.3: Diagrams for rare b meson decays: a) Cabibbo suppressed spectator and b) electromagnetic penguin.

In addition to the rare b decays proceeding via charge changing transitions, evidence for FCNC decays of b hadrons has been reported recently. The most significant of these decay modes is the one-loop $b \to s$ transition diagram, known as the 'penguin' diagram (fig. 2.3b). Penguin contributions lead to significant

amplitudes in b decays because the $b \to s$ loop contains the heavy top quark with the couplings $|V_{tb}|$ and $|V_{ts}|$, the largest possible couplings in penguin decays. The observation of the decay $B \to K^*(892)\gamma$, reported by the CLEO Collaboration [39], was the first direct evidence for penguin diagrams. This decay is described by the electromagnetic transition $b \to s\gamma$, where the $b \to s$ penguin loop is accompanied by the radiation of a photon. Its branching ratio as well as the inclusive $B \to X_s\gamma$ width determine the ratio of the CKM matrix elements $|V_{ts}\,/\,V_{cb}|$ and contribute in testing the unitary of the CKM matrix.

Charmless semileptonic decays

The first evidence for a non-zero matrix element $|V_{ub}|$ was obtained by studying the spectra of charged leptons in inclusive semileptonic B decays [40]. The excess of leptons beyond the kinematic endpoint for the decay $B \to D\,l\,\bar{\nu}$ directly visualizes the contribution from $b \to u\,l\,\bar{\nu}$. In order to normalize the contribution from $b \to u\,l\,\bar{\nu}$ to the dominant mode $b \to c\,l\,\bar{\nu}$ a prediction of the q^2 dependence of the form factors is needed. The q^2 domain spanned by the decays $b \to u\,l\,\bar{\nu}$ is much bigger as that of $b \to c\,l\,\bar{\nu}$ and makes the determination of $|V_{ub}\,/\,V_{cb}|$ more difficult than that of $|V_{cb}|$. The calculations for inclusive semileptonic decays are based on the assumption of quark-hadron duality. Model dependence is introduced by the predicted shape of the q^2 distributions.

On the other hand, exclusive channels, as for instance $\bar{B}^0 \to \pi^+\,l\,\bar{\nu}$ and $\bar{B}^0 \to \rho^+\,l\,\bar{\nu}$ can be studied, but the branching ratios need to be normalized according the probability that a hadronic system X_u consists of a single particle π or ρ. Nevertheless exclusive channels can be used to check different theoretical predictions in more detail. In particular, a measurement of the ratio between the partial widths to vector and pseudoscalar final states can discriminate between several phenomenological models. The combined analysis of inclusive and exclusive decays [41] determines the ratio $|V_{ub}\,/\,V_{cb}|$ to:

$$\left|\frac{V_{ub}}{V_{cb}}\right| = 0.080 \pm 0.015\,, \tag{2.10}$$

which corresponds to the constraint:

$$\rho^2 + \eta^2 = (\,0.36 \pm 0.07\,)^2\,. \tag{2.11}$$

At the present time the model dependence still dominates the error.

Potential sources of information on $|V_{ub}|$ are also the purely leptonic decays $B^+ \to \tau^+\nu_\tau$ and $B^+ \to \mu^+\nu_\mu$. These processes, which have not been observed yet, will provide information on the product of the CKM matrix element $|V_{ub}|$ and the B decay constant f_B. The present experimental limits for $B^+ \to \tau^+\nu_\tau$ and $B^+ \to \mu^+\nu_\mu$ by L3 [42] and CLEO-II [43] are still more than one order of magnitude above the theoretical predictions [44], giving so far no stringent constraints for $f_B|V_{ub}|$.

Electromagnetic penguin decays

The electromagnetic penguin decays $B \to X_s\gamma$, $B \to K^*\gamma$ and their Cabibbo-suppressed counterparts $B \to X_d\gamma$, $B \to \rho\gamma$ are important for determining the top quark couplings to the strange and down quark, $|V_{ts}|$ and $|V_{td}|$. The rate for inclusive radiative penguin decays $B \to X_s\gamma$ has been measured by the CLEO experiment [45], operating at the $\Upsilon(4S)$ resonance. The experimental signature of a hard photon with an energy of ~ 2.5 GeV in the CLEO electromagnetic calorimeter has been used to detect $b \to s\gamma$ transitions. An excess from $B \to X_s\gamma$ events was observed in the photon spectrum after the expected background from continuum and other B decays was subtracted. The dominant background was initial-state radiation from the continuum. The strange quark from the X_s system has been reconstructed by a $K_s^0 \to \pi\pi$ decay or by a measurement of the ionization energy loss in the drift chamber consistent with a $K^\pm$.

The exclusive channels $B^0 \to K^{*0}\gamma$ and $B^- \to K^{*-}\gamma$ have been analyzed by a full reconstruction of K^{*0} and K^{*-} decay modes [46]. The measured branching ratios [45, 46]:

$$\begin{aligned} \mathcal{B}(B \to X_s\gamma) &= (2.32 \pm 0.57 \pm 0.35) \times 10^{-4} , \\ \mathcal{B}(B \to K^*\gamma) &= (4.2 \pm 0.8 \pm 0.6) \times 10^{-5} , \end{aligned} \tag{2.12}$$

determine the ratio of the CKM matrix elements $|V_{ts}\,/\,V_{cb}|$ [47]:

$$\left|\frac{V_{ts}}{V_{cb}}\right| = 0.85 \pm 0.12\,(\mathrm{exp}) \pm 0.10\,(\mathrm{theo}) , \tag{2.13}$$

which is within errors consistent with unity, as expected from the unitarity of the CKM matrix.

In addition CLEO has searched for exclusive $b \to d\gamma$ decays in the modes: $B^0 \to \rho^0\gamma$, $B^0 \to \omega\gamma$ and $B^- \to \rho^-\gamma$. The decays $\rho(770) \to \pi\pi$ have been distinguished from $K^*(892) \to K\pi$ decays by a π/K separation using ionization and time of flight measurements and a reconstruction of the invariant mass assuming the particles were either a $K\pi$ or $\pi\pi$ pair. No signal for $b \to d$ transitions was found. The upper bounds on the branching ratios [46] have been converted into an upper limit on the ratio of the CKM matrix elements $|V_{td}\,/\,V_{ts}|$:

$$\left|\frac{V_{td}}{V_{ts}}\right| < 0.56 \qquad (90\%\,\mathrm{C.L.}) . \tag{2.14}$$

In the preceding discussion of electromagnetic penguin decays it has been always assumed that $|V_{tb}| = 1$. Indeed the hierarchy of the CKM matrix allows deviations of $|V_{tb}|$ from unity only at a level of $\mathcal{O}(\lambda^4)$. However, the only measurement of $|V_{tb}|$ has been performed by studying top quark decays at the Tevatron and its precision is far from $\mathcal{O}(\lambda^4)$. The dominant coupling of top quarks to bottom quarks has been used to identify top quarks in the reaction $p\bar{p} \to t\bar{t}X \to bW^+\bar{b}W^-X$. The lifetime of b quarks was used to distinguish b jets from other quark jets. A

comparison of the number of events with a single b tag and those with a double b tag allowed the determination of the top quark cross section and the coupling strength $|V_{tb}|$. The probability that a top quark decays to a b quark is related to the CKM matrix elements containing a top quark via:

$$b = \frac{\mathcal{B}(t \to bW)}{\mathcal{B}(t \to qW)} = \frac{|V_{tb}|^2}{|V_{td}|^2 + |V_{ts}|^2 + |V_{tb}|^2} \tag{2.15}$$

Under the assumption of three families the denominator is identical to unity and b reduces to $|V_{tb}|^2$. A measurement of b by the CDF Collaboration [48] yielded:

$$b = 0.94 \begin{matrix} +0.06 \\ -0.30 \end{matrix} . \tag{2.16}$$

Assuming three families implies $|V_{tb}| = 0.97 \begin{matrix} +0.03 \\ -0.17 \end{matrix}$.

2.2.2 Observation of $B^0 - \overline{B}^0$ and search for $B_s - \overline{B}_s$ oscillations

The behaviour of neutral particles under charge conjugation has already occupied the pioneers of quantum mechanics. This discussion was mainly stimulated by Enrico Fermi. We will begin with a review of the history of oscillations, which were first predicted for the neutral kaon system.

Review of oscillations in the $K^0 - \overline{K}^0$ system

It was believed that neutral particles fall into two classes according to their behaviour under CP transformation.

(1) On one side there are particles that transform under CP into themselves and which are thus their own antiparticles. For example, the photon and the π^0 meson are bosons that behave in this fashion.

(2) On the other side there are neutral particles that behave like charged ones in that they have antiparticles distinct from themselves. The conservation of a charge-like quantum number prohibits transitions between particle and antiparticle states. A member of this class is provided by the neutron where the conserved quantity is the baryon number.

M. Gell-Mann and A. Pais [49] have first pointed out in 1955 that neutral particles could exist that belong neither to class (1) nor to class (2). It was known that the K^0 meson decays into two charged pions. They argued that the $\pi^+\pi^-$ state is a CP eigenstate and if CP is conserved in nature the CP mirror process $\overline{K}^0 \to \pi^+\pi^-$ must also occur. If decays of two particles can lead to the same final state then also virtual transitions $K^0 \Leftrightarrow \pi^+\pi^- \Leftrightarrow \overline{K}^0$ can take place. However, K^0 and $\overline{K}^0$ mesons can be distinguished by the sign of the electric charge of the K^+, K^- meson associated with the production of K^0 and $\overline{K}^0$ in a typical fixed target experiment. This distinction is possible due to conservation of strangeness

in the strong interaction. The K^0 particle is distinct from its antiparticle $\overline{K}^0$ if it is observed via its strong interaction, but nevertheless transitions between K^0 and $\overline{K}^0$ occur in the weak interaction.

This mixing of the K^0 and $\overline{K}^0$ particles in the weak interaction is responsible for interesting new phenomena. These phenomena cannot be found for the photon nor for the neutron, but are specific for the neutral mesons only. Some of the predicted properties of the K^0 meson state were:

(I) The existence of a K_2 particle for which two-pion decay is prohibited and which has a lifetime considerably longer than that for the two-pion decay of the K_1 particle. As far as CP is conserved the decay modes for K_1 and K_2 are distinct from each other and their rates of decay are quite unrelated. There are thus two independent lifetimes, one for K_1 and one for K_2. For this reason these are called K_S^0 (short-lived) and K_L^0 (long-lived). In addition, the weak interaction responsible for $K^0 - \overline{K}^0$ transitions will produce small level shifts in the masses of K_1 and K_2.

(II) The content of K^0 and $\overline{K}^0$ mesons in an initial pure K^0 state will oscillate in time. These oscillations can be observed by the strong interaction of the K^0 particle with matter or by flavour tagging K^0 decays, as for instance semileptonic decays. The oscillation process is sensitive to the K_1 - K_2 mass difference.

In order to understand the $K^0 - \overline{K}^0$ system on a deeper level a short mathematical description is presented here [50]. The $K^0 - \overline{K}^0$ system is an example of a quantum mechanical two-state system. We choose the base states as $|K^0\rangle$ and $|\bar{K}^0\rangle$. The amplitudes that any state $|\Psi\rangle$ of a neutral K particle is in either of the two base states are denoted by:

$$C_+ = \langle K^0|\Psi\rangle \ , \qquad C_- = \langle \bar{K}^0|\Psi\rangle \ . \tag{2.17}$$

The Hamilton equations for the $K^0 - \overline{K}^0$ system are given by:

$$\begin{aligned} i\,\frac{dC_+}{dt} &= A_0 C_+ + A_w C_- + A_w C_+ \\ i\,\frac{dC_-}{dt} &= A_0 C_- + A_w C_+ + A_w C_- \ , \end{aligned} \tag{2.18}$$

in which we used the convention $\hbar = 1$. The first terms on the right-hand side characterize the free motion of the K^0 and $\overline{K}^0$ mesons, respectively. The terms proportional to A_w are induced by the weak transitions from $\overline{K}^0$ to K^0 and K^0 to K^0 as described by the first equation. The second equation contains the respective counterparts. As far as CP is conserved in these transitions all terms are proportional to a single amplitude A_w. Both amplitudes A_0 and A_w are, in general, complex numbers.

These equations of motion can be decoupled from each other by transforming to new base states $|K_1\rangle$ and $|K_2\rangle$ that are given by the sum and difference of $|K^0\rangle$ and $|\bar{K}^0\rangle$:

$$\begin{aligned} |K_1\rangle &= (|K^0\rangle + |\bar{K}^0\rangle)/\sqrt{2} \\ |K_2\rangle &= (|K^0\rangle - |\bar{K}^0\rangle)/\sqrt{2} \ . \end{aligned} \tag{2.19}$$

The time-behaviour of the amplitudes C_1 and C_2 of the new base states

$$C_1 = \langle K_1|\Psi\rangle \ , \qquad C_2 = \langle K_2|\Psi\rangle \tag{2.20}$$

is governed by the independent Hamilton equations:

$$\begin{aligned} i\,\frac{dC_1}{dt} &= A_0 C_1 + 2A_w C_1 \\ i\,\frac{dC_2}{dt} &= A_0 C_2 \ . \end{aligned} \tag{2.21}$$

The solutions are plane waves:

$$\begin{aligned} C_1(t) &= C_1(0)\exp\left(-i\,(A_0 + 2A_W)\,t\right) \\ C_2(t) &= C_2(0)\exp\left(-i\,A_0\,t\right) \ . \end{aligned} \tag{2.22}$$

Choosing the real and imaginary parts of the amplitudes as

$$A_0 = M_0 - \frac{i}{2}\Gamma_0 \ , \qquad 2A_w = \Delta M - \frac{i}{2}\Delta\Gamma \tag{2.23}$$

$C_1(t)$ and $C_2(t)$ describe the time-evolution of two unstable particles that are characterized by a mass splitting of ΔM and a decay rate difference of $\Delta\Gamma$. The reference scales are given by the mass M_0 and by the decay width Γ_0 of the K_2 particle.

If a K^0 particle is produced in a strong interaction, for instance in the process $\pi^- + p \to K^0 + \Lambda^0$, the initial conditions of the kaon beam are:

$$C_+(0) = 1 \ , \qquad C_-(0) = 0 \ , \tag{2.24}$$

which is equivalent to

$$C_1(0) = \frac{1}{\sqrt{2}} \ , \qquad C_2(0) = \frac{1}{\sqrt{2}} \ . \tag{2.25}$$

The time-dependence of the C_- amplitude is given by:

$$C_-(t) = (C_1(t) - C_2(t))/\sqrt{2} = \frac{1}{2}\exp\left(-i\,A_0\,t\right)\left(\exp\left(-2i\,A_w\,t\right) - 1\right) \ . \tag{2.26}$$

The probability of observing a $\bar{K}^0$ particle at a time t is equal to:

$$|C_-(t)|^2 = \frac{1}{4}\exp\left(-\Gamma_0\,t\right)\left(1 + \exp\left(-\Delta\Gamma\,t\right) - 2\exp\left(-\frac{\Delta\Gamma}{2}\,t\right)\cos(\Delta M\,t)\right) \ . \tag{2.27}$$

This is a remarkable result! Although a $\overline{K}^0$ component was not present in the initial K^0 beam it is produced by the interference of the two mass eigenstates K_1 and K_2 if they develop in time.

Already in 1956, one year after the prediction of a longlived K^0 particle, it was discovered by L. M. Ledermann *et al.* [51]. K_L^0 decays were observed in a cloud

chamber placed more than 100 mean lives of the K_S^0 particle from the production target. They observed decays into two charged particles, so called V^0 events, that were kinematically unlike $K^0 \to \pi^+\pi^-$ and were interpreted as semileptonic decays of K_L^0 mesons. The oscillations have been first observed by L. M. Ledermann *et al.* [52] in 1957 by noting a K^0 meson that interacted with a helium nucleus to produce a hyperon of negative strangeness. Further confirmation on $K^0 - \overline{K}^0$ oscillations has been obtained from the observation of a time-dependent charge asymmetry in the semileptonic decay $K^0 \to \pi^- e^+ \nu$ (see for instance [53]). The charge asymmetry was defined as the fraction of "wrong sign" electrons (e^-) to the "right sign" electrons (e^+) from an initial pure K^0 state.

The oscillation phenomenon of neutral mesons is equivalent to a modified Stern-Gerlach experiment. The creation of a pure K^0 state, a strangeness eigenstate, can be simulated by a Stern-Gerlach apparatus where one of the atom beams inside the magnetic field is blocked by a plate. This modified apparatus can be called a Stern-Gerlach filter [50]. The time evolution of a pure K^0 state is equivalent to a series of Stern-Gerlach filters. In the kaon beam the weak interaction produces intermediate states of dominantly even CP parity (the two pion state). However, the strangeness S and the CP parity form a pair of complementary variables. They cannot be measured simultaneously with infinite accuracy. The situation is equivalent to the one if the polarized atoms of the first Stern-Gerlach filter are passed through a second filter with the direction of the field axis rotated by 90^0 with respect to the first one. In case of the kaon beam the weak interaction is responsible for blocking the CP-odd component in the kaon state. After the kaons have passed through the "filter of the weak interaction" the original information on the strangeness S is lost. A third Stern-Gerlach filter with the magnetic field directed along the original field direction can be used to measure the presence of an atom state of opposite polarization to that which was selected by the first filter. For the kaon beam the role of the third Stern-Gerlach filter is taken by strong interactions or semileptonic decays of kaons. The result is that if the second Stern-Gerlach filter has a blocking mask there will be a $\overline{K}^0$ component detected by the third filter, but if not, the beam will stay in a pure K^0 state. The important point is the filter in the second apparatus, not the beam separation in the apparatus itself.

Observation of $B^0 - \overline{B}^0$ oscillations

Some evidence for $B^0 - \overline{B}^0$ mixing was first found by the UA1 Collaboration in proton-antiproton collisions at CERN [54]. The experimental method was the same as for $K^0 - \overline{K}^0$ oscillations: a search for a charge asymmetry in semileptonic B^0 decays. The UA1 Collaboration observed a like-sign dilepton signal, which was a 2σ deviation from the expected background. $B^0 - \overline{B}^0$ oscillations produce leptons with the "wrong sign" of electric charge. They contribute to the fraction of like-sign lepton pairs. In addition, several background sources, as for instance semileptonic charm decays, pollute this sample. The majority of the scientific community of that time believed that it was impossible to observe $B^0 - \overline{B}^0$ mixing. Therefore

the UA1 signal was interpreted as being due to $B_s - \overline{B}_s$ mixing. However also this explanation was not satisfactory because the signal was much larger with respect to the suppression of the B_s production fraction.

It was the merit of the ARGUS Collaboration to clear up this situation. The clearest signals are fully reconstructed $\Upsilon(4S)$ events that decay into $B^0\,B^0$ or $\overline{B}^0\,\overline{B}^0$ meson pairs. In 1987 ARGUS succeeded in finding one fully reconstructed $\Upsilon(4S) \to B^0\,B^0$ decay [4]. In this event, shown in fig. 2.4, all final particles (μ, π, K) were well identified and the masses of the intermediate states agreed well with the masses of D and D^* mesons. Kinematic considerations showed that the event was complete. The background for this event was found to be completely negligible.

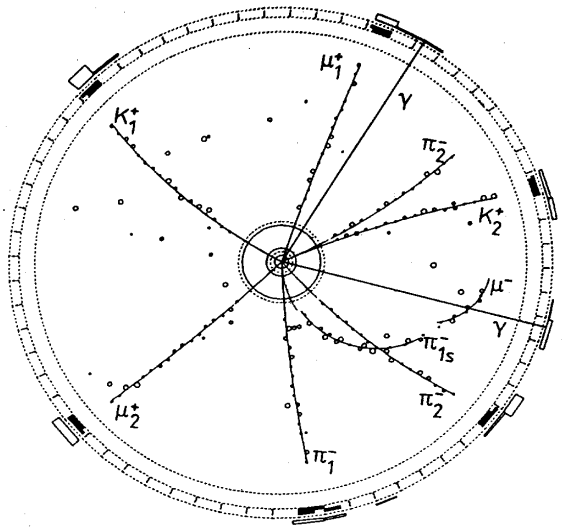

Figure 2.4: Completely reconstructed $\Upsilon(4S) \to B^0\,B^0$ event observed by the ARGUS Collaboration [4].

This one event demonstrates that the phenomenon of $B^0 - \overline{B}^0$ oscillation must exist. The direct evidence derived from this single mixed event was complemented by a statistical analysis of like-sign lepton pairs in semileptonic decays. The ARGUS collaborators could extract a $B^0 - \overline{B}^0$ oscillation signal in the like-sign lepton sample of more than 4 standard deviations. The mixing strength was measured to be [4]:

$$r = \frac{N(B^0\,B^0) + N(\bar{B}^0\,\bar{B}^0)}{N(B^0\,\bar{B}^0)} = 0.21 \pm 0.08\ . \tag{2.28}$$

Does the Standard Model agree with the ARGUS measurement? From the historical point of view the measurement of r was a stunning surprise because $B^0 - \overline{B}^0$ oscillations were expected with very tiny mixing amplitudes much smaller than the measured value. How could this happen?

The calculation of $B^0 - \overline{B}^0$ transition amplitudes relies on $2W^\pm$ exchange box

diagrams, illustrated in fig. 2.5. These box diagrams represent flavour changing neutral currents (FCNC) with $|\Delta B| = 2$, which are governed by the GIM mechanism. The GIM mechanism named after Glashow, Iliopoulos and Maiani [1] gives a quantitive description of FCNC transitions, which are only allowed if the participating quarks are not degenerate in mass.

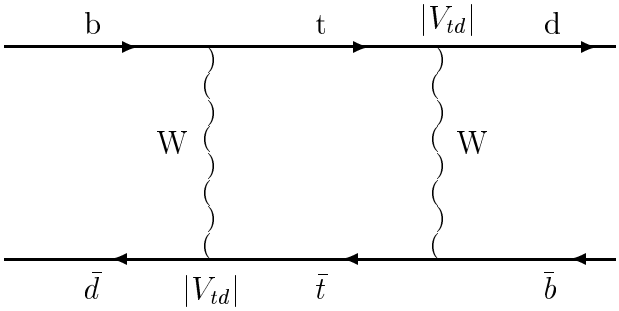

Figure 2.5: Box diagram for $B^0 - \overline{B}^0$ mixing.

The mass splitting in the B^0 system induced by the SM box diagram contributions can be expressed by [55]:

$$\Delta M = \frac{G_F^2 f_B^2 m_B}{12\pi^2}\, m_t^2\, \xi_t^2 \ . \tag{2.29}$$

Here G_F is the Fermi-constant, f_B the decay constant of the B^0 meson, describing its wave function at the origin and m_B the B^0 meson mass. ΔM is proportional to the square of the top mass m_t. This dependence is a consequence of the dimension of the Fermi-constant. A second-order weak process diverges quadratically in energy. The GIM mechanism cancels this divergency at an energy scale defined by the heaviest quark involved in the process. Finally ΔM is proportional to the relevant combination of CKM matrix elements: $\xi_t = V_{tb} V_{td}^*$. The contribution from the top quark is dominant relative to the charm and up quark due to $m_t \gg m_b$. It is the high value of the top quark mass of $m_t = 175 \pm 6$ GeV [18] (which was not known in 1987) that is responsible for observable $B^0 - \overline{B}^0$ mixing.

The leading terms to $\Delta\Gamma$ are determined by transitions with charm and up quarks in the intermediate state. These correspond to Feynman diagrams as in fig. 2.5 where the top quark is replaced by a charm or up quark, respectively.

$$\Delta\Gamma = -\frac{G_F^2 f_B^2 m_B}{8\pi}\, m_b^2\, (\xi_c + \xi_u)^2 = -\frac{G_F^2 f_B^2 m_B}{8\pi}\, m_b^2\, \xi_t^2 \tag{2.30}$$

The unitary relation $\xi_c + \xi_u = -\xi_t$ relates the combination of u- and c-quark CKM elements to that of the t-quark. The important consequence is that the leading contributions to ΔM and $\Delta\Gamma$ are both proportional to the same combination of CKM elements.

The experimental parameter r of $B^0 - \overline{B}^0$ mixing measured by ARGUS can be expressed in terms of ΔM and $\Delta\Gamma$. In the limit $\Delta\Gamma = 0$, which is reasonable because of $m_t \gg m_b$, the expression for r is given by [56]:

$$r = \frac{\Delta M_{B^0}^2}{2\Gamma^2 + \Delta M_{B^0}^2} \; . \tag{2.31}$$

Equation 2.31 is only valid on the $\Upsilon(4S)$ resonance where the $B^0\,\overline{B}^0$ pair is produced in a coherent state [56]. In order to get a rough estimation for r the values $f_{B^0} = 200$ MeV, $m_{B^0} = 5.3$ GeV, $m_t = 175$ GeV, $|V_{td}| = 0.01$ and $\tau_b = 1.55$ ps have been inserted into equation (2.29) and (2.31). The prediction for the mass difference ΔM_{B^0} is of the order: $\sim 7 \times 10^{-4}$ eV ~ 1 ps^{-1} and the mixing parameter r is of observable magnitude: $r \sim 0.5$. Vice versa, the measurement (2.28) can be converted into $\Delta M_{B^0} = 0.47 \pm 0.12$ ps^{-1}.

A direct measurement of ΔM_{B^0} can be obtained by studying the time dependence of the mixing amplitude. The oscillation frequency is equal to the mass difference, as shown in equation (2.27). The time dependence of $B^0 - \overline{B}^0$ mixing has been measured at LEP [57]. Here the high kinetic energy of B^0 mesons produced in Z decays can be exploited to measure the proper time of the decaying B^0 mesons (which is not possible at the $\Upsilon(4S)$ resonance). An example of a time-dependent charge asymmetry measurement by L3 is shown in fig. 2.6. This measurement has been performed in an inclusive sample of B hadrons, which consists of $\sim 40\%$ B^0 mesons. The b flavour has been tagged by the charge of the lepton originating from b decay. The observed oscillation pattern has been interpreted to come from B^0 oscillations.

The present LEP average in the mass difference $\Delta M_{B^0} = 0.466 \pm 0.019$ ps^{-1} [57] is in excellent agreement with the first measurement of ΔM_{B^0} by ARGUS and has a factor 10 better accuracy.

What do we learn from the measurement of ΔM_{B^0} in terms of the CKM matrix elements? The value of $|V_{td}|$ can be determined from equation (2.29) by an estimate of the factor between ΔM_{B^0} and $|V_{td}|$. All parameters that enter in this factor are measured except of one, the B^0 meson decay constant f_{B^0}. At present its value was calculated by means of lattice-QCD methods up to a precision of $\sim 20\%$. In reference [58] a value of:

$$|V_{td}| = 0.086 \pm 0.020 \tag{2.32}$$

was obtained. The error is dominated by the uncertainty in f_{B^0}. The value of $|V_{td}|$ constrains the combination $(1-\rho)^2 + \eta^2$ in the Wolfenstein parametrization. The allowed range is:

$$(1-\rho)^2 + \eta^2 = (\,0.97 \pm 0.23\,)^2 \; . \tag{2.33}$$

In the preceding discussion of $K^0 - \overline{K}^0$ and $B^0 - \overline{B}^0$ oscillations it was assumed at first that CP is a good symmetry of both the strong and weak interactions. In this case the physical states with well-defined masses and lifetimes are CP eigenstates

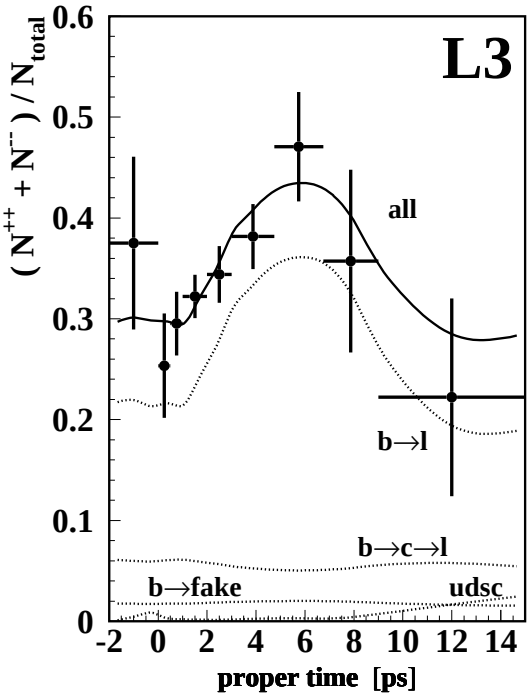

Figure 2.6: Fraction of hadronic events containing two same-charged leptons normalized to the total number of hadronic events with two leptons. The ratio has been measured by the L3 Collaboration in dependence on the b hadron decay time.

as in eq. (2.19) for the K^0 particle. However in 1964, Christenson, Cronin, Fitch and Turlay observed the decay $K_2 \to \pi^+\pi^-$ [28], which is strictly forbidden if CP is a good symmetry. Since that year it is known that neither the parity P nor the combination of charge conjugation times parity CP are conserved in nature. The experiment [28] carried out at Brookhaven found that the CP violating decay had a branching ratio of about 2×10^{-3}. A similar situation is expected for the neutral B meson system. The mass eiganstates $|B_{1,2}\rangle$ can be chosen as an asymmetric superposition of the strong interaction eigenstates $|B^0\rangle$ and $|\bar{B}^0\rangle$ with the CP impurity parameter ϵ:

$$|B_{1,2}\rangle = \frac{1}{\sqrt{2(1+|\epsilon|^2)}} \left[(1+\epsilon)\,|B^0\rangle \pm (1-\epsilon)\,|\bar{B}^0\rangle \right] . \qquad (2.34)$$

This situation can be described by a Hamilton operator (2.18) which has different matrix elements for transitions from $B^0 \to \overline{B}^0$ and $\overline{B}^0 \to B^0$. The CP impurity parameter ϵ is a complex number. The identity of $B^0 \to \overline{B}^0$ and $\overline{B}^0 \to B^0$ transitions can be violated by a difference in the transition strength or a phase difference between both amplitudes. However only the real part of ϵ is a physical observable, while the imaginary part is not. A difference in the transition strength between $B^0 \to \overline{B}^0$ and $\overline{B}^0 \to B^0$ results in a non-vanishing value for Re ϵ. It can be determined

from a measurement of the charge asymmetry in same-sign dilepton events:

$$Re\,\epsilon = \frac{1}{4}\,\frac{N(B^0\,B^0) - N(\bar{B}^0\,\bar{B}^0)}{N(B^0\,B^0) + N(\bar{B}^0\,\bar{B}^0)}\;. \tag{2.35}$$

A search for an asymmetry in the same-sign dilepton sample at the $\Upsilon(4S)$ resonance was used to put a limit on $|\mathrm{Re}\;\epsilon| < 0.045$ [59]. In the limit $m_t \to \infty$, the real part of ϵ vanishs, $\mathrm{Re}\;\epsilon \to 0$.

However, the imaginary part of ϵ is a phase convention dependent, unphysical parameter. The Hamiltonian (2.18) describes only one part in a physical process, the transition from B^0 to $\overline{B}^0$, but an observable can only be defined for final decay channels of the B^0 particle. There are physical consequences of CP violating terms in the Hamiltonian (2.18) beside Re ϵ, namely that CP violation can be induced from interference between a mixing amplitude and a decay amplitude in decays of neutral B mesons. We shall see later on explicitly how $B^0 - \overline{B}^0$ mixing is related to CP violation.

Search for $B_s - \overline{B}_s$ oscillations

Measurements of the time-integrated mixing strength $\chi = r/(1-r)$ at LEP and at the $\Upsilon(4S)$ resonance allow the extraction of the mixing parameter χ_d and χ_s of B^0 and B_s mesons, respectively. We can benefit here from the different composition of the neutral B meson samples at LEP and at the $\Upsilon(4S)$ resonance. The $\Upsilon(4S)$ measurements $\chi^{\Upsilon(4S)} = \chi_d = 0.156 \pm 0.024$ [57] are only sensitive to the fraction of mixed B^0 mesons, whereas the LEP measurements $\chi^{LEP} = f_d\chi_d + f_s\chi_s = 0.1217 \pm 0.0046$ [57] observe a fraction of mixed B^0 and B_s mesons. The weights f_d and f_s are the branching ratios $\mathrm{Br}(\mathrm{b} \to B^0) \sim 0.4$, $\mathrm{Br}(\mathrm{b} \to B_s) \sim 0.1$ that a b quark hadronizes into a B^0, B_s meson at LEP. Both measurements are only compatible at values of $\chi_s \sim 0.5$ implying maximal mixing of B_s mesons. We can conclude that the B_s oscillations occur at a time scale much shorter than the average b lifetime, $\Delta M_{B_s} \gg \Delta\Gamma_{B_s}$. But it is not possible to derive a value for ΔM_{B_s} from $\chi_s = 0.5$.

A time-dependence of B_s mixing has not been observed yet, because the present experimental resolution on the decay length does not allow to resolve very fast B_s oscillations. The task so far is to derive limits on ΔM_{B_s} of B_s mesons from a search for such oscillations. One possibility of determining limits on B_s oscillations is provided by the amplitude method [57]. This method is inspired by a Fourier analysis. The Fourier-spectrum of the observed time distribution of mixed B_s events at LEP does not show a peak at a certain value of ΔM_{B_s} . A limit has been placed on regions of ΔM_{B_s} where peaks can be excluded. The combined lower limit from all LEP experiments is $\Delta M_{B_s} > 8.0$ ps^{-1} at 95%C.L. [57].

This high limit for ΔM_{B_s} may have its origin in the hierarchy of the CKM matrix elements. The ratio $\Delta M_{B^0}\,/\,\Delta M_{B_s}$ reflects the transition strength $|V_{td}|$ relative to

that of $|V_{ts}|$:

$$\frac{\Delta M_{B^0}}{\Delta M_{B_s}} = \left(\frac{f_{B^0}}{f_{B_s}}\right)^2 \frac{m_{B^0}}{m_{B_s}} \left|\frac{V_{td}}{V_{ts}}\right|^2 . \tag{2.36}$$

A future measurement of ΔM_{B_s} will allow an estimate of the ratio $|V_{td}\,/\,V_{ts}|$ and thus of $|V_{td}|$ (2.3) with better accuracy as compared to eq. (2.32). The uncertainty in the absolute value of f_{B^0} can be avoided by the use of the ratio $\Delta M_{B^0}\,/\,\Delta M_{B_s}$ rather than of ΔM_{B^0} alone. The ratio of the decay constants f_{B^0}/f_{B_s} is known with a much better accuracy than f_{B^0} because $f_{B^0}/f_{B_s} \sim 1$ except of deviations coming from the breaking of the SU(3) flavour symmetry [60].

The lower limit on ΔM_{B_s} can be converted into an upper limit on $|V_{td}\,/\,V_{ts}|$ [61]:

$$\left|\frac{V_{td}}{V_{ts}}\right| < 0.28 \qquad (95\%\,\text{C.L.}) , \tag{2.37}$$

which just reaches the upper boundary in the allowed range of $|V_{td}|$ from eq. (2.32).

2.2.3 Lifetime differences of neutral B mesons

In order to understand $B^0 - \overline{B}^0$ oscillations as a quantum mechanical interference phenomenon it is necessary to establish experimentally the existence of two kinds of B^0 particles, a short lived and a long lived one. However a similar observation to that of the K^0_L particle [51] is much more difficult for the B^0 particle. The huge lifetime difference of $(\Delta\Gamma/\Gamma)_{K^0} \sim 600$ is a special property of the K^0 particle. The final states of K^0 decays with definite CP parity are two pion and three pion states. The K^0_S particle decays dominantly to two pions, whereas three pion states are reserved for the K^0_L particle. These decay modes differ in their available phase space. The three pion final state is kinematically strongly suppressed, because the masses of three pions almost add up to the mass of the kaon. But in the limit of CP conservation, there is no other CP eigenstate than that of three pions available for the K^0_L particle. The small decay width for the K^0_L particle appears here as an "accident in phase space" and is not correlated to the values of CKM matrix elements. If, on the contrary, the masses of the final state mesons are small compared to the mass of the decaying meson, the original dependence of $\Delta\Gamma$ on its relevant CKM elements is no longer hidden under special phase space configurations. This is the case of neutral B mesons.

The expected lifetime differences according to eq. (2.30) are of the order $\sim 1\%$ for the B^0 meson and $\sim 10\%$ for the B_s meson [62]. Possible lifetime differences of neutral B mesons have not been investigated yet, neither for the B^0 meson nor for the B_s meson. These measurements are awaited because they will improve the knowledge in the values of CKM matrix elements. Of particular interest is a measurement of $\Delta\Gamma$ of the B_s meson because it allows the determination of the ratio $|V_{td}\,/\,V_{ts}|$. In the SM $\Delta\Gamma_{B_s}$ and ΔM_{B_s} are proportional to each other:

$$\frac{\Delta\Gamma_{B_s}}{\Delta M_{B_s}} \sim \left(\frac{m_b}{m_t}\right)^2 . \tag{2.38}$$

The calculation in [62] determined the factor between $\Delta\Gamma_{B_s}$ and ΔM_{B_s} as 5.6×10^{-3}. The known ratio of $\Delta\Gamma_{B_s}\,/\,\Delta M_{B_s}$ offers a new possibility to measure $|V_{td}\,/\,V_{ts}|$. B_s oscillations can be observed until a lower limit on ΔM_{B_s} so that the oscillation frequency is small enough to be resolvable or until an upper limit on ΔM_{B_s} where the decay width difference $\Delta\Gamma_{B_s}$ is big enough to be detectable. A measurement of $\Delta\Gamma_{B_s}$ is sensitive to small values of $|V_{td}\,/\,V_{ts}|$ and is thus complementary to that of ΔM_{B_s}. Experimental limits on ΔM_{B_s} are upper limits on $|V_{td}\,/\,V_{ts}|$, whereas a limit on $\Delta\Gamma_{B_s}$ would be a lower limit on $|V_{td}\,/\,V_{ts}|$. The expected magnitude of $\Delta\Gamma_{B_s}$ as a function of $|V_{td}\,/\,V_{ts}|$ is shown in fig. 2.7.

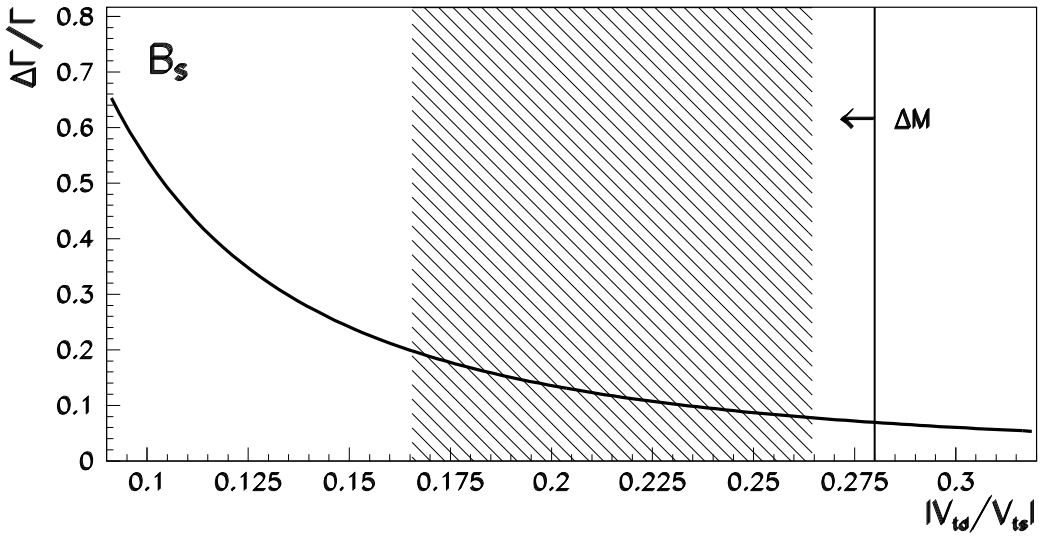

Figure 2.7: The expected difference in decay rates of the B_s meson as a function of the ratio of CKM elements $|V_{td}\,/\,V_{ts}|$. The prediction relies on the measurement of ΔM_{B^0} of B^0 mesons. The hatched region corresponds to the predicted values according to a theoretical estimate of the B^0 decay constant [58]. Also shown is the limit on ΔM_{B_s} from a measurement of the B_s oscillation frequency [61].

It is one of the major concerns of this thesis to point out the possibility for a measurement of lifetime differences of neutral B mesons at LEP. Fig. 2.8 shows the effect of $\Delta\Gamma$ of B^0 and B_s mesons on the proper decay time distribution of all B hadrons assuming an exponential decay law for each b hadron and neglecting all measurement uncertainties. The average lifetime of B mesons was set to 1.5 ps and that of b baryons to 1.2 ps, in agreement with the current world averages of b lifetimes. A b hadron composition of eq. (1.8) has been assumed. Differences to the case $\Delta\Gamma = 0$ are observable at long-time scales in the inclusive decay time distribution. This influence arises from the non-linearity of the decay law. At short

decay times the sum of a shortlived and longlived component is almost identical to a decay law with a single average lifetime because the decay distribution is in good approximation a linear function. However at long-time scales higher order effects in the exponential decay law are important and the presence of a longlived B^0 component influences significantly the shape of the decay time distribution.

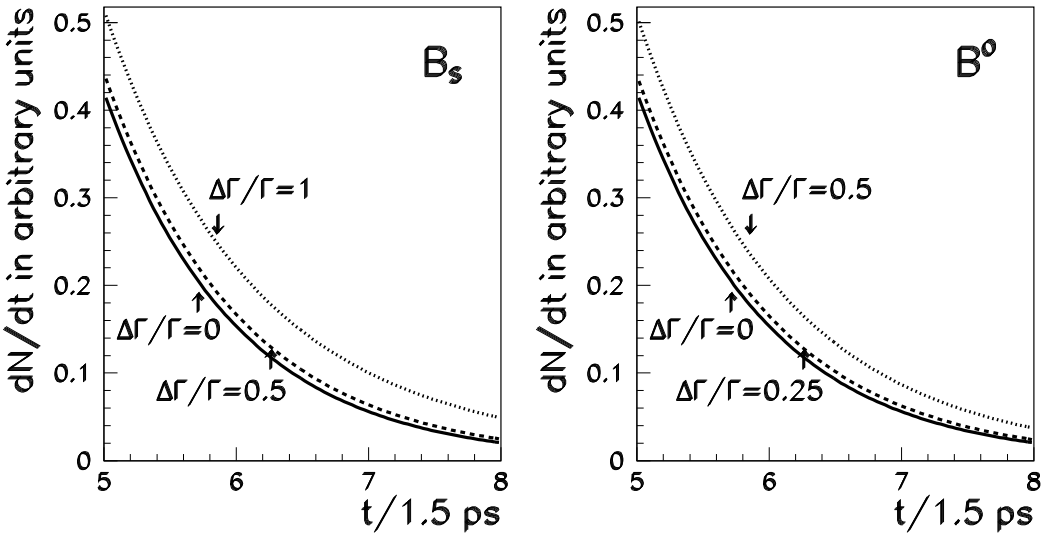

Figure 2.8: Proper time distribution for b hadron decays in case of a short- and longlived B_s and B^0 meson. The distributions are shown for lifetimes bigger than five mean B meson lives, where the deviations to $\Delta\Gamma = 0$ are most significant. The distributions are normalized to be identical at $t = 0$. The fractions of b hadrons were assumed to be $\Lambda_b : B_s : B^+ : B^0 = 1 : 1 : 4 : 4$ and the average lifetime of B mesons was set to 1.5 ps and that of b baryons to 1.2 ps.

Fig. 2.8 illustrates that it is possible to observe a lifetime difference between two CP eigenstates of neutral B mesons even if the CP state is not explicity reconstructed. The LEP statistics do not allow the reconstruction of CP eigenstates of B hadrons due to very tiny B branching ratios for CP eigenstates [5]. But nevertheless thanks to the non-linearity of the decay law it is possible to observe $\Delta\Gamma$ as a statistical significant deviation from the decay distribution with a single average lifetime. Assuming the ratio of $(\Delta\Gamma)_{B_s}/(\Delta\Gamma)_{B^0} \sim 10$, as a consequence of the hierarchy of the CKM transitions, it follows that a lifetime difference of the B_s meson produces the more significant effects on the decay time distribution and will be observed first. In the following we will rely on that assumption and concentrate the discussion on the B_s meson.

The question is, how many events are necessary to establish that the deviations

are statistically significant? As an example fig. 2.9 shows the number of B hadron events necessary to extract a $\Delta\Gamma \neq 0$ signal with a significance of three standard deviations. Note that the number of B events represents the total number of B decays from which only 10% consist of B_s mesons. The sensitivity could be improved by a B hadron flavour separation. This is also shown in fig. 2.9 for the example of 50% non-B_s background suppression. The sensitivity is almost independent of the resolution on the decay time if the resolution is better than five average lifetimes. In an extreme case it would be possible to measure $\Delta\Gamma$ only with the number of b decays that occur after five mean lives with almost the same accuracy as obtained from a fit to the full decay time distribution. As it will be pointed out in chapter 4 the L3 resolution on the decay length is $\sim 0.2\,\tau_b$ in the inclusive sample described before and therefore the detection of $\Delta\Gamma$ is in good approximation as precise as in fig. 2.9.

There exist several calculations for $\Delta\Gamma$ relying on different assumptions. An early calculation within the parton model was performed by J. Hagelin [55] in 1981, i.e. even before the lifetime of the B hadron was measured. Rescaling this early estimate to the actual value of the top mass gives $\Delta\Gamma/\Gamma \sim 0.2$. In 1993 $\Delta\Gamma$ was estimated as a sum over exclusive decay modes, where the major contributions come from $D_s\bar{D}_s$, $D_s^*\bar{D}_s^*$ and $D_s\bar{D}_s^* + \bar{D}_s D_s^*$ [63] with the result $\Delta\Gamma/\Gamma \sim 0.15$. A recent calculation using the operator product expansion taking into account Λ_{QCD}/m_b and α_s power corrections [62] yielded: $\Delta\Gamma/\Gamma = 0.16^{+0.11}_{-0.09}$. The large uncertainty is the same that occurs in the extraction of $|V_{td}|$ from ΔM_{B^0} coming from uncertainties in the hadronic matrix elements. Fig. 2.9 illustrates that the statistics collected by L3 seem to be sufficient to be sensitive to the predicted values of $\Delta\Gamma/\Gamma$ within the SM.

Fig. 2.9 demonstrates in a quantitive manner that the smaller the lifetime difference the more events are needed to observe it. If, for instance, the sensitivity should be improved by a factor of two in $\Delta\Gamma$, a ten times bigger data sample has to be analyzed. The difficulty in observing very small lifetime differences arises from the fact that only the time distribution of a superposition of both CP eigenstates of the B_s meson can be observed at LEP. If it would be possible to measure the lifetimes in two separate CP eigenstate samples much fewer events would be sufficient to measure the same value of $\Delta\Gamma$. For instance 100 B_s mesons, consisting of 50% CP even and 50% CP odd states, that are measured separately would allow a three sigma significant observation of $\Delta\Gamma/\Gamma = 0.6$ and an increase in statistics by a factor of four would extend the sensitivity up to $\Delta\Gamma/\Gamma = 0.3$.

One important systematic uncertainty regards lifetime differences between the B hadron species that are in principle not distinguishable from lifetime differences of neutral B mesons if the inclusive time distribution alone is considered. Lifetime differences between B hadrons are expected to be small due to the high value of the b quark mass. As a first estimate of the systematic error on $\Delta\Gamma/\Gamma$ I have evaluated how the significance for $\Delta\Gamma/\Gamma$ changes if the lifetime of one B hadron is varied relative to the average B hadron lifetime. The results are shown in fig. 2.10. It is sufficient to vary three lifetime ratios because the lifetime of the fourth B

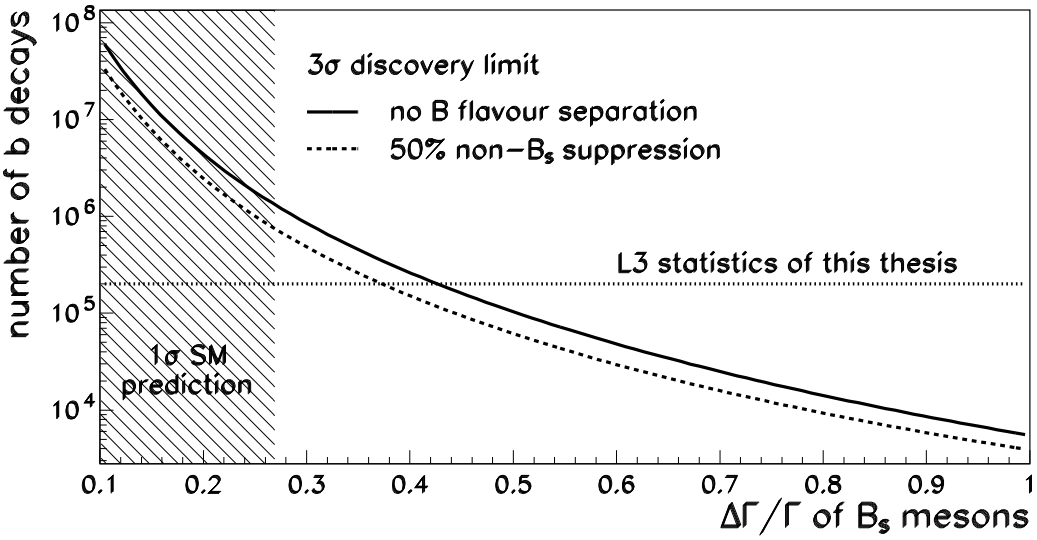

Figure 2.9: Discovery potential for a short- and longlived B_s meson in dependence on the magnitude of $\Delta\Gamma/\Gamma$. The number of B decays necessary for a 3σ significant observation of $\Delta\Gamma$ is shown by the solid curve, the improvement obtained from 50% non-B_s background suppression is indicated by the dashed curve. The curves show the statistical sensitivity, systematic errors have been neglected. The sensitivity of the L3 experiment in this thesis is getting close to the SM prediction of $\Delta\Gamma/\Gamma = 0.16^{+0.11}_{-0.09}$ [62].

hadron is constrained by the average B lifetime. Fig. 2.10 indicates the influence of the lifetime of b baryons, the mean lifetime of both B_s mesons and the lifetime of charged B mesons for the example $\Delta\Gamma/\Gamma$=0.5.

The most important reduction in significance for $\Delta\Gamma$ arises from the uncertainty in the mean value of the lifetimes of the short- and longlived B_s meson followed by the uncertainty in the lifetime ratio of B^+ and B^0 mesons, whereas the uncertainty in the b baryon lifetime is less important. The measurement of $\Delta\Gamma$ is more precise if the mean B_s lifetime is longer than the average lifetime because this leads to a background reduction at long lifetimes. Vice versa, the measurement of $\Delta\Gamma$ becomes more difficult if the background species as B^+ and Λ_b have a longer lifetime than the B_s mesons. In our example of $\Delta\Gamma/\Gamma$=0.5 the signal was statistically significant by 4σ and has still a significance of 3σ taking into account the systematic error from B lifetimes. To summarize, the lifetime differences between B hadrons are a source of systematic uncertainty, but within the current accuracy in lifetime ratios the systematic error on $\Delta\Gamma/\Gamma$ is well under control.

It is constructive to compare the properties of particle-antiparticle mixing for

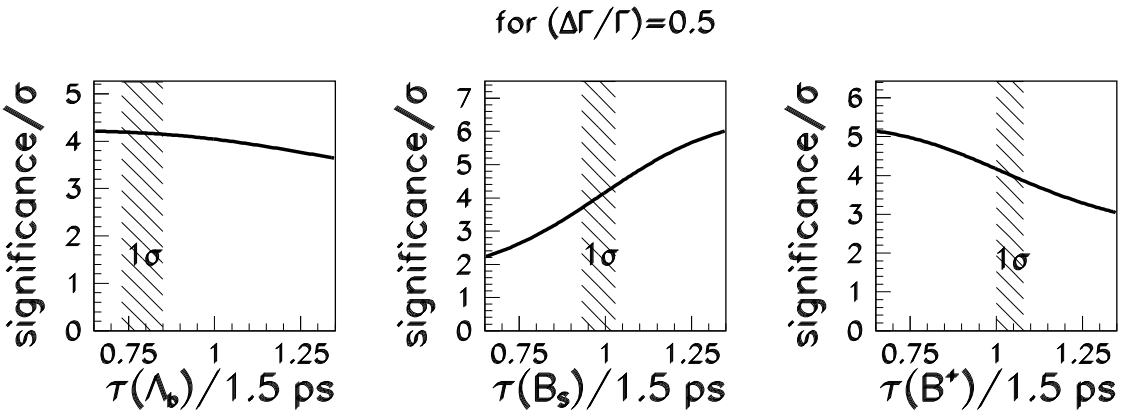

Figure 2.10: Influence of uncertainties in the average lifetimes of Λ_b, B_s, B^+ or B^0 hadrons on the significance for $\Delta\Gamma$ of B_s mesons. The curves illustrate the variation of the significance for the example $\Delta\Gamma/\Gamma$=0.5 using the L3 statistics of this thesis of 2×10^5 b hadrons as a function of the respective lifetime ratios. All other average lifetimes except that which was varied were fixed to 1.5 ps for B mesons and 1.2 ps for b baryons. The hatched regions indicate the measured lifetime ratios.

the different neutral mesons: K^0, D^0, B^0 and B_s. The important characteristics are collected in tab. 2.2.

	K^0	D^0	B^0	B_s
$\Delta\Gamma/\Gamma$	$\Gamma_1 = 579\ \Gamma_2$	~ 0	~ 0	$\sim 0.16 \pm 0.10$
$\Delta M/\Gamma$	0.95	~ 0	0.73 ± 0.05	$\sim 25 \pm 15$

Table 2.2: Important properties of neutral K, D and B mesons. $\Delta\Gamma$ and ΔM denote the rate and mass difference of the neutral two-state systems, respectively. The values are given in units of the average decay width $\Gamma = (\Gamma_1+\Gamma_2)/2$. The kaon entries and ΔM for B^0 mesons are experimental results, the remaining numbers theoretical expectations.

In principle the process of particle-antiparticle transitions is the same for all neutral mesons. However the transition amplitudes are rather different due to different masses and CKM elements of the participating quarks. A crucial feature of the kaon system is the very large difference in decay rates between the two mass eigenstates. A similar hierarchy in decay rates is expected for the B_s meson, although far less pronounced as $\Gamma_1/\Gamma_2 = \mathcal{O}(1)$. In the case of B^0 $\Delta\Gamma/\Gamma$ is essentially negligible. A special role is taken by the D^0 meson where $\Delta\Gamma/\Gamma$ and $\Delta M/\Gamma$ are expected to have values close to zero. The $D^0 - \overline{D}^0$ transitions are dominated by the exchange of virtual d- and s-quarks. They contribute with amplitudes that have the same magnitude, but opposite sign (due to $m_c \gg m_d, m_s$ both amplitudes

cancel each other: $m_c^2\, V_{cd}\, V_{ud}^* = -m_c^2\, V_{cs}\, V_{us}^*$).

2.2.4 Possible scenarios for values of $|V_{ub}|$ and $|V_{td}|$

Measurements of $|V_{ub}\,/\,V_{cb}|$ and $|V_{td}\,/\,V_{ts}|$ are estimates of two independent combinations of ρ and η, the parameters of the Wolfenstein parametrization describing transitions from the first to the third family. The values for ρ and η can thus be determined separately. In principle, measurements of magnitudes alone fully constrain all free parameters in the CKM matrix including the complex phase η, responsible for CP violation. The relations between magnitudes and phases of CKM matrix elements in the SM can be submitted to experimental tests. This section shows the consequences of measurements of $|V_{ub}\,/\,V_{cb}|$ and $|V_{td}\,/\,V_{ts}|$ for CP violation in the SM. The main task is to find out if the measurements are already precise enough to give stringent predictions of CP violation magnitudes.

The allowed range in values of ρ and η according to the estimates (2.11) and (2.33) is shown in fig. 2.11. The most likely point in the (ρ, η) plane forms the upper corner of an triangle, which is a geometrical interpretation of an unitarity relation among CKM matrix elements. A path along the triangle sides in fig. 2.11 is identical to summing up three complex numbers,

$$\frac{V_{ud}\, V_{ub}^*}{V_{cd}\, V_{cb}^*} + \frac{V_{td}\, V_{tb}^*}{V_{cd}\, V_{cb}^*} + 1 = 0 \ , \tag{2.39}$$

with the result of zero. The sides of the triangle can be determined from measurements of magnitudes of CKM elements, as illustrated in fig. 2.11. The angles of the triangle correspond to CP violation effects. They visualize a phase difference between products of CKM elements. CP violation is induced for instance by $B^0 - \overline{B}^0$ mixing through the interference of the two amplitudes $B^0 \to f$ and $B^0 \to \overline{B}^0 \to f$. We can observe CP violation effects if the angles in the triangle are different from 0^0 and 180^0. The approach of testing the SM is to measure the sides *and* the angles of the unitarity triangle and to see if they are consistent.

Of primary interest is the question, whether the triangle collapses to a line, in which case CP violation cannot come from quark mixing. This can be excluded by measurements of $|V_{ub}\,/\,V_{cb}|$ and $|V_{td}\,/\,V_{ts}|$ at least within 68% CL. It is worth remarking that the (db) triangle of fig. 2.11 together with the (ut) combination,

$$V_{ud}\, V_{td}^* + V_{us}\, V_{ts}^* + V_{ub}\, V_{tb}^* = 0 \ , \tag{2.40}$$

are the only non-trivial triangles in the SM. In all other cases the triangles are almost degenerate to a line. This is just a consequence of the hierarchy of the triangle's sides. Only the (db) and (ut) triangles have sides of approximately the same magnitude. In the other triangles representing transitions from the first to the second and from the second to the third family one side is much shorter than the others so that all angles are close to 0^0 or 180^0.

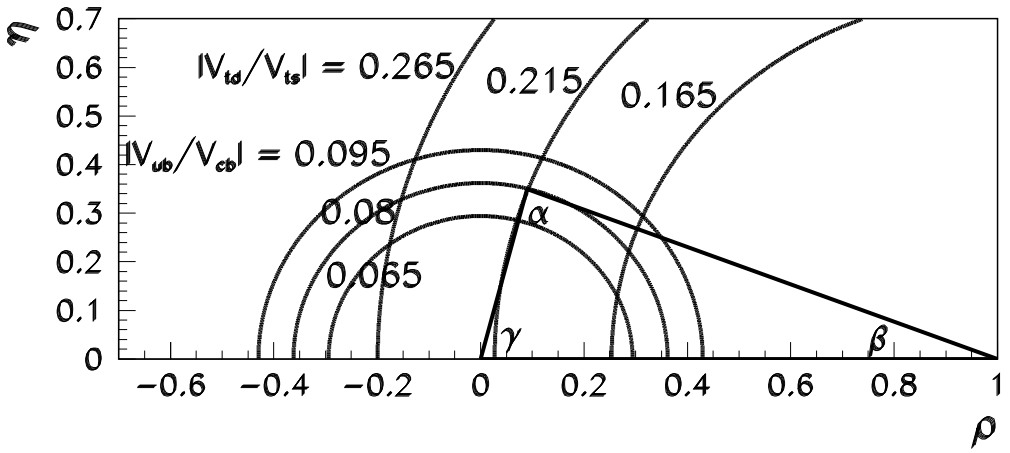

Figure 2.11: Curves in the (ρ, η) plane associated with fixed values of $|V_{ub}\,/\,V_{cb}|$ and $|V_{td}\,/\,V_{ts}|$. The labels were chosen according the present 1σ uncertainties in $|V_{ub}\,/\,V_{cb}|$ and $|V_{td}\,/\,V_{ts}|$.

CP violation can be observed by measuring a time-dependent asymmetry between B^0 decays to a CP eigenstate f_{CP} and that of $\overline{B}^0$ to the same CP eigenstate f_{CP}:

$$\mathcal{A}(t) = \frac{\Gamma(B^0(t) \to f_{CP}) - \Gamma(\bar{B}^0(t) \to f_{CP})}{\Gamma(B^0(t) \to f_{CP}) + \Gamma(\bar{B}^0(t) \to f_{CP})} \; . \tag{2.41}$$

In the limit $\Delta\Gamma = 0$ the asymmetry $\mathcal{A}(t)$ obtains the simple form [32]:

$$\mathcal{A}(t) = \xi \sin 2\Phi_W \, \sin(\Delta M_{B^0} t) \; , \tag{2.42}$$

where ξ is the CP eigenvalue of f_{CP} and Φ_W is the process specific weak phase. The CP violating asymmetry $\mathcal{A}(t)$ oscillates in time with the oscillation frequency ΔM_{B^0} and the amplitude $\xi \sin 2\Phi_W$. Two familiar examples [64] are: (i) $B^0 \to J\Psi K^0_S$, where $\xi = -1$ and $\Phi_W = \beta$,

$$\mathcal{A}(t) = -\sin 2\beta \, \sin(\Delta M_{B^0} t) \; , \tag{2.43}$$

and (ii) $B^0 \to \pi^+\pi^-$, where $\xi = 1$ and $\Phi_W = \beta + \gamma = \pi - \alpha$,

$$\mathcal{A}(t) = \sin 2(\beta + \gamma) \sin(\Delta M_{B^0} t) = -\sin 2\alpha \, \sin(\Delta M_{B^0} t) \; . \tag{2.44}$$

The two asymmetries in our example measure the angles α and β.

What can we conclude now from measurements of $|V_{ub}\,/\,V_{cb}|$ and $|V_{td}\,/\,V_{ts}|$ for the CP asymmetry amplitudes $\sin(2\alpha)$ and $\sin(2\beta)$? Curves in the ($\sin(2\alpha)$,$\sin(2\beta)$)

plane associated with fixed values of $|V_{ub}\,/\,V_{cb}|$ and $|V_{td}\,/\,V_{ts}|$ are shown in fig. 2.12. The existing measurement of $|V_{ub}\,/\,V_{cb}|$ provides stringent constraints on $\sin(2\beta)$ whereas the present estimation of $|V_{td}\,/\,V_{ts}|$ cannot restrict the range in $\sin(2\alpha)$. Improvements in the prediction for $\sin(2\alpha)$ are expected from an observation of B_s oscillation, either a measurement of the lifetime difference $\Delta\Gamma_{B_s}$ or the oscillation frequency ΔM_{B_s} of the B_s meson.

It would be interesting if measurements of magnitudes alone could predict *direct* CP violation [29]. *Indirect* CP violation characterizes the situation in which CP violation of the CKM mechanism cannot be distinguished from the one of a superweak force. Generally the amplitudes of CP asymmetries of different decay channels could differ both in sign and magnitude. In a superweak model, however, the amplitudes differ only by the sign ξ of the CP parity of the final state ($\Phi_W =$ constant). Superweak models are geometrically located at $\sin(2\alpha) = -\sin(2\beta)$. The differentiation between them and the SM depends crucially on the value of $|V_{td}\,/\,V_{ts}|$. However, the present range in values of $|V_{td}\,/\,V_{ts}|$ still includes the possibility of no direct CP violation.

The question of direct CP violation was first formulated for the neutral kaon system. Several experimental groups searched for a difference in the CP violating magnitude between K^0 decays to $\pi^+\pi^-$ and $\pi^0\pi^0$. The present experimental results [5] do not allow to dismiss the possibility of only indirect CP violation. If different CP violating amplitudes would be observed in different decay channels, it would imply that CP violation cannot come from particle-antiparticle mixing alone but rather is also a property of the weak deacys of neutral mesons. The question, whether CP violation comes from mixing or decay is only meaningful, if two decay channels are compared. As far as only one decay channel is considered, only the sum of both phases from mixing and decay is well defined, whereas the individual phases are parametrization dependent. This is the same reason, why Im ϵ is not an observable. However, if CP violating effects are different in different decay channels, there exists a non-trivial phase from weak decay that cannot be removed by reparametrizations of the CKM matrix.

Note that the absolute signs of $\sin(2\alpha)$ and $\sin(2\beta)$ are not determined as long as the sign of ΔM_{B^0} has not been measured. Nevertheless the relative sign between $\sin(2\alpha)$ and $\sin(2\beta)$ is well defined. It is thus possible to rule out the superweak model even if $\sin(2\alpha)$ and $\sin(2\beta)$ would have the same magnitude but also the same sign.

Finally I would like to remark that CP violation in the SM is a phenomenon restricted to the microscopic world because it appears only in quantum mechanical interference processes. An observation of macroscopic CP violation effects would revolutionize our present physical theory.

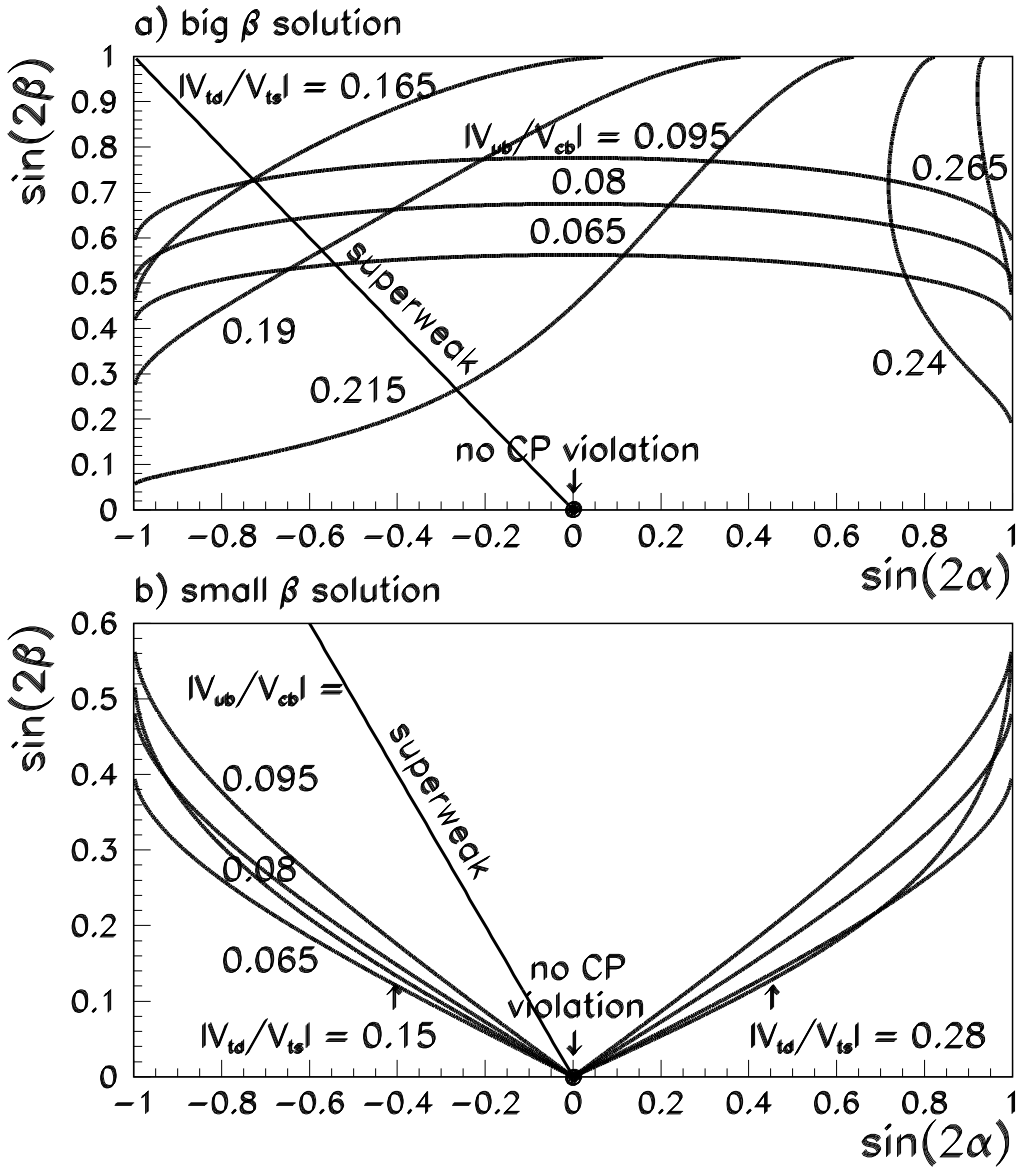

Figure 2.12: Values of CP asymmetries $\sin(2\alpha)$ and $\sin(2\beta)$ associated with fixed values of $|V_{ub}\,/\,V_{cb}|$ and $|V_{td}\,/\,V_{ts}|$. The big β solution shown in figure a) is only valid within 1σ uncertainty in the best estimates of $|V_{ub}\,/\,V_{cb}|$ and $|V_{td}\,/\,V_{ts}|$. At a level of 2σ uncertainty the region of allowed values extends to small $\sin(2\beta)$ values (figure b). The point $\sin(2\alpha)$=$\sin(2\beta)$=0 of no CP violation is still contained in the 90%C.L. region.

Chapter 3

The L3 detector at LEP

3.1 The LEP e^+e^- storage ring

The Large Electron Positron collider LEP situated at the CERN laboratory has been designed to study the electroweak interaction at energy scales of up to 200 GeV. The physics goals of LEP are twofold. In a first phase, electrons and positrons are annihilated at center-of-mass energies close to the Z resonance. The main purpose of this stage is a measurement of the neutral-current couplings of the leptons and quarks to the Z boson. The Z resonance in e^+e^- annihilations is especially suitable for this object. The difficulty is to disentangle the Z boson contribution to the neutral current from the electromagnetic one which dominates at energies below the Z mass. However, the Z resonance in e^+e^- annihilations is a pure weak resonance above a negligible electrodynamic background. The resonance in the e^+e^- annihilation cross section is shown in fig. 3.1.

Moreover the large amount of Z bosons produced at the LEP e^+e^- storage ring can be used to study the properties of heavy fermions, such as fermions of the second and third family into which the Z boson decays. In this thesis the Z resonance has been exploited only in its property to deliver large amounts of bottom hadrons. The e^+e^- cross section at the Z resonance together with a large branching ratio for $Z \to b\overline{b}$ of $\sim 15\%$ make the LEP collider an ideal b hadron factory. A big sample of in total ~ 6 million high-energetic bottom hadrons has been collected by the four experiments at the LEP collider. The most precise determination of bottom hadron lifetimes and the time-dependent measurement of $B^0 - \overline{B}^0$ oscillations were made with these data samples at LEP.

In a second stage of the LEP program, which started in 1995, the energy of the LEP beams has been increased to allow e^+e^- annihilations into pairs of W^+W^- bosons. The present center-of-mass energy is 183 GeV and will be increased further up to ~ 200 GeV until the end of the LEP program in the year 2000. The energy was increased to study the gauge boson self interaction - a crucial feature of the SM and to search for the Higgs particle as well as for new phenomena beyond the SM.

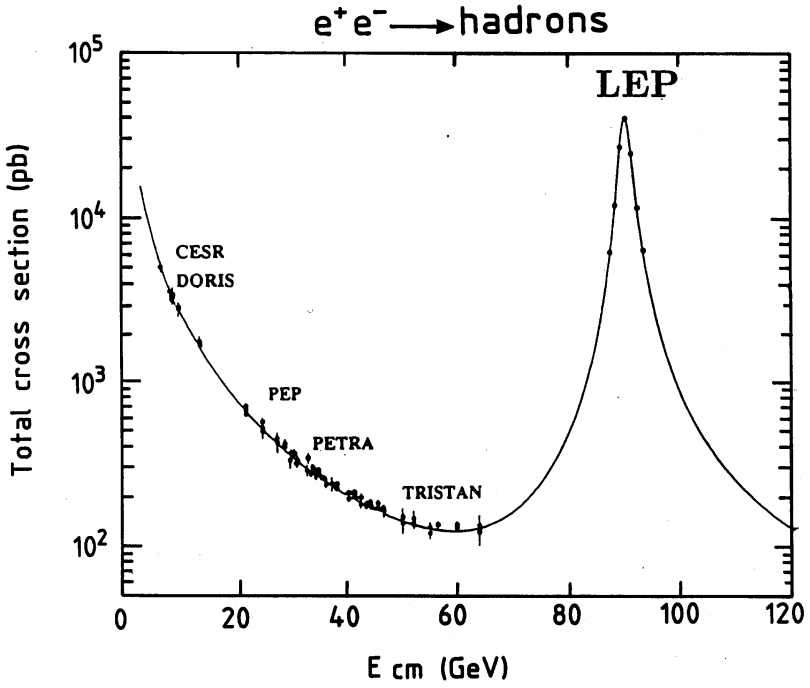

Figure 3.1: Cross section for e^+e^- annihilation into hadrons as a function of the center of mass energy E_{cm}. The LEP collider works at the peak of the Z resonance and exploits the maximum cross section. Note the logarithmic scale for the cross section.

3.1.1 The LEP accelerator system

The LEP ring has a circumference of 26.7 km and is located in a tunnel underneath the Swiss-French border near Geneva at a depth which varies between 50 and 150 m. It consists of eight circle segments and eight straight sections, as shown in fig. 3.2. Four to eight $\sim$ 1 cm long bunches of electrons and positrons circulate, in opposite directions, in the same vacuum vessel. To keep the electrons and positrons in their orbit 3304 dipole magnets, which produce a field of 0.048 T each, are installed in the curved sections. In addition the e^+ and e^- bunches are steered with focusing quadrupole and sextupole magnets onto their required trajectories. The beams collide at four interaction points in the straight sections around which the four experiments ALEPH [65], DELPHI [66], L3 [67] and OPAL [68] are placed.

The energy loss by synchrotron radiation of 120 MeV per turn at a beam energy of 45 GeV is replenished by radiofrequency (RF) copper cavities placed on two of the straight sections. The LEP ring was chosen with its large radius in order to reduce the energy loss by synchrotron radiation which is inversely proportional to the radius of curvature. The 128 cavities are capable of providing up to 16 MW of power. They are also used to accelerate the particles from their injection energy of

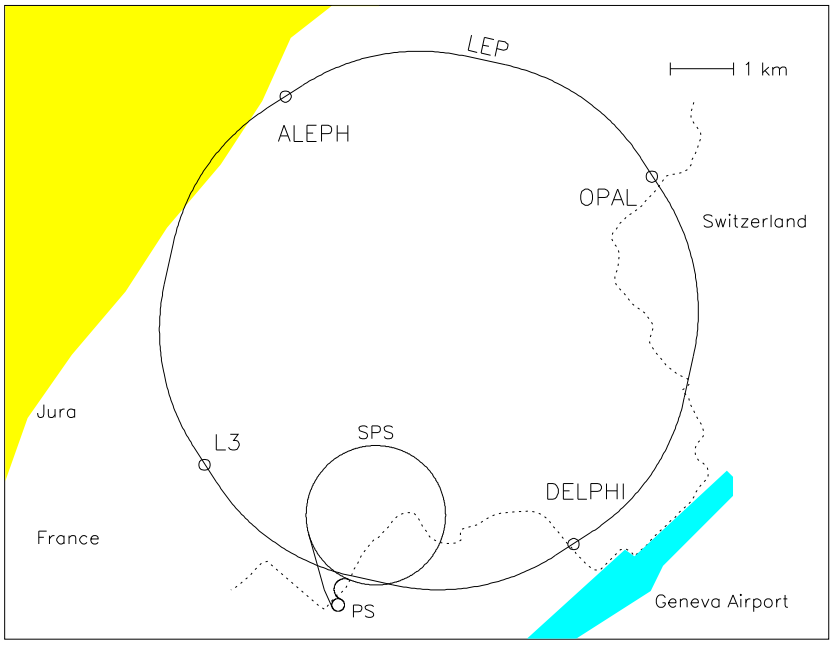

Figure 3.2: The LEP e^+e^- storage ring at CERN located at the border between France and Switzerland. Its circumference extends from the Jura mountains in the northwest to the Geneva Airport in the southeast.

20 GeV up to the final beam energy. In the LEP II program the beam energy was increased by a factor of two, from 45 GeV to 90 GeV. This enhances the energy lost by synchrotron radiation by a factor of 16 to 2 GeV per turn because it scales with the fourth power of the particle beam energy. The necessary RF power for LEP II was provided by the installation of additional 240 superconducting cavities.

The pre-acceleration of electrons and positrons for the LEP ring uses previously built facilities at CERN. The pre-acceleration steps are described in [69]. The LEP beam energy is measured by monitoring the current going through calibrated dipole magnets. In particular at the Z resonance the calibration can be improved by means of the so-called "resonant depolarization" method [70]. This method makes use of the transverse polarization of the electrons that is caused by the Sokolov-Ternov effect [71]. The calibration has a precision of ~ 5 MeV at beam energies of 45 GeV and is responsible for the high accuracy in the determination of the Z mass with a relative precision of better than 10^{-4} [17].

For a measurement of bottom hadron lifetimes the dimensions of the e^+ and e^- bunches and the environment near to the interaction point are of great importance. The average decay length of b hadrons at LEP is of the order 3 mm. At the interaction point the beam has a vertical extension of ~ 20 μm and a horizontal extension of ~ 200 μm. The beam is broader horizontally than vertically because

the synchrotron radiation emitted in the accelerator plane causes momentum and thus orbit changes. The beam profile dimensions show the typical uncertainty in the position of the primary interaction point relative to which the secondary bottom decay position has to be determined.

The central beam is accompanied by a halo which extends over radial distances of a few cm. As a compromise between long beam lifetimes and spatial resolution near to the interaction point the vacuum beam pipe has a radius of 5 cm in the interaction region. It is made of beryllium with a thickness of 1 mm. The radial dimension of the beam pipe implies that the first measurements of the particle trajectories are made at distances that are much larger than the average decay length of b hadrons. The b hadrons decay before they can reach the detector! Therefore excellent measurements of the particle trajectory are needed at distances > 5 cm. The resolution requirement can be expressed in a simple rule. The single point resolution of the tracking detectors has to be small compared to the average decay time $c\,\tau_b \sim 400$ μm of b hadrons in their rest frame. This is the accuracy that has to be achieved by the experimental apparatus.

3.1.2 Luminosity

For precision measurements large amounts of Z bosons have to be produced. The event rate N is equal to the product of the cross section σ and the luminosity L,

$$N = \sigma L \qquad L = \int \mathcal{L}\, dt\ . \tag{3.1}$$

The LEP energy is optimized on the peak of the cross section at the Z mass, as shown in fig 3.1. At the peak the cross section for e^+e^- annihilation into hadrons is ~ 30 nb. In order to measure the shape of the resonance the beam energy was varied close to the maximum position. This energy scan is necessary for the determination of the total width of the Z boson from which the number of neutrino species can be derived. The typical instantaneous luminosity $\mathcal{L}$ of LEP is 10^{31} cm^{-2} s^{-1}. The LEP performance is organized in fills where one fill extends over ~ 10 hours. One fill yields thus about 400 nb^{-1} of integrated luminosity. The total luminosity delivered to the L3 experiment at the Z resonance was 155 pb^{-1} from which 80 pb^{-1} were taken in the years 1994 and 1995. The luminosity is proportional to the number of bunches per particle species in the ring, the current per bunch and the single turn frequency. The single turn frequency, which is fixed by the circumference of the LEP ring, is 11.2 kHz. The typical bunch current is 0.32 mA and the number of bunches was initially four and increased to eight since 1992. The limiting factor for the luminosity is the maximum current per bunch, which, in turn, is determined by the beam-beam interactions. Therefore, to increase the luminosity the LEP machine has to be filled with more bunches.

The luminosity to produce on average one Z event is 2.5×10^{31} cm^{-2}. With the typical LEP luminosity of 10^{31} cm^{-2}s^{-1} it yields a Z production frequency of 0.4 Hz. This can be compared with the beam crossing rate of 90 kHz for eight

bunches and implies that the electron and positron beams have to cross each other 200,000 times before one Z boson is produced.

Detailed information on the LEP machine and its performance can be found in [69].

3.2 The L3 detector

The L3 detector [67] is one of the four LEP experiments located at the LEP e^+e^- storage ring. A perspective view of the detector is shown in fig. 3.3. The axis of the electron direction is signed as the z direction within the L3 coordinate system. The origin of the L3 coordinate system lies in the center of the detector. The y direction points vertically upwards and the x direction points to the center of the LEP ring.

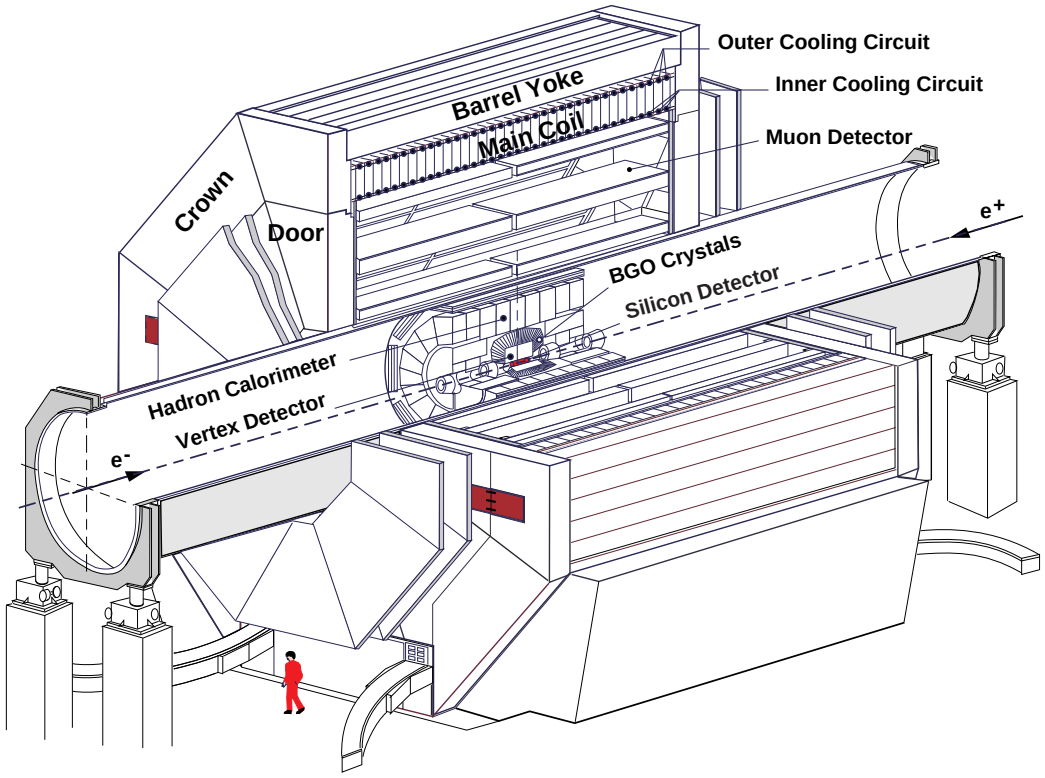

Figure 3.3: The L3 detector.

The design has been optimized towards the accurate energy and position measurement of jets, muons, electrons and photons. To achieve this, L3 is divided into several sub-detectors.

From inside out, they are:

- a silicon microvertex detector, the SMD, to provide few very accurate charged particle position measurements for the determination of momenta and production vertices.

- a time expansion chamber, the TEC, to extend the charged particle tracking system over a bigger lever arm for the measurement of track momenta and production vertices.

- a z chamber to measure the charged particle trajectories in the z direction.

- an electromagnetic calorimeter composed of BGO crystals to identify electrons and photons and to determine their energy.

- a luminosity monitor, to measure the luminosity by counting small angle Bhabha events.

- an array of scintillators to reject cosmic rays.

- a hadron calorimeter to measure, in conjunction with the BGO, jet energies.

- a muon spectrometer to identify muons and to measure their momenta.

All detector elements are installed in a 12 m inner diameter solenoidal magnet, which provides a uniform magnetic field of 0.5 T along the beam direction. In this magnetic field charged particles move on helicoidal trajectories along the symmetry axis of the beam direction. From the helix curvature the particle momentum transverse to the beam direction can be determined. Except for the muon system, all subdetectors are installed inside a steel support tube, which is 32 m long and has a diameter of 4.45 m. The muon chambers are mounted outside of this support tube.

I will describe now the L3 detector components from inward to outward. The description will go into more detail for the inner detectors, on which the measurement of bottom hadron lifetimes relies. However this is a biased view of the L3 detector which has many more applications [72]. Most of the L3 subdetectors consist of a barrel part and an endcap part. These parts cover different polar angle regions and differ in their relative resolution. For instance the θ determination of tracks outside the z chamber is performed with the forward tracking chamber (FTC) located at the TEC endflanges. The measurement of b hadron lifetimes, however, relies on the precise tracking information of the TEC chamber. Therefore only measurements inside the barrel part of the detector ($|\cos\theta| < 0.74$) are relevant for this thesis and no detailed description of the endcap detector part is presented here.

3.2.1 The silicon microvertex detector

The first measurements of bottom hadron lifetimes have been performed using the impact parameter of leptons from b hadron decays [30]. The leptons can be identified with the relevant detector components and offer a clean signature for events containing bottom hadrons. The impact parameter is defined as the shortest distance between the lepton track and the primary production vertex. The MAC and MARK-II Collaborations at SLAC succeeded at first to measure the b lifetime with the impact parameter method [30]. However, those charged particle tracking detectors had a rather modest impact parameter resolution. Another restriction of the semileptonic decay is the loss of statistics by a factor of 5 to 10 due to the semileptonic branching ratio (10% for muons and 10% for electrons).

Silicon microvertex detectors were built as detectors of very high spatial resolution for the recognition of secondary decays on an event-by-event basis. In the last 15 years a lot of effort has been put into the development of high resolution silicon strip detectors that have been incorporated into the detector systems at LEP, in particular into L3, and at $p\bar{p}$ colliders like the Tevatron. The silicon detectors are a tool for the identification of heavy flavours independent and superior to the lepton tag discussed above. Therefore I will describe now the basic principles underlying the design of these detectors followed by a detailed presentation of the L3 silicon microvertex detector.

Particle detection with silicon

Silicon detectors are an application of p-n junction diodes. Historically they have been used almost exclusively for energy measurements until the end of the '70s. In this case the primary particle is absorbed within the semiconductor and the electrical signal is proportional to the primary energy. The discovery of the charm quark [9] in 1974 and the fact that it is relatively long-lived motivated the improvement of the spatial resolution of silicon detectors. The high spatial resolution is achieved by the segmentation of the silicon diode in a series of strips. A traversing particle creates a signal in the strips near to the particle crossing path.

The detection principle of particles in silicon is similar to the one in gas detectors. Relativistic charged particles passing through matter lose energy primarily by ionization. In case of a gas atoms are ionized under the emission of electrons, in case of a semiconductor electron-hole pairs are created. However, there are quantitative differences. The binding energy of an electron in a typical drift chamber gas like argon is $\sim$ 26 eV. This is much more than the energy gap between valence and conduction band in silicon. The energy to create an electron-hole pair is only $\sim$ 3.6 eV. The high density of silicon leads to a large stopping power for charged particles. Very thin silicon layers (typical thickness of 300 μm) are sufficient to generate detectable amounts of signal charge.

The physical processes in a semiconductor detector are the following: The

application of a reverse bias voltage on the p-n junction depletes the silicon layer of mobile charge carriers (that would be present otherwise by thermal excitation) and sets up an electrical field for the separation of electron-hole pairs generated by the passage of ionizing particles. A typical voltage for the depletion of a 300 μm thick silicon layer is $\sim$ 50 V. When a charged particle traverses the depleted region it generates electron-hole pairs along its path in a very narrow tube. 99.9% of the generated electrons remain inside a radius of 0.1 μm. The electrons and holes drift to opposite sides of the electrodes where they cause a change in the induced surface charges and create a short current pulse. The collection of charge carriers from the production until their arrival on the electrodes takes $\sim$ 8 ns for electrons and $\sim$ 25 ns for holes. The front and back side of the silicon substrate can be equiped with silicon implantation strips so that both, the electrons and holes, can be detected simultaneously. The strips on both sides can be oriented perpendicular to each other so that two coordinates of the transversing particle can be measured. A three dimensional tracking performance can be obtained by a series of silicon detector layers placed one behind the other.

Last but not least, the fabrication of silicon detectors is already so advanced that complicated geometries and very small structures (of the order a few μm) can be produced in mass production. The strip distance should be a reasonable compromise between the resolution requests and the intrinsic limitations. The resolution is limited by the transverse diffusion during charge collection (typically 5 μm for 300 μm thickness) and by δ-electrons (high energetic electrons that lead to further ionization). A typical resolution is of the order 10 μm. In the simplest case, if only the strip with the highest signal is used for the position measurement, the resolution σ is related to the strip distance d by: $\sigma = d \,/\, \sqrt{12}$. Thus, to achieve the best possible resolution the strip distance should be of the order 30 μm.

It is still rather expensive to read out big detector areas with strip distances of $\sim$ 30 μm. One possibility to reduce the number of electronic read-out channels by only a small worsening of resolution is given by the method of capacitive charge division. Here the number of strips is as high as before, but not all of them are read out anymore. The strips are coupled by a capacity. A charge collected in a non-readout strip induces a certain charge in the neighbour strip. This can be repeated until a readout channel is reached. From the signal heights in the two read-out channels enclosing the particle path the position can be extrapolated.

A detailed report about the use of silicon detectors and their application to heavy flavour physics can be found in [73].

SMD detector components

The L3 silicon microvertex detector (SMD) is a cylindrical detector directly surrounding the beam pipe and is composed of two concentric layers of silicon strip sensors at distances of 6 cm and 8 cm from the interaction point. The inner and outer silicon layers consist of respectively 12 subunits, called ladders. The geomet-

rical location of the ladders is shown in fig. 3.4.

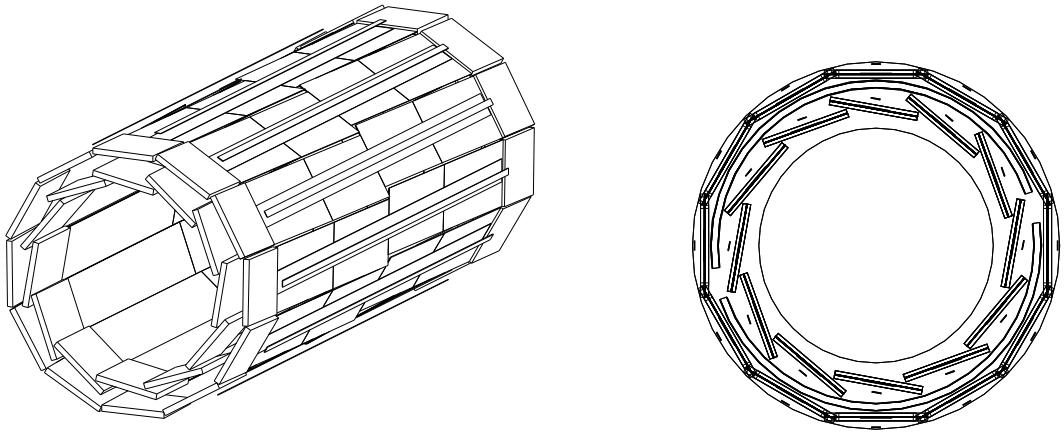

Figure 3.4: The L3 silicon microvertex detector.

The silicon sensors have readout strips on both sides. The strips on the one side (p^+ doped) run parallel to the beam direction and measure the azimuthal angle ϕ and the strips on the other side (n^+ doped) run perpendicular to the beam and measure the z coordinate. Together with the radial position of the ladder given by the mechanical holding frame, the position of a single particle hit is determined in cylindrical coordinates r, ϕ and z.

The ϕ coordinate measuring p^+ doped strips are made of boron implantations, the z coordinate measuring n^+ doped strips of phosphor implantations. In between the n doped active silicon layer is sandwiched. The strip pitch on the p^+ junction side is 25 μm and every second strip is read out. On the n^+ ohmic side the strip pitch is 50 μm and the readout pitch depends on the polar angle, either 150 μm or 200 μm. The total number of readout channels amounts to about 73,000.

In the r-ϕ direction the sensitive areas of adjacent ladders are arranged so that they match each other in case of the outer layer and overlap each other by $\sim$ 2 mm in case of the inner layer. In this way the full 2π azimuthal angular region is covered. An average number of four and a maximum number of six hits is obtained for a charged particle traversing the detector. The length of the sensitive region in the z direction is 30 cm. Therefore the SMD covers the polar angular region from 22^0 to 158^0.

In the case of multi-hadronic events a solution has to be found how the ϕ hits can be correlated to the z hits. Ambiguities can occur due to accidental matching of ϕ hits and z hits of different particles. To resolve these ambiguities the sensors of the outer layer are rotated by 2^0 relative to the beam direction, as it can be seen in fig. 3.4. This means, that the strips in the outer sensors do not measure the "true" ϕ and z coordinates but rather orthogonal superpositions of both. Due to the z component in the ϕ hit of the outer layer it can be derived which hits belong to

each other and the number of combinatorial background tracks is strongly reduced.

The mechanical support structure of the SMD consists of a 1 m long carbon fibre cylinder. The silicon sensors are mounted onto rings made of aluminum. The structure was chosen to be mechanically stable, resistant against temperature changes and to contain a minimum amount of material (to reduce the effect of multiple scattering). The aluminium rings host the water cooling circuit. Components of the readout electronics are implemented into the carbon fibre cylinder which is electrically screened with a thin aluminized foil.

SMD alignment

In order to achieve the desired high precision in vertex reconstruction an accurate alignment of the SMD has to be performed. The alignment begins with the control of the strips under a microscope during assembly of the SMD detector sensors. Before installation of the SMD detector into the L3 experiment a complete survey of the ladder positions on the carbon cylinder has been performed with a high precision mechanical measuring device. Once installed, the ladder positions have to be monitored as a function of time. This is done by laser light spots. They are generated by laser diodes, distributed by optical fibres and focused on the silicon detector surface. The system is capable of a precision of several microns. The optical alignment is further improved by off-line software alignment using reconstructed tracks.

The final alignment concerns both the global SMD detector position with respect to the rest of the L3 experiment and the relative positions of SMD sensors to each other. The global alignment is performed by the use of a sample of dimuon events with the muons measured in the time expansion chamber and the muon chamber. The discrepancy between the SMD hits and the track extrapolation points is minimized using as free parameters that of the translations and rotations of the whole detector. In the local alignment each ladder position is described by translations and rotations relative to a SMD coordinate frame. The parameters are determined as before by minimizing the residuals of the hit positions with respect to the track fit. In order to become independent of the systematic error from the rest of the tracking system the local alignment is done with the SMD alone. Tracks that are passing through the r-ϕ overlap region of the inner ladders constrain neighbour ladders to each other. Tracks that have hits in the inner and outer layer relate both detector layers to each other. In addition dimuon and Bhabha events allow to constrain opposite sides of the detector due to their back-to-back structure. As a result the relative ladder positions can be determined with a resolution of 5 μm in the r-ϕ projection and of 10 μm in the r-z projection.

Further details on the design and construction principles of the L3 silicon microvertex detector and its alignment system can be found in [74]. The SMD detector has been implemented into the L3 experiment at the beginning of the 1993 running period. It was fully operational from 1994 onwards. L3 has collected

data at the Z resonance containing SMD measurements in the years 1994 and 1995 which amount to a luminosity of 80 pb^{-1}. The thesis relies on this data sample.

SMD performance

A study of the SMD performance in 1994 and 1995 was performed with $\mu^+\mu^-$ and e^+e^- events [74, 75]. The SMD hardware was found to be operational to 79% [75]. The average detection efficiency for the operational part was estimated to 84% [75]. A spatial resolution of 15 μm was measured in the r-ϕ projection and of 25 μm in the r-z projection [74].

3.2.2 The time expansion chamber

The time expansion chamber is a precise wire chamber for the position measurement of charged particles. The chamber extends over a radial distance of 37 cm and is operated in the so-called "time expansion mode". Following its principle [76], the time expansion chamber (TEC) combines a large volume with a low, homogeneous drift field with a very small volume of high fields to achieve the necessary gas amplification. The chamber is filled with a mixture of 80% CO_2 and 20% isobutane iso-C_4H_{10}, at a pressure of 1.2 bar. This gas mixture has a low diffusion coefficient and enables the use of low electric fields (0.9 kV/cm). Thus the electrons produced by ionization have a low drift velocity of 6 μm/ns which improves the position resolution. A single-wire resolution of $\sim$ 50 μm is obtained.

The chamber is made up of two concentric cylinders operating in a common volume that is limited by an inner wall at a radius of 9 cm and by an outer wall at a radius of 46 cm. A segment of the cylindrical chamber is shown in fig. 3.5. Its sensitive length is 98 cm. The inner drift chamber is divided into 12, the outer into 24 sectors along the ϕ direction. The different number of sectors accounts for the longer drift distances in the outer chamber and enables to resolve left-right ambiguities. These ambiguities occur because only the drift distance, but not its direction can be determined. Each sector contains anode, cathode and grid wires stretched parallel to the beam direction, as it can be seen in fig. 3.5. The grid wires situated close to the anodes separate the drift region from the amplification region. The inner chamber measures 8, the outer 54 coordinate points of an ionization track. All sensitive wires measure the ϕ coordinate. In addition some of the wires are prepared for z coordinate measurement and left-right ambiguity resolution. Information on the z coordinate can be obtained by a divison of the signal charge that is transported to both ends of the wire and a comparison of its pulse heights. The drift direction can be determined by the readout of groups of grid wires to further reduce left-right ambiguities.

The drift time is determined relative to the beam-crossing time delivered by the LEP machine. The anode pulses are sampled by 100 MHz flash analog-to-digital converters (FADC) in order to obtain a precise drift time measurement by

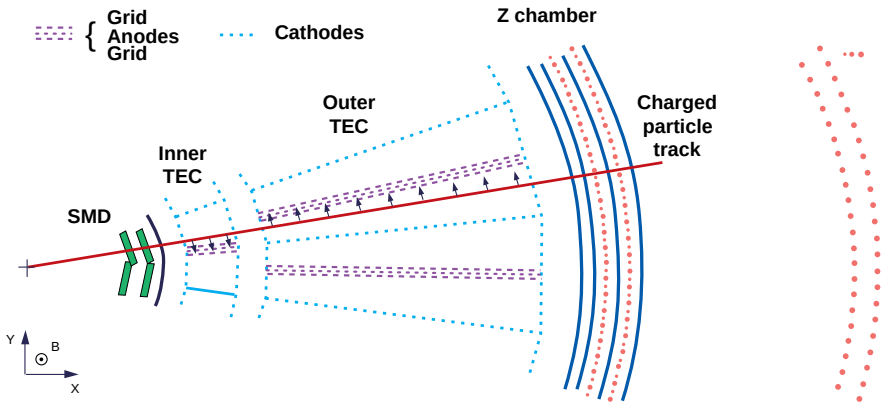

Figure 3.5: Charged particle detection in the silicon microvertex detector (SMD), the $r\phi$ drift chamber (TEC) and the z chamber.

a weighted average of the arrival times of the electrons. A precise calibration of the drift velocity is necessary to transform the time measurement into a position measurement. The TEC itself can be used to parametrize the time-to-distance relation. The calibration parameters are determined from a minimization of the residuals of the single hit positions with respect to the track fit. The parametrization of the time-to-distance relation depends on the drift time. It is different for the amplification region between anode and grid wires, the drift region and the cathode region. The difficulty is that the track fit has to be repeated for each new configuration of parameters. This problem can only be solved iteratively. In order to minimize the free parameters in the calibration it was assumed that the parametrization is the same for all wires in the inner TEC and for all wires in the outer TEC. This is of course a simplification of the real situation.

A new possibility to calibrate the TEC chamber is offered by the SMD detector. This calibration has the advantage that it is independent of the TEC chamber. In dimuon events a precise track fit can be performed with the muon chambers and the SMD. The TEC is now calibrated by comparing this track trajectory with the time measured in the TEC. The particular advantage is that the residual minimization is non-iterative and directly yields the calibration parameters. As a result a more realistic parametrization can be chosen by enlarging the number of free parameters. For instance, small corrections to the linear time-to-distance relation in the drift region can be described by the inclusion of a quadratic term. Most important, the parameters are determined separately for each single wire, so that the calibration gets drift time, wire, sector and chamber dependent. In total, about 16,000 parameters were fitted with the SMD calibration method. The single-wire resolution could be improved by 20% in the drift region and by a factor of two in the worse-resolution regions close to the cathode and amplification region.

The only drawback is that the TEC and SMD calibrations become dependent from each other because the resolution is only as precise as the position of the SMD with respect to the TEC is known. A data sample not used in the SMD calibration has been used to cross check the impact of SMD systematic uncertainties on the TEC calibration which was found to be small. To summarize, the use of an external detector, namely the SMD, allowed a reduction of systematic uncertainties in the TEC calibration so that the intrinsic resolution of the TEC chamber of better than 50 μm could be reached.

The details of the design, construction and performance of the TEC are described in [76].

The transverse momentum resolution obtained with the combination of SMD and TEC measurements is $\delta(1/p_\perp) = 0.010$ GeV^{-1}. The inclusion of the SMD improves the $\delta(1/p_\perp)$ resolution by a factor of two mainly due to the increase in the lever arm of the tracking system. In addition the presence of the SMD has a considerable effect on the impact parameter resolution. A track fit with the TEC alone yields a resolution of 120 μm for high-momentum tracks that is improved to 32 μm by including the SMD. Here the high resolution points nearest to the interaction point account for the improvement in the resolution.

3.2.3 The z chamber

In addition to the SMD measurements a second z measurement is provided by the z chamber at a radial distance of $\sim$ 50 cm. The z chamber consists of two thin cylindrical multiwire proportional chambers containing four layers of cathode strips on their surfaces. Its radial dimension extends from 47 to 49 cm at a length of 107 cm. In the gas volume anode wires are strung in the beam direction. If a particle traverses the gas the charge avalanche around the anode wires induces a mirror charge on the cathode strips at the chamber surface. These cathode strips are read out. The readout pitch is 4.45 mm. In two layers the cathode strips are inclined perpendicular to the beam axis so that they measure the z coordinate, whereas the strips in the remaining two layers form a helix with a stereo angle of $+69^0$ and -69^0. The stereolayers are used to match the z measurements with the ϕ measurements of the TEC. The resolution of the z measurement is 450 μm [77].

3.2.4 Outer detector components

The calorimeter system

The energy of particles emerging from e^+e^- annihilations is measured by the total absorption technique [5] with an electromagnetic and a hadron calorimeter. Two calorimeters are combined in the L3 detector to get an optimum energy measurement for electrons and photons on one side and for hadrons on the other. A schematic view of the L3 calorimeter system is shown in fig. 3.6.

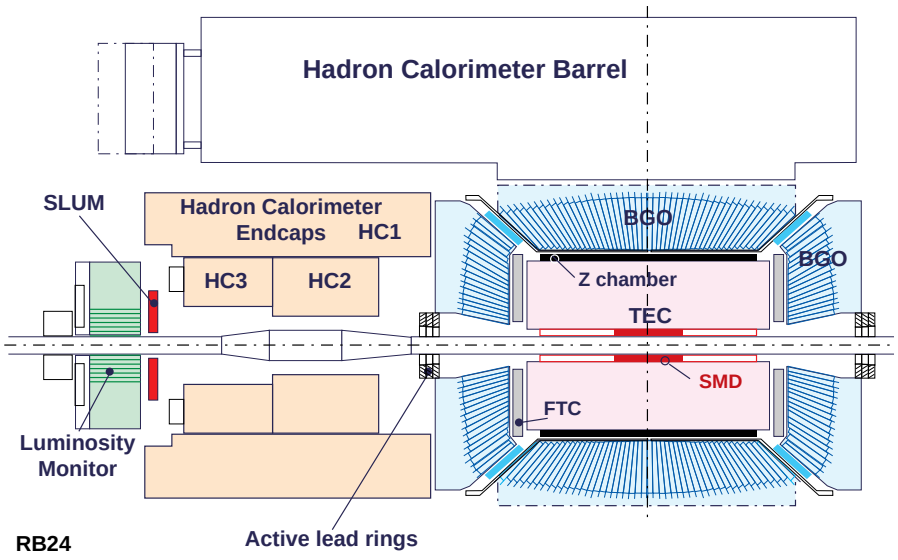

Figure 3.6: The L3 calorimeter system contains the electromagnetic BGO crystal calorimeter and the hadron calorimeter composed of uranium modules. Also shown are the BGO and silicon (SLUM) luminosity monitors placed at small polar angles.

The electromagnetic calorimeter consists of $\sim$ 11,000 BGO (Bismuth Germanate) crystals which transform electromagnetic energy depositions into a scintillation light signal. An optimum energy resolution is achieved by the use of the BGO crystal as the showering and detection medium. This is different from the design of the hadron calorimeter which is a sampling calorimeter where only a fraction of the total energy is measured. The small radiation length of BGO (1.2 cm) makes it possible to use a unique calorimeter material. Each crystal has a length of 24 cm with a frontface of 2×2 cm^2 and a backface of 3×3 cm^2. The scintillation light is read out by photodiodes mounted on the crystal backface.

The energy resolution obtained for electrons and photons is about 2% for energies above 2 GeV. The measured spatial resolution for energies above 2 GeV is better than 2 mm.

In hadronic events electrons and photons can be separated from hadronic particles by the transverse shower shape. The energy of electromagnetic showers is concentrated in almost one crystal due to the small Moliere radius of BGO (2.2 cm). On the contrary the energy of hadron-induced showers is distributed over many crystals. One application of this separation tool is the identification of electrons from semileptonic b decays.

As already mentioned the hadron calorimeter is a sampling calorimeter. It consists of uranium absorbers interspersed with proportional chambers, which act as the sampling medium. The high stopping power of uranium minimizes the

uncertainty due to intrinsic shower fluctuations and reduces the hadron background in the muon chambers. Combining the information from the BGO and hadron calorimeters, a resolution of 10% in the total energy and of 40 mrad in the direction of jets has been obtained in hadronic Z events.

The luminosity monitor

The luminosity delivered by the LEP collider to the L3 interaction region is measured by two dedicated BGO calorimeters. In the limit of small polar angles the cross section for Bhabha scattering $e^+e^- \to e^+e^-$ is identical to Rutherford scattering with purely photon exchange. It is assumed that the cross section is well known from QED so that the number of observed events can be converted into a value of the luminosity. The calorimeters are situated symmetrically on either side of the interaction region at $z = \pm 2.7$ m. They cover the polar angular range of 25 mrad $< \theta$, $(\pi - \theta) < 70$ mrad, respectively. The limiting factor on the luminosity measurement is the definition of the fiducial volume. In order to improve the angular resolution a silicon detector (SLUM) was installed in front of each of the calorimeters [78]. The precision obtained with this luminosity monitor system is 0.2%.

The scintillation counters

An array of 30 scintillation counters is situated in the region between the BGO and the hadron calorimeter. The aim of these scintillators is a discrimination of cosmic muons by precise timing measurements.

The muon spectrometer

The muon spectrometer consists of three layers of drift chambers which measure the muon trajectory in the region between the support tube and the magnet coil. A momentum precision of 2.5% is reached for 45 GeV muon tracks. Tracks measured in only two layers have a precision of $\sim 20\%$. In 1996 the barrel muon system has been complemented by forward muon chambers. The polar angular acceptance of both muon detectors covers the range from $36^0 < \theta < 158^0$.

3.2.5 Trigger system

As mentioned earlier, the Z production rate is five orders of magnitude smaller than the beam crossing rate. Therefore the readout performance of the L3 detector is an essential task.

The readout sequence of the L3 detector starts at each bunch crossing and, unless it is aborted, takes 500 μs or 45 bunch crossings to complete. While the readout sequence is active no new input will be accepted. To minimize this "dead"

time a trigger system is designed in three stages such that beam crossings without e^+e^- annihilations can be recognized at time scales of 9 μs. This allows in case of a negative trigger decision to reset the readout in time for the next bunch crossing. In each of the subsequent trigger levels more time can be consumed to process the remaining events. Under normal running conditions the dead time is less than 8%.

The level-1 trigger decision is based on the signals in five independent subdetectors, the calorimeter system, the TEC chamber, the muon chamber, the scintillation counters and the luminosity monitors. The event is retained in the buffer if at least one of these subtriggers contains a signal. Events that satisfy only one level-1 subtrigger are subjected to the level-2 decision. This trigger level is more complex and aims toward a rejection of obvious background events such as cosmic events, beam-gas or beam-wall interactions and detector noise. The level-3 trigger has access to the full detector information. Tighter cuts are performed on the correlations between detector components. For instance, tracks from the TEC trigger need to be correlated with an energy deposition in the calorimeters. Events accepted by the level-3 trigger are recorded on tape for off-line analysis.

3.2.6 Event simulation

To understand the detector response in terms of specific physics processes in e^+e^- annihilations, events are simulated with a Monte Carlo generator. A Monte Carlo event generator simulates the evolution of a multiparticle configuration from an initial e^+e^- annihilation up to a time of $\sim c\tau = \mathcal{O}$ (1 cm). The Monte Carlo program used for this analysis is the Lund JETSET version 7.4 generator [79]. The JETSET parameter settings were tuned on the values obtained in L3 measurements. Subsequently the particles are passed through the L3 detector simulation, based on the GEANT program [80]. This program is responsible for the propagation of particles through a geometrical description of the detector, taking into account the interactions of the particles with the detector material. It calculates the signal response of the various sensitive detector elements as well as the distortion occuring by the passage of particles through detector material, as for instance multiple scattering. In the last step the Monte Carlo events are reconstructed in the same way as the "real data". In this reconstruction step the primary information about drift times and pulse heights is converted into values of kinematical variables of particles. For instance, the measured drift times in the TEC are associated to *hits* that are fitted to a particle trajectory. The charge collected on the wires of the hadron calorimeter chambers is converted to an energy deposit that is combined with other signal wires to form topological *clusters*. Finally the information from various subdetectors is combined to construct objects that roughly correspond to one final particle. Distributions of kinematical variables of these "reconstructed final particles" are used to derive the fundamental properties of the original leptons and quarks produced in e^+e^- annihilations.

Chapter 4

Measurement of the b hadron production and decay location

The processes in which bottom quarks are involved that lead finally to observable effects in a physical detector should be discussed now in more detail. Due to its short lifetime of ~ 1 ps the b hadron cannot be observed directly in the detector. However its decay products as pions and kaons have lifetimes long enough to interact with the detector material. It is the aim of this chapter to explain how the b hadron decay length can be reconstructed from position measurements of its decay particles.

4.1 Hadronic event selection

The selection of hadronic events was identical to the one used for the measurement of the hadronic cross section [81]. The selection is mainly based on calorimetric information. Hadronic events are characterized by a large amount of energy deposited in the detector and a high particle multiplicity in the final state. The following cuts have been applied:

The total visible energy normalized to the center-of-mass energy was restricted to the range: $0.5 < E_{vis}/\sqrt{s} < 2.0$.

The energy balance of the final state has been analyzed with two variables. The vector sum of all cluster energies has been projected on the beam axis ($E_{||}$) and on the bending plane ($E_{\perp}$). For Z events with the total final state energy visible in the calorimeters both values should be identical to zero within the measurement accuracy. The longitudinal energy imbalance normalized to the center-of-mass energy, $E_{||}/\sqrt{s}$, should be below 0.6 removing beam gas events. The cut on the normalized transverse energy imbalance was $E_{\perp}/\sqrt{s} < 0.5$.

The number of energy clusters should be greater than 13. This cut removed $e^+e^- \to \tau^+\tau^-$ events that have a typical cluster multiplicity of 5, whereas the mean cluster multiplicity in hadronic events is about 30.

In addition to these selection criteria a cut has been applied to the number of TEC tracks. More than four tracks should be measured in the TEC chamber to ensure that the chamber was in operation. The efficiency of the selection has been estimated to $99.2 \pm 0.1\%$ [81]. It is mainly given by the polar angle coverage of the hadron calorimeter. The hadronic event sample has a high purity. The remaining background contamination is at the per thousand level. The biggest background is that of $e^+e^- \to \tau^+\tau^-$ events with a fraction of $0.20 \pm 0.02\%$. Background from all other Z decays is negligible. The fraction of non-resonant background amounts to $0.10 \pm 0.04\%$.

An event contained in the hadronic event sample is shown in fig. 4.1. In total, 2.141×10^6 hadronic events have been selected in the data sample of the years 1994 and 1995 corresponding to a luminosity of 79.7 pb^{-1}.

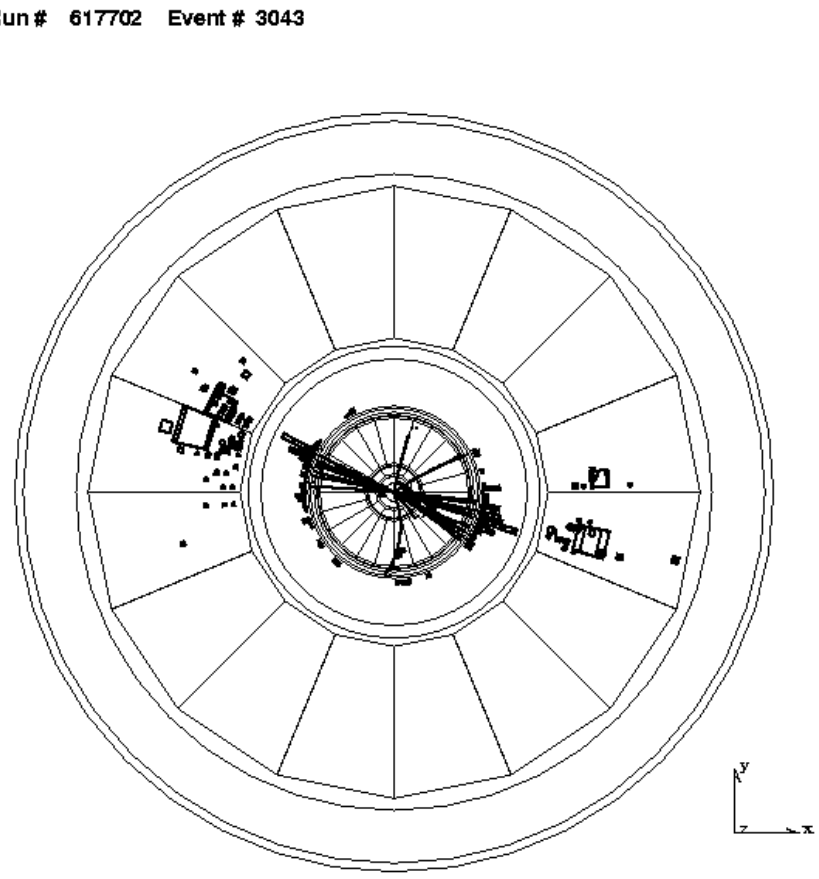

Figure 4.1: A hadronic event from 1994 data shown in the $r\phi$ plane of the L3 detector at the size of the hadron calorimeter.

4.2 Charged particle trajectory

The trajectory of a charged particle inside a uniform magnetic field is a helix spiraling along the direction of the magnetic field (the z direction). The particle moves at a circle in the bending plane and the z displacement is proportional to the length of arc on the circle. A particle trajectory obeying cylinder symmetry can be described by five parameters.

The circle in the xy plane can be mathematically described by:

$$(x - x_c)^2 + (y - y_c)^2 = R^2 \ , \tag{4.1}$$

where R is the radius of curvature and (x_c, y_c) the center of the circle. The curvature C is defined as $1/R$. A graphical representation is given in fig. 4.2.

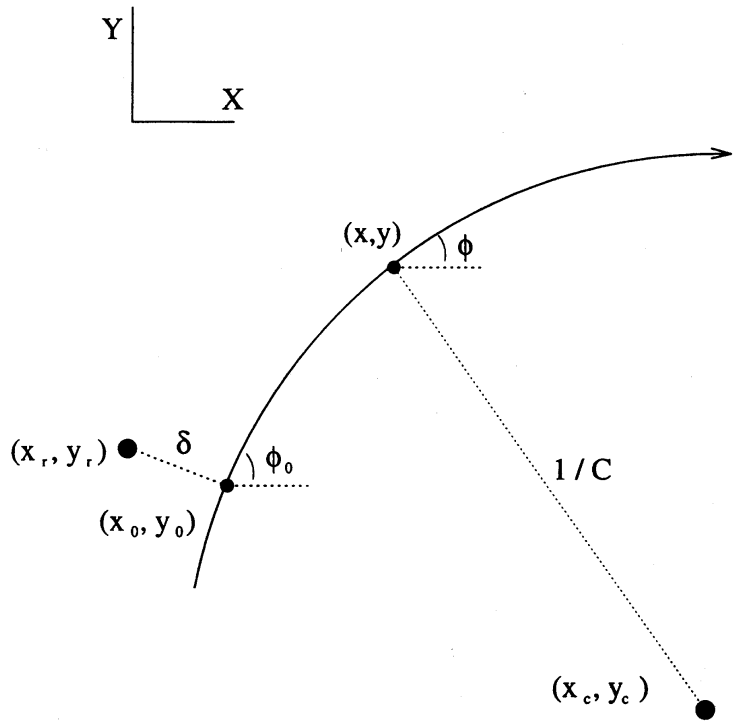

Figure 4.2: The particle trajectory in the xy plane. In the L3 coordinate system the projection of a helix in the xy plane is a circle. The parameters used in the text are shown in the figure.

An equivalent description of the central point (x_c, y_c) is given by the parameters $\delta^{r\phi}$ and ϕ_0 that relate the position of the circle to a specific reference point, as for instance the e^+e^- interaction point. $\delta^{r\phi}$ is the distance of closest approach to the reference point (x_r, y_r). In the following also the term impact parameter will be used for it. ϕ_0 is the azimuth angle of the momentum vector at the position of

closest approach to the reference point. The relation to (x_c, y_c) is given by:

$$\begin{aligned} x_c &= x_r + (R - \delta^{r\phi}) \sin\phi_0 \\ y_c &= y_r - (R - \delta^{r\phi}) \cos\phi_0 \ . \end{aligned} \tag{4.2}$$

The equation of the trajectory in the z direction can be parametrized by:

$$z = z_0 + \frac{s}{\tan\theta} \ , \tag{4.3}$$

where s denotes the arc length when the particle moves from (x_0, y_0), the point of closest approach, to (x, y). The z coordinate at the point (x_0, y_0) is given by z_0 and θ is the polar angle of the momentum vector. We can consider equation (4.2) as a "straight line fit in the sz plane", taking $1/\tan\theta$ as the slope in the sz plane.

4.3 Common vertex of several tracks

The common vertex is found as the point $\vec{x}_r = (x_r, y_r, z_r)$ that minimizes the weighted sum of distances of closest approach $\delta_i^{r\phi}$ and δ_i^z to the tracks:

$$\chi^2_{vertex} = \sum_{i=1}^{n} \left(\frac{\delta_i^{r\phi}(\vec{x}_r)}{\sigma_i^{r\phi}} \right)^2 + \left(\frac{\delta_i^z(\vec{x}_r)}{\sigma_i^z} \right)^2 \ . \tag{4.4}$$

Here $\delta_i^{r\phi}$ are the distances of closest approach to the point (x_r, y_r) in the xy plane and $\delta_i^z = z_{0,i} - z_r$ are the differences in the z coordinates of the i-th track and the vertex $\vec{x}_r$. The estimated errors are denoted by $\sigma_i^{r\phi}$ and σ_i^z, respectively.

A numeric solution for the minimization of χ^2_{vertex} in equation (4.4) can be derived from the transformation law of the track parameters $\delta_i^{r\phi}, \delta_i^z$ under a change of the reference position $\vec{x}_r$. The change from the first reference point (x_r, y_r, z_r) to the new reference point $(\tilde{x}_r, \tilde{y}_r, \tilde{z}_r)$ is described by:

$$\begin{aligned} \tilde{x}_r &= x_r + \Delta x \\ \tilde{y}_r &= y_r + \Delta y \\ \tilde{z}_r &= z_r + \Delta z \ . \end{aligned} \tag{4.5}$$

It is the task of the χ^2 fit to find that values of $\Delta x, \Delta y$ and Δz for which χ^2 is minimal.

How do the track parameters $\delta_i^{r\phi}$ and δ_i^z change under this change of the reference position? In the limit $C \to 0$, which is reasonable for most of the tracks in hadronic events, the transformation law is given by:

$$\begin{aligned} \tilde{\delta}^{r\phi} &= \delta^{r\phi} + \Delta x \sin\phi_0 - \Delta y \cos\phi_0 - \frac{C}{2(1 - C\delta)} \left(\Delta x^2 + \Delta y^2 \right) \\ \tilde{\delta}^z &= \delta^z + \frac{\Delta x \cos\phi_0 + \Delta y \sin\phi_0}{\tan\theta} - \Delta z \ . \end{aligned} \tag{4.6}$$

If the first reference point is already close to the final one, we can linearize the problem by neglecting the terms proportional to $(\Delta x^2 + \Delta y^2)$. In this linear limit an analytic solution exists for the vertex coordinates $(\tilde{x}_r, \tilde{y}_r, \tilde{z}_r)$ [5]. The analytic expressions will be given in section 4.7. The procedure continues by a cross check on the error induced by the linearization: $C/[2(1 - C\delta)]\,(\Delta x^2 + \Delta y^2)$. If the accuracy is not sufficient the process should be iterated redefining the start position (x_r, y_r, z_r). The parameters $\delta^{r\phi}, \delta^z$ are thereby calculated using the exact transformation laws. The iteration can be stopped if the required precision on $\vec{x}_r$ is reached.

4.4 Track resolution near the e^- beam location

4.4.1 Impact parameter resolution

The uncertainty in the measurement of the impact parameter with respect to a fixed point contains two contributions. One reflects the intrinsic accuracy of the tracking system and the other originates from multiple scattering of charged particles in the Coulomb field of nuclei. The latter one is strongly momentum dependent. It is possible to determine both error contributions separately by studying Bhabha and dimuon events on one side and hadronic events on the other. In case of leptonic Z decays $Z \to e^+e^-$, $\mu^+\mu^-$ the error from multiple scattering is negligible relative to the intrinsic impact parameter resolution.

Intrinsic impact parameter resolution

The impact parameter resolution can be measured by the distribution of the distance at which tracks of dilepton events miss each other at the beam center. The tracks from $Z \to e^+e^-$, $\mu^+\mu^-$ events are known to come from the same vertex. Therefore this distribution, shown in fig. 4.3, serves as a measure of the impact parameter resolution. The plotted variable is defined as a relative distance between two lepton tracks in order to get independent from an external reference position. This has the advantage that it is not necessary to locate precisely the e^+e^- annihilation point, which would introduce an additional uncertainty. From the width of the distribution a resolution of $\sigma_{tk}^{r\phi} = 32\mu$m was obtained. It was derived by scaling the distribution's width by $1/\sqrt{2}$, because both tracks contribute to the uncertainty.

Impact parameter error due to multiple scattering

The deflection of a charged particle traversing a homogeneous medium can be described by a Gaussian distribution with a width given by [5]:

$$\theta = \frac{13.6\ \text{MeV}}{p\,[\text{MeV}]}\sqrt{\frac{x}{X_0}}\ . \tag{4.7}$$

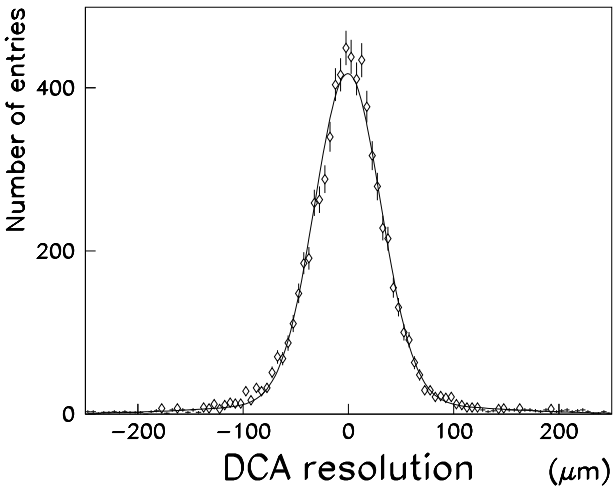

Figure 4.3: The resolution on the impact parameter. It was derived from the distribution of the distance at which electrons from Bhabha events miss each other at the beam center by scaling the distribution's width by $1/\sqrt{2}$. The superimposed Gaussian fit has a width of 32 μm.

x/X_0 is the thickness of the scattering medium in units of the radiation length. The value of θ is the mean angular deflection of a relativistic particle carrying unit charge and incident momentum p.

Table 4.1 lists the material that contributes to multiple scattering of charged particles in the tracking detectors of L3.

	Radius [mm]	Thickness	x/X_0 [%]
beam tube	55.0	1.1 mm Be	0.32
inner silicon layer	61.9	300 μm Si	0.33
carbon support tube	71.2 - 74.8	900 μm C	0.96
outer silicon layer	77.4	300 μm Si	0.33
air	55.0 - 85.5	3 cm air	0.02
inner TEC wall	85.5	1.5 mm Be	0.42
TEC gas	85.5 - 460	i-C_4H_{10}/CO_2	0.38
TEC wires	85.5 - 460	average	0.11

Table 4.1: Material contained in the tracking system.

In order to get a first estimation of the uncertainty induced by the amount of material in the tracking system we assume that the extrapolation from the particle trajectory to the interaction point can be approximated by a line connecting the two most inner hits. In this approximation equation (4.7) leads to an uncertainty

in the impact parameter of:

$$(\sigma_{ms}^{r\phi})^2 = \left(\frac{13.6\,\mathrm{MeV}}{p\,[\mathrm{MeV}]}\frac{1}{|\sin\theta|^{3/2}}\right)^2 \left[\sum_{i=1}^{N_1}\left(\frac{x}{X_0}\right)_i R_i^2 + \sum_{i=N_1+1}^{N_2-1}\left(\frac{x}{X_0}\right)_i R_{N_1}^2\right] . \quad (4.8)$$

All layers of matter, $i = 1, \ldots, N_2 - 1$, in front of the second inner hit contribute to $\sigma_{ms}^{r\phi}$. The lever arm for the deflection angle in the layers in front of the first inner hit, $i = 1, \ldots, N_1$, is the respective layer radius R_i. However, the lever arm of all layers in between the first and second hit, $i = N_1 + 1, \ldots, N_2 - 1$, is fixed to R_{N_1}. The radiation thickness of the layers for normally incident particles is denoted by $(x/X_0)_i$. The dependence $\sigma_{ms}^{r\phi} \sim 1/|\sin\theta|^{3/2}$ is caused by the increase of the lever arm $\sim 1/|\sin\theta|$ and by the increase of the layer thickness $\sim 1/|\sin\theta|^{1/2}$ in dependence of the polar angle θ of the incident particle.

In the optimum case where both SMD $r\phi$ hits were used in the track fit, multiple scattering in the beam tube, the first silicon layer and the carbon support tube adds up to an uncertainty of 105 μm $/(p_\perp/\,\mathrm{GeV}\sqrt{\sin\theta})$. This is in agreement with the amount of multiple scattering seen in the data. The error from multiple scattering can be directly obtained from data by studying the transverse momentum dependence of the width of the impact parameter distribution. It is illustrated in fig. 4.4. This method relies on the assumption that the intrinsic error on the impact parameter is independent of the momentum. A two parameter fit was performed assuming that the distribution's width can be described by a quadratic sum of the intrinsic uncertainty $\sigma_{tk}^{r\phi}$ and the $1/p_\perp$ momentum dependent uncertainty from multiple scattering $\sigma_{ms}^{r\phi}$. In order to ensure a small error $\sigma_{tk}^{r\phi}$ a sample of tracks with azimuth angles ϕ close to $0^0, 180^0$ was selected in which the uncertainty resulting from the reference point is minimal (see next section). The fit result was $(110 \pm 2)\mu\mathrm{m}/(p_\perp/\,\mathrm{GeV}\sqrt{\sin\theta})$.

Table 4.2 summarizes the uncertainty in the impact parameter due to multiple scattering for different SMD $r\phi$ hit pattern situations. The error varies between 105 μm $/(p_\perp/\,\mathrm{GeV}\sqrt{\sin\theta})$ with two SMD $r\phi$ hits used in the track fit and 152 μm $/(p_\perp/\,\mathrm{GeV}\sqrt{\sin\theta})$ if no SMD $r\phi$ hits were available.

SMD $r\phi$ hit pattern	$\sigma_{ms}^{r\phi}$ $/(p_\perp/\,\mathrm{GeV}\sqrt{\sin\theta})$
inner and outer	105 μm
inner only	128 μm
outer only	149 μm
non	152 μm

Table 4.2: Uncertainty from multiple scattering in dependence on the number of available SMD $r\phi$ hits.

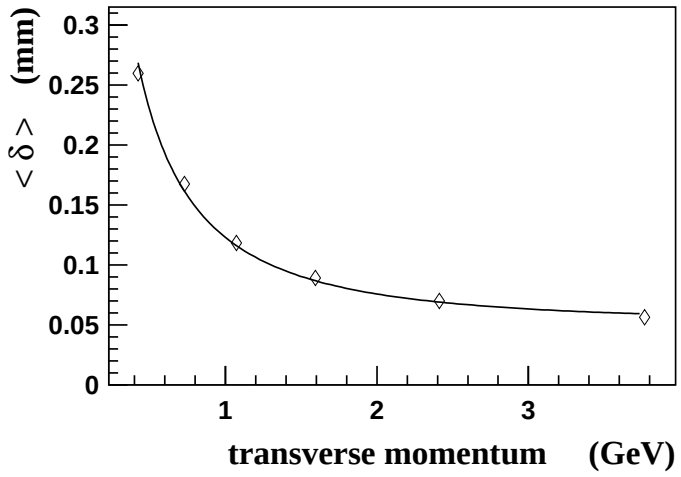

Figure 4.4: The transverse momentum dependence of the impact parameter resolution. The width of the impact parameter distribution of tracks containing both SMD $r\phi$ hits is shown for different bins of $p_\perp$.

Detector dependent correction on the impact parameter resolution

In order to obtain a precise understanding of the L3 tracking detectors the impact parameter resolution has been checked for residual detector systematics. This test was performed in a similar way as the error of multiple scattering was estimated in the previous section. The width of the impact parameter distribution has been studied as a function of the local azimuth angle. The local azimuth angle is related to the TEC chamber geometry consisting of 12 identical units. One unit contains one inner and two outer TEC sectors. All 12 units are mapped onto each other and the bins in the azimuth angular region represent $\Phi_{local} \in [0^0, 30^0]$. Fig. 4.5 shows the corrections applied to the impact parameters of the standard Monte Carlo (MC). They were derived from the quadratic difference of the distribution's width in data and MC. The maximum deviations occured at the positions of the outer anodes (at $\Phi_{local} = 7.5^0, 22.5^0$) and smaller deviations were found at the position of the outer cathodes (at $\Phi_{local} = 0^0, 30^0$) and of the inner anodes (at $\Phi_{local} = 15^0$). The distributions in fig. 4.5 have been fitted by a sum of five Gaussian functions located at the angular wire positions. The corrections were applied in dependence of the track momentum. The deviations were found to be greater and narrower located to the wire positions the higher the track momentum. The corrections fall into the worse-resolution regions of the TEC chamber where the calibration of the time-to-distance relation is difficult. This behaviour is understood and was described by a Gaussian smearing of the MC impact parameters with a Φ_{local} and $p_\perp$ dependent width. The smearing was done before the vertex positions have been calculated in the vertex fit.

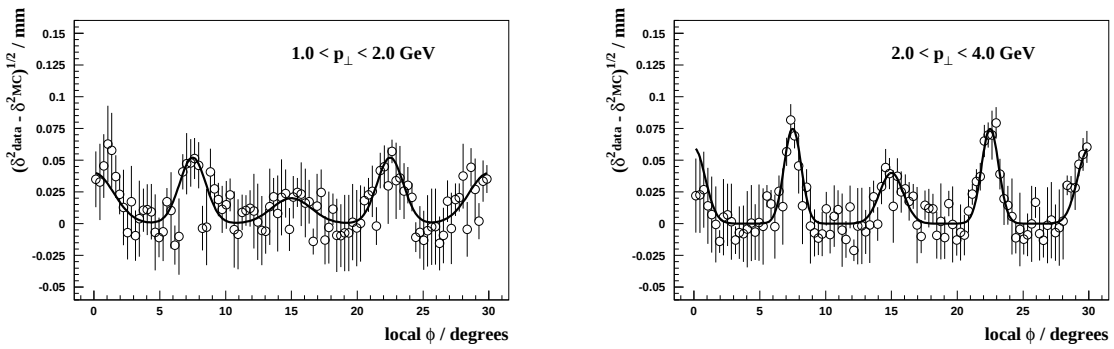

Figure 4.5: The impact parameter resolution correction in dependence of the local azimuth angle Φ. The difference between the width of the impact parameter distribution in data and MC is shown for two momentum regions. Deviations occur at the positions of anode and cathode wires. (The sign of $\sqrt{\delta^2_{data} - \delta^2_{MC}}$ is the sign of $\delta^2_{data} - \delta^2_{MC}$.)

4.4.2 z_0 resolution

The z_0 resolution has been studied in hadronic events which were found to be compatible with a single vertex in the $r\phi$ plane. In this way a sample enriched in light flavour events (u,d,s) was obtained. In these events all tracks should have a common z coordinate. The z_0 resolution can be measured by the z residual distribution of the z track coordinates with respect to the mean z event position. In order to separate the intrinsic track resolution from the multiple scattering contribution only the residuals of high-energetic hadron tracks have been considered. Fits relying on Gaussian functions have been performed to the residual distribution separately for different z quality categories. If at least one SMD z hit was used in the track fit a resolution of $\sigma^z_{tk} = 350\mu$m was found in the data. This can be compared with a resolution of $\sigma^z_{tk} = 3$ mm obtained with the z chamber alone. The SMD is essential for accurate z_0 measurements because it delivers precise z measurements very close to the interaction point at radial distances of 6 and 8 cm, respectively. The z chamber alone can only provide information about the polar angle θ but not about z_0 because the z coordinate is measured at only one radius of about 50 cm. However in combination, both detectors can exploit the big lever arm from 6 cm to 50 cm to give precise predictions for the z_0 coordinate.

The error from multiple scattering on the z_0 coordinate is similar to the one of the impact parameter. The mean deflection angles in ϕ and θ are the same. However, the lever arm increases more rapidly with $1/\sin\theta$. The z_0 error from multiple scattering can be parametrized by $\sim 1/(p_\perp/\,\mathrm{GeV}|\sin\theta|^{3/2})$ with the same values as in tab. 4.2.

4.5 Beam position measurement

The beam position is essential for the b lifetime measurement in its use as an approximate event origin.

4.5.1 Central beam spot position

The central beam position at the L3 interaction point is determined by fitting a common vertex to a set of charged tracks passing loose quality criteria, as explained in section 4.3. Tracks of hadronic events with momenta above 600 MeV and at least 15 TEC hits were considered to ensure precise position information near the origin.

Usually the beam spot position is varying considerably over time and it is useful to group the beam positions in short time intervals. In the L3 analysis samples of ~ 200 hadronic Z decays were constructed corresponding to a mean time interval of about 16 minutes. These data samples contain typically ~ 1700 tracks which were constrained to a single production vertex. The result of this procedure is the so-called 200-event vertex. The statistical error in the determination of the central beam position was determined to $\sigma_x = 15$ μm in the horizontal direction and $\sigma_y = 10$ μm in the vertical direction. Fig. 4.6 shows the variation of the 200-event vertex positions within a fill for the x and y coordinate, respectively. Large fluctuations of up to $\mathcal{O}(100$ μm) can be seen. In particular the x position is affected by large orbit corrections to the LEP beam.

Independent information on the beam spot position can be obtained from the beam orbit monitors located at $z = \pm 4.7$ m and $z = \pm 64$ m on either side of the L3 interaction point. The beam orbit monitors (BOM) consist of a set of 4 electrodes in which the field of the passing electron and positron bunches induces short current pulses. These measurements of the beam position in x and y can be extrapolated to the interaction point. They provide useful cross checks for the estimation of the 200-event vertex. The accuracy of the BOM system in the y direction reaches that one obtained with the tracking detectors of $\sigma_y = 10$ μm. This is due to the narrow width of the beam shape in y.

4.5.2 Beam spot dimension

How do we measure the beam spot shape? The standard technique uses Bhabha and dimuon events where the high momentum of the leptons assures a minimum contribution from multiple scattering errors. The beam spot size is measured by plotting the distance of closest approach to the estimated central beam position versus the azimuth angle ϕ of the track at the same position. The width of this distribution $\langle \delta^{r\phi} \rangle$ for different ϕ bins reflects directly the dimension of the beam spot folded with the impact parameter resolution. As explained in the previous section the impact parameter resolution $\sigma_{tk}^{r\phi}$ can be taken out by measuring the

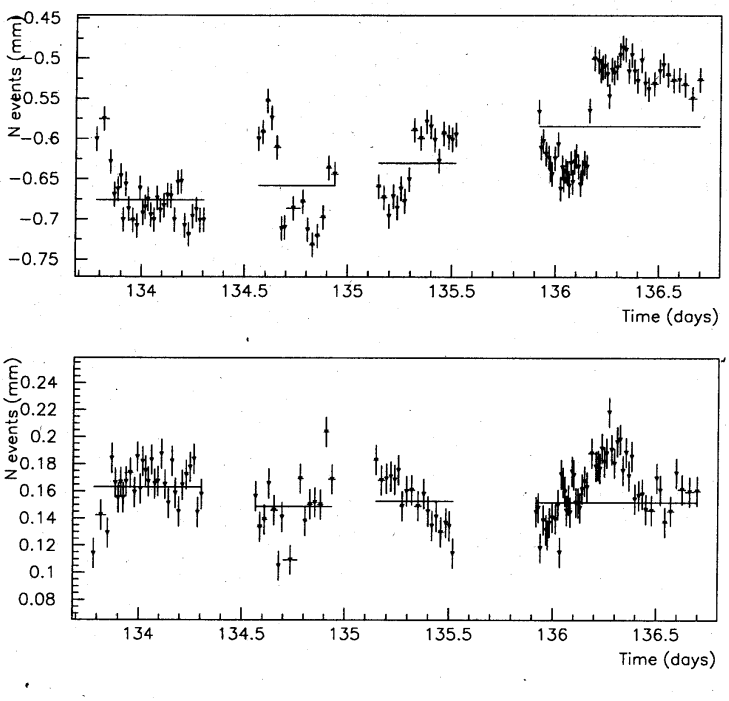

Figure 4.6: Time-distribution of the fill and 200-event vertices in four fills. The upper plot shows the value in x and the lower one the value in y. The lines are the average fill vertex values and the dots the 200-event vertices with their errors.

distance between two back-to-back tracks at their point of closest approach. The widths of the impact parameter distributions were determined using Gaussian fits. The correlation between $\langle \delta^{r\phi} \rangle$ and ϕ can be parametrized by:

$$\langle \delta^{r\phi} \rangle^2 = (\sigma_{tk}^{r\phi})^2 + \left[(\sigma_{BS}^x)^2 \sin^2 \phi + (\sigma_{BS}^y)^2 \cos^2 \phi \right] . \tag{4.9}$$

σ_{BS}^x and σ_{BS}^y are the one standard deviation width and height of the LEP beam shape at the L3 interaction point. A fit to the L3 Bhabha event sample of 1994 yielded the dimensions of $\sigma_{BS}^x = 133 \pm 6$ μm and $\sigma_{BS}^y = 22 \pm 10$ μm. The resolution on the y dimension of the beam spot is limited by the intrinsic track resolution that dominates the total error for $\phi \to 0^0, 180^0$ due to $\sigma_{tk}^{r\phi} > \sigma_{BS}^y$.

4.6 Track quality selection

Tracks fulfilling the following quality cuts were used in the calculation of the b hadron decay length. The selection criteria were designed to remove tracks with badly measured impact parameters while keeping the efficiency high.

The transverse momentum with respect to the beam axis should be greater than 300 MeV in order to restrict the uncertainty due to multiple scattering. At

least 25 hits should be included in the track fit and the difference between the outermost minus the innermost wire number should exceed 35. In addition at least two of the used hits have to belong to the inner TEC chamber. The track should contain at least one SMD hit from the inner $r\phi$ ring to ensure a good extrapolation to the interaction point.

Tracks from identified decays of K_S^0 and Λ hadrons were antiselected to reduce the number of downstream secondary vertices. An additional cut on the the impact parameter, to be smaller than 4 mm with respect to the 200-event vertex, was applied to remove remaining tracks from longlived hadrons and secondary tracks produced in interactions in the beam tube or the SMD.

Tracks that satisfy the above criteria were used for the calculation of the xy position of the event vertices. If in addition the track was well measured in the z projection it has been used in the calculation of the three dimensional vertex position. The track criteria for the z projection were: At least one SMD hit from the inner rz ring has to be included in the track fit. The z distance at closest approach to the interaction point should be smaller than 1.5 cm.

4.6.1 Antiselection of tracks from identified K_S^0 and Λ decays

In addition to b hadrons other longlived particles are produced in Z decays. Several strange hadrons originating from the fragmentation process or from decays of heavy quarks have decay paths of $\sim$ 10 cm and are visible in the tracking detector. Particles from those decays cause a systematic uncertainty in the measurement of the b hadron decay position. In order to minimize this uncertainty tracks of decays of strange hadrons were antiselected from the sample used for the b lifetime fit.

In particular, K_S^0 and Λ hadrons decay inside the volume of the tracking detector and are produced frequently in Z decays. A measurement of the L3 Collaboration [82] yielded an average multiplicity per Z decay of 1.02 ± 0.07 for K_S^0 and of 0.37 ± 0.04 for Λ hadrons. K_S^0 and Λ hadrons are neutral hadrons that have high branching ratios for two-body decay channels [5]. The selection of this analysis relies on the $\pi^+\pi^-$ decay of the K_S^0 meson and on the $p\pi^-$ ($\bar{p}\pi^+$) decay of the Λ ($\bar{\Lambda}$) baryon. The experimental signature are two tracks of opposite curvature that have a common vertex downstream of the interaction point. The total momentum vector points in the direction to the interaction point. The following cuts have been applied to select K_S^0 and Λ decays:

Tracks have to be well measured in the TEC chamber as well as in the z chamber. A minimum number of 10 hits in TEC chamber and at least one z-measuring wire in the z chamber were required. The momentum transverse to the beam axis should exceed 150 MeV.

From all possible two-track combinations of opposite charge those were selected that are geometrical consistent with the so called V^0 form. A powerful rejection of

background from randomly intersecting tracks was achieved by a cut on the angle between the transverse flight direction $\vec{d}_\perp$ and the total transverse momentum of the pair $\vec{p}_\perp$ required to be less than 15 mrad. A stronger cut was performed on the minimum hit number in dependence of the transverse flight path $|d_\perp|$. A minimum number of at least 25 hits for $|d_\perp| < 10$ cm and $25 - 1.3\,(|d_\perp|\,[cm] - 10)$ hits for $|d_\perp| > 10$ cm should be distributed over a span of at least 35 wires for $|d_\perp| < 10$ cm and $35 - 1.3\,(|d_\perp|\,[cm] - 10)$ wires for $|d_\perp| > 10$ cm. The radial distance $|d_\perp|$ was required to be separated from the primary vertex by more than 15 standard deviations and to be included in a fiducial volume of a maximum radius of 35 cm.

The two-track combinations should show typical kinematic properties of K^0_S and Λ decays. Each track pair was considered as a K^0_S and a Λ candidate. In case of a K^0_S candidate both tracks were assumed to be pions, in case of a Λ candidate the track with the higher momentum was assumed to be the proton (antiproton) and the other one the pion. Due to the large mass difference $m_p - m_\pi$ the probability of a wrong assignment has been found to be less than 0.6%. The total momentum p of a K^0_S candidate was required to be greater than 200 MeV and that of a Λ candidate greater than 500 MeV. The masses of the final state particles determine the average fractions of momenta carried by them. The momentum asymmetry, $(|p_1 - p_2|)/(p_1 + p_2)$, should be smaller than 0.7 for a K^0_S candidate and should lie between 0.5 and 0.8 for a Λ candidate. The proper decay time $t = (m/p)\,|d_\perp|/\sin\theta$, as derived from position and momentum measurements, had to be greater than a minimum fraction of the average decay time, 0.05 $\tau_{K^0_S}$ in case of a K^0_S candidate and 0.10 τ_Λ in case of a Λ candidate.

The resolution in the masses of the K^0_S and Λ resonances has a linear dependence on the total momentum p. The widths of 68% acceptance have been fitted by $(5 + 760\,p/p_{beam})$ MeV for K^0_S and by $(5 + 170\,p/p_{beam})$ MeV for Λ decays. All track pairs that fulfil the preceding cuts and which masses fall into these mass windows have been counted as tracks from decays of longlived hadrons.

The described cuts have been found by an iterative procedure in which the signal and background distributions of individual variables were studied while all other cuts have been applied. The invariant mass distribution of $\pi\pi$ and pπ combinations are shown in fig. 4.7. The combinatorial background decreases exponentially with increasing mass. In addition p/π misidentification causes ambiguities in the separation of the K^0 and Λ decays. The small shoulder below the K^0 mass in the $\pi\pi$ mass spectrum is produced from Λ decays interpreted as $\pi\pi$ decays. The mirror process of misidentified K^0 decays is responsible for the shoulder above the Λ mass in the pπ mass distribution.

Within the described cuts the detection efficiency was 15.3% for selecting a K^0_S meson and 8.0% for selecting a Λ baryon, as estimated from the Monte Carlo. A purity of 61.6% and 26.6% was obtained for K^0_S and Λ, respectively. The values of the efficiency are normalized to the total number of K^0_S and Λ decays in the considered decay channels. However most of K^0_S and Λ hadrons decay outside of

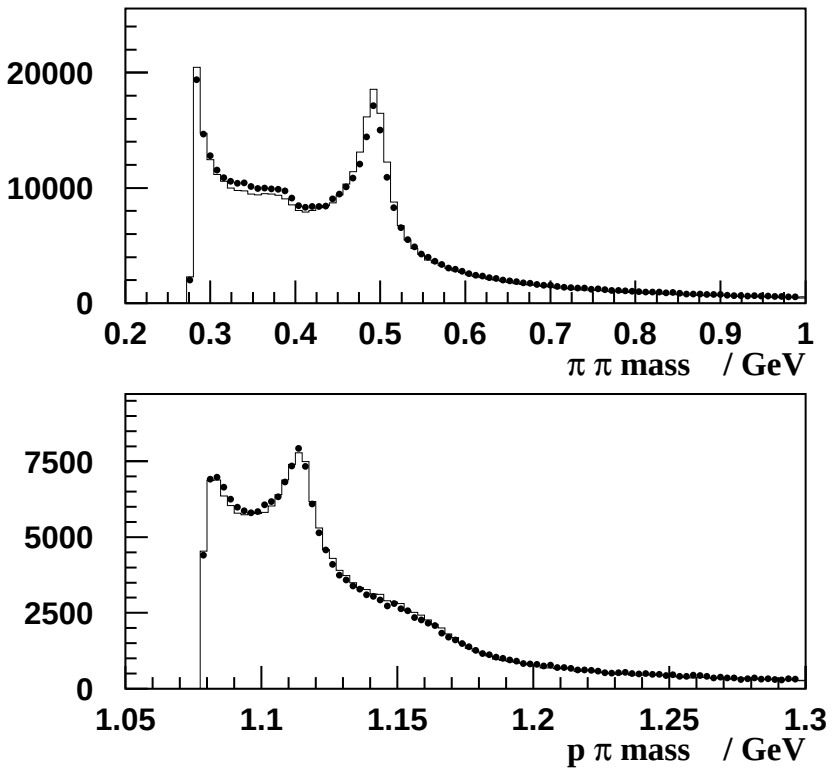

Figure 4.7: The measured $\pi\pi$ and pπ invariant mass distributions in 1994 data (points). The solid line shows the MC distribution. All selection cuts except that on the invariant mass have been applied. The K^0 and Λ signals are clearly visible.

the L3 tracking detector and have no influence to the track reconstruction. The efficiency normalized to the number of visible decays in the TEC chamber was 39.8% for K^0_S and 29.4% for Λ.

4.7 Reconstruction of Z decays into $b\overline{b}$

The pair production of b quarks is characterized by two decay positions (secondary vertices) separated on average by ≈ 3 mm from the e^+e^- interaction point (primary vertex). The daughter particles of b hadrons arise at the secondary vertices and additional particles produced in the fragmentation process originate at the primary e^+e^- vertex. Therefore in contrast to Z decays into other quark species $b\overline{b}$ events consist of three distinct vertices: one primary and two secondary. This situation is illustrated in fig. 4.8. The same event as in fig. 4.1 is seen in an enlarged view of the vertex region. In both jets secondary vertices are visible that are distinct from

the primary e^+e^- vertex.

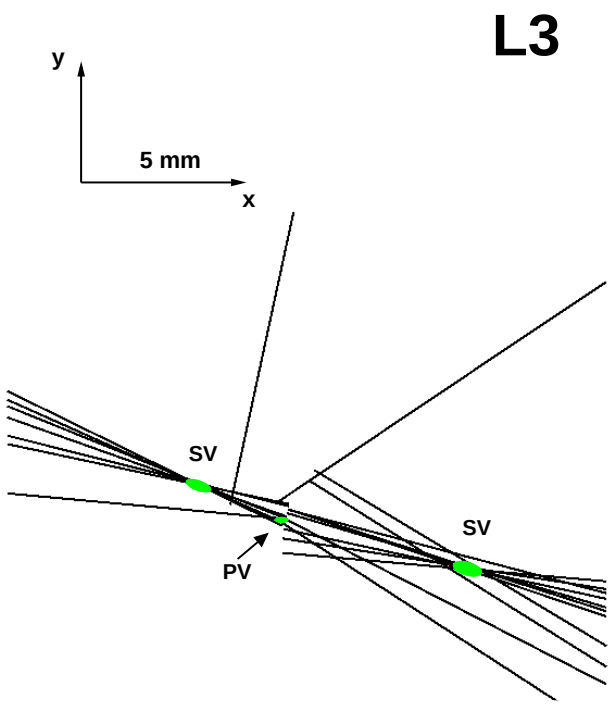

Figure 4.8: The same hadronic event as in fig. 4.1 in a zoom of the vertex region. The event has a high probability to be a $b\overline{b}$ event due to the secondary vertices clearly visible in both jets.

In principle even five vertices would be expected because b quarks are members of the third quark family and two decay cascades take place with c hadrons as intermediate state. However the resolution did not allow to resolve the b from the c decay point. Therefore they were merged into one decay position. In this analysis we have assumed that three vertices exist and tried to find the best description under this hypothesis.

Hadronic jets were reconstructed from energy clusters in the calorimeter using the JADE algorithm [83] with a cut on the scaled invariant mass squared $y_{\rm cut} = m^2/s$ of 0.04. This resulted mostly in two jet events and ensured that all decay particles from one b hadron were contained in the same jet.

The tracks in the event were associated to the closest jet. The two most energetic jets in the event have been considered to contain the original b quarks. Both of these jets must point into a fiducial region delimited by the barrel part of the detector, $|\cos\theta| < 0.74$. In case of three or more jet events tracks in the less energetic jets were not used for the lifetime measurement.

The three vertex hypothesis was tested with tracks that fulfiled the quality cuts described in the previous section. In order to assign the selected tracks to

one of the three vertices we considered all associations and selected the most likely combination by a χ^2 fit, which included lifetime and kinematical information:

$$\chi^2_{vertex} = \sum_{i=1}^{n}\left[\left(\frac{\delta_i^{r\phi}(\vec{x}_j)}{\sigma_i^{r\phi}}\right)^2+\left(\frac{\delta_i^{z}(\vec{x}_j)}{\sigma_i^{z}}\right)^2\right]+\sum_{k=1}^{3}\left(\frac{(\vec{x}_1-\vec{x}_{BS})\vec{e}_k}{\sigma_{BS}^{k}}\right)^2-2\sum_{i=1}^{n}\ln P_l(\eta_i)$$

$$\begin{aligned}&\mathrm{i}=1,\cdots,\mathrm{n\ tracks},\quad \mathrm{j}=1,2,3\ \text{vertices}\\ &\mathrm{k}=\mathrm{x,y,z\ projections},\quad \mathrm{l}=1,2\ \ \text{b hadron/fragmentation}\,.\end{aligned}\tag{4.10}$$

The first two terms contain the sum of quadratic deviations of all track positions to the respective vertices in $r\phi$ and z. The parameter $\delta_i^{r\phi}$ denotes the impact parameter of the track in the bending plane and δ_i^z is the z difference, both with respect to the vertices $\vec{x}_j$ (j=1,2,3). The associated errors $\sigma_i^{r\phi}$ and σ_i^z were defined as the sum of uncertainties from the track fit and multiple scattering, added in quadrature. If a track did not belong to the z selected sample, the error σ_i^z was set to infinity.

The primary vertex $\vec{x}_1$ was constrained to be identical to the beam spot position $\vec{x}_{BS}$, within the horizontal beam spot size o f $\sigma_{BS}^x = 135$ μm, the vertical size of $\sigma_{BS}^y = 25$ μm and the longitudinal size of $\sigma_{BS}^z = 1$ cm.

The last term in the expression for χ^2 exploits the high mass and high energy of b quarks to distinguish b decay from fragmentation tracks. A suitable variable that combines the high momentum and small angles of b decay tracks is the rapidity $\eta = 1/2\ \ln(E+p_{||})/(E-p_{||})$, where E stands for the particle energy (assuming pions) and $p_{||}$ for the momentum parallel to the jet axis. The track configurations in equation (4.11) were weighted with the probability that the measured rapidities η_i belong to either the b decay or the fragmentation distributions $P_l(\eta_i)$ (l=1,2). The probability distributions are shown in fig. 4.9. Rapidity distributions in the reconstruction of b decays have first been used by the DELPHI Collaboration in the application to b hadron spectroscopy [84]. By means of equation (4.11) they can be implemented into a b lifetime measurement because the rapidity contains independent information on the particle origin that is derived from curvature and angle measurements.

The minimum value of χ^2 was found in two steps. At first the vertex coordinates were estimated for a given track combination. In order to decide which track came from which vertex the calculation was repeated for all possible configurations and that one with the minimum value of χ^2 as defined in equation (4.11) was selected. In this selection of the most likely track configuration the rapidity term was applied complementing the pure position measurements.

The χ^2 problem was simplified by assuming the track measurements were independent from each other. Under this assumption the χ^2 function formulated for three vertex positions splits up into three separate terms for a single vertex position. The procedure for the calculation of a common vertex of a set of tracks followed that one described in section 4.3. The χ^2 function was assumed to be linear dependent on the vertex coordinates $\vec{x}_j$ (j=1,2,3). Small nonlinear terms due

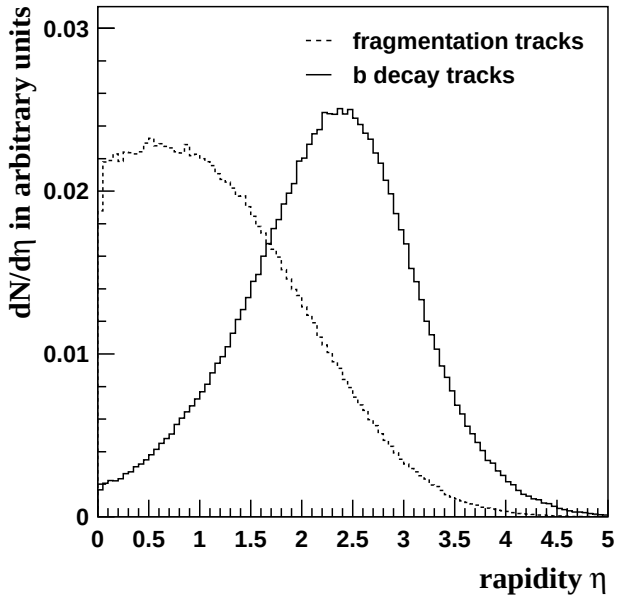

Figure 4.9: Rapidity distributions for b decay and fragmentation tracks, respectively.

to the track curvature and the dependence of the track error on the coordinates itself have been neglected. This offered the possibility of a fast analytic solution for a linear problem. Deviations from linearity were taken into account in an iterative solution of the linearized χ^2 function.

At first the three coordinates (x_{PV}, y_{PV}, z_{PV}) of the primary vertex were calculated. So far only measurements in the tracking system were used for the definition of χ^2. However, due to the big lever arm, the calorimeters provide precise measurements of the b flight direction. The direction of the b momentum vector was better defined with the calorimeters than the direction of the decay distance was measured in the tracking system. Therefore the flight direction, given by the line connecting primary and secondary vertex, was fixed to the jet axis, defined with the clusters in the calorimeter. The secondary vertices were constrained on a line starting from the primary vertex and pointing in the direction of the jet axis. The χ^2 function for the secondary vertices was expressed by:

$$\chi^2_{SV} = \underbrace{\sum_{i=1}^{N}(\alpha_i + \beta_i\, r)^2}_{xy\,fit} + \underbrace{\sum_{i=1}^{N}(\gamma_i + \delta_i\, r)^2}_{z\,fit} \tag{4.11}$$

with the coefficients of the linear expansion given by:

$$\alpha_i \;=\; \frac{\delta_i^{r\phi} + (x_{PV} - x_r)\sin\phi_i - (y_{PV} - y_r)\cos\phi_i}{\sigma_i^{r\phi}} \tag{4.12}$$

$$
\begin{aligned}
\beta_i &= \frac{\cos\phi_J \sin\theta_J \sin\phi_i - \sin\phi_J \sin\theta_J \cos\phi_i}{\sigma_i^{r\phi}} \\
\gamma_i &= \frac{z_{0,i} + \left[(x_{PV} - x_r)\cos\phi_i + (y_{PV} - y_r)\sin\phi_i\right] / \tan\theta_i - z_{PV}}{\sigma_i^z} \\
\delta_i &= \frac{\left[\cos\phi_J \sin\theta_J \cos\phi_i + \sin\phi_J \sin\theta_J \sin\phi_i\right] / \tan\theta_i - \cos\theta_J}{\sigma_i^z} \; .
\end{aligned}
$$

Here r is the decay length and ϕ_J, θ_J are the azimuth and polar angle of the jet axis, respectively. The impact parameters $\delta_i^{r\phi}$ are given with respect to a reference point (x_r, y_r). The reference point for z is chosen at $z_r = 0$. The solution for r can easily be obtained by:

$$
\begin{aligned}
(\Delta r)^2 &= \left(\sum_{i=1}^{N} (\beta_i^2 + \delta_i^2) \right)^{-1} \\
r &= -(\Delta r)^2 \left(\sum_{i=1}^{N} (\alpha_i \, \beta_i + \gamma_i \, \delta_i) \right) \; . \qquad (4.13)
\end{aligned}
$$

The role of the jet axis as a constraint for the decay length direction can be illustrated for the case that no track belongs to the z selected sample ($\gamma_i = \delta_i = 0$ for all i = 1, N). In that limit the solution (4.13) is identical to a two-dimensional fit in which the projection of the decay length in the $r\phi$ plane is scaled by $1/\sin\theta_J$ into a three dimensional value of r.

No constraint was imposed on the sign of r. A negative value for r denotes an unphysical situation with the b hadron decay length and momentum pointing in opposite directions. The fraction of b decays with negative values of their decay length serves as a measure of the decay path resolution and constitutes an important cross check. The sign of the decay length is unambiguously defined by (4.11) due to the beam spot and rapidity terms that are sensitive to the distinction of fragmentation and b decay tracks. Chapter 5 shall refer to that sign in its description of the b lifetime fit.

The solution (4.13) was calculated for all possible track combinations. In general the number of track combinations was 3^n where n is the number of selected tracks in the two most energetic jets. A reasonable simplification was to assume that all tracks at the secondary vertex belong to the same jet which reduced the number of combinations to 2^n. Apart from that at least one track from each jet was required at the primary vertex and at least three tracks at the secondary vertex to reduce fake vertices of random track crossing.

In order to prevent the procedure from poorly-measured tracks and remaining tracks from decays of longlived hadrons, all $r\phi$ impact parameters $\delta^{r\phi}$ and z differences δ^z were checked if they were below 1 mm and 3 mm, respectively. If a impact parameter was greater than 1 mm the track was taken out from the vertex calculation and if a z difference to the estimated vertex was greater than 3 mm, the track was removed from the z selected sample and only the $r\phi$ impact parameter was used in a new evaluation of the vertex positions. The χ^2 minimization

was repeated up to a maximum of two times. Finally all tracks should satisfy the criteria for the described quality cuts. Otherwise the event was not considered to allow a unique interpretation as a $b\overline{b}$ event with three vertices and it was removed from the selected sample.

The fit results were the three-dimensional coordinates of one primary vertex and two secondary vertices. Only that combination with the minimum χ^2 value was kept for the further analysis. The vertex positions have been calculated in 445 k hadronic events in the data sample of the years 1994 and 1995. This event number corresponds to a total efficiency of 21% relative to the number of selected hadronic events. The efficiency was determined by the luminosity fraction with an operational SMD detector (79%), the angular acceptance fraction (66%) and the fraction of events with a minimum number of selected tracks (40%). A breakdown of the selection steps is given in table 4.3. The efficiency of 40% to have the minimum number of tracks for the vertex calculation was mainly determined by the SMD hit requirement. The rejected events had at least one jet with less than four quality tracks. Due to the higher multiplicity of $b\overline{b}$ events the b purity was slightly increased from 22% to 27%.

Selection step	Event number	Efficiency to previous step
Hadronic events in 1994/95	2,141 k	99%
SMD detector status	1,692 k	79%
Barrel angular range	1,110 k	66%
Events with vertex positions	445 k	40%

Table 4.3: Event statistics in different stages of the selection.

Chapter 5

Average b hadron lifetime

This chapter describes the fit procedures used to extract the average lifetime τ_b from the locations of the primary event vertex and the secondary decay vertices as determined in chapter 4.

5.1 Principle of measurement

Lifetime measurements with hadronic b events at LEP already reach a statistical precision that is small compared to the systematic uncertainties in modeling heavy quark decays [85–88]. Our main purpose was thus to perform a fit where the values of poorly known model parameters were determined from the data itself. The most relevant parameters were the b hadron energy spectrum, the average b decay multiplicity and the background of longlived mesons.

Two variables sensitive to the b lifetime are analyzed here. One is the decay length, which measures the distance between primary and secondary vertex. The other is the impact parameter, here defined as the impact parameter of those tracks attached to a secondary vertex in the minimum χ^2 configuration. The advantage of the impact parameter is that for relativistic b hadrons its mean value is proportional to τ_b, whereas the decay length is proportional to $(p/m)\,\tau_b$, where m and p are the rest mass and momentum of the b hadron in the laboratory frame respectively. The average impact parameter of tracks from b decays at LEP is therefore less sensitive to the b hadron momentum and to a precise knowledge of the b quark fragmentation parameters. In this thesis two lifetime fits have been performed, one to the decay length distribution and the other to the impact parameter distribution. The comparison of both results has been used to measure the value of the average b hadron energy $E = \sqrt{(m^2 + p^2)}$.

The τ_b value was obtained from a binned χ^2 fit to the respective distributions, with the lifetime dependent expected distribution predicted by a Monte Carlo simulation [79, 80]. The lifetime dependence was introduced by reweighting the

simulated events according to

$$\left(\frac{\tau_{MC}}{\tau_b}\right)^2 \frac{e^{-t_1/\tau_b}}{e^{-t_1/\tau_{MC}}} \frac{e^{-t_2/\tau_b}}{e^{-t_2/\tau_{MC}}} \ . \tag{5.1}$$

Here t_1 and t_2 are the proper decay times of the weakly decaying b hadrons in jet 1 and 2 and τ_{MC} is the lifetime value in the Monte Carlo, 1.55 ps. The one parameter lifetime fit is based on the assumption that all b hadrons have the same lifetime.

In order to allow small discrepancies in the resolution function between data and Monte Carlo additional resolution parameters were introduced. The Monte Carlo distribution was convoluted with two Gaussian functions with a standard deviation $s_{1,2}$ applied to a fraction $f_{1,2}$ of Monte Carlo events. The resolution correction parameters have been measured by the shape of the respective distributions on the negative side.

The background of fragmentation tracks attached to the secondary vertices constitutes another important source of uncertainty. Monte Carlo studies showed that this background fraction is dependent on the average b decay charged multiplicity $\langle n_b \rangle$ [1].

Secondary vertices far from the primary event vertex tend to include one or two tracks from decays of longlived strange hadrons, mainly K_s^0 and Λ decays. In the following $\langle n_K \rangle$ denotes the fraction of K_s^0 and Λ hadrons produced in Z decays.

In order to make the measurement of the b lifetime independent of the described parameters, the resolution correction parameters $f_{1,2}, s_{1,2}$, the average b decay multiplicity $\langle n_b \rangle$ and the fraction of longlived hadrons $\langle n_K \rangle$ were fitted together with τ_b. A binned χ^2 fit has been performed to the multiplicity distribution, to the impact parameter distribution and to the decay length distribution. The expression for χ^2 was defined as:

$$\chi^2 = \sum_{i=1}^{n} \frac{(N^i_{data} - N^i_{MC}(\tau_b; \vec{f}_{int}, \vec{f}_{res}))^2}{(\Delta N^i_{data})^2 + (\Delta N^i_{MC}(\tau_b; \vec{f}_{int}, \vec{f}_{res}))^2} \qquad \text{i} = 1, \cdots, \text{n bins} \ , \tag{5.2}$$

where $\vec{f}_{int} = (\langle n_b \rangle, \langle n_K \rangle)$ and $\vec{f}_{res} = (f_1, s_1, f_2, s_2)$ stand for the intrinsic MC parameters and the resolution correction parameters, respectively. N^i_{data}, N^i_{MC} denote the entries in the i-th bin of the fitted distribution and ΔN^i_{data}, ΔN^i_{MC} are the statistical errors.

5.2 Monte Carlo simulation of bottom hadrons

The simulation of b hadrons includes two main steps: the production of b hadrons and their subsequent decays.

[1] The definition used here includes only the direct decay products pions, kaons, leptons and protons. Tracks from decays of K^0 and Λ's are not included.

5.2.1 Bottom quark fragmentation

A reliable model of the quark to hadron transition following the $Z \to b\overline{b}$ decay is of primary importance for identifying bottom hadrons and measuring their lifetime. The description of the first stage of the hard gluon radiation of the primordial partons is based on the JETSET parton shower approach [79]. The parton shower approach is a QCD calculation where instead of the full matrix-element expressions only approximations simplifying the kinematics and the helicity structure are used. The calculation is performed as a summation of leading logarithms and is suitable formulated for a Monte Carlo event simulation: the evolution of the parton shower cascade is looked upon as an arbitrary number of branchings of one parton into two or more. There is no upper limit on the number of partons. Thus it provides a good description of the multijet structure of hadronic events. The probabilities for parton branchings are described by the Altarelli-Parisi equation [89]. A typical property of heavy quarks in the gluon radiation phase is the suppression of high energy losses leaving more energy to the leading particle than in light quark jets.

An often applied description of the subsequent fragmentation process is the scheme of the string fragmentation (SF), which is also used in this analysis within the framework of the JETSET program [79]. The physical picture is that of a colour flux tube stretched between $q\overline{q}$ pairs produced in e^+e^- collisions. The QCD confinement mechanism is implemented by a linear increase of potential energy stored in the string if the quarks move apart until the string breaks by the production of new $q\overline{q}$ pairs. The string break-ups will proceed until only colourless and on-mass-shell hadrons remain. For the sharing of energy and momentum at each step the SF model employs a probability distribution $f(z)$, called fragmentation function, wherein z is the fraction of the quark energy retained in the hadron, $z = (E + p_{\|})_{hadron}/(E + p_{\|})_{quark}$.

For the light quarks (u,d,s) the Field-Feynman parametrization [90]

$$f(z) = 1 - a + 3a(1 - z)^2 \tag{5.3}$$

is commonly used with $a = 0.77$. In contrast to light-quark hadronization, the fragmentation of heavy quarks is hard because heavy quarks are only softly deaccelerated by taking up light quarks. Hard fragmentation for b and c quarks has been observed in many experiments [5]. An often used parametrization is the one of Peterson et al. [91]:

$$f(z) = \frac{1}{z}\left(1 - \frac{1}{z} - \frac{\epsilon_q^2}{1 - z}\right)^{-2} . \tag{5.4}$$

Here ϵ_q is a free parameter and its value is expected to decrease with increasing quark mass, i.e. $\epsilon_q \propto 1/m_q^2$.

The LEP experiments have measured the mean b hadron energy, scaled by the beam energy $\sqrt{s}/2$, and obtained [92]:

$$\langle x_E \rangle_b = \frac{2E_{b-hadron}}{\sqrt{s}} = 0.702 \pm 0.008 , \tag{5.5}$$

which can be compared with $\langle x_E \rangle$ for c quarks [92]:

$$\langle x_E \rangle_c = 0.484 \pm 0.008 \; . \tag{5.6}$$

Other parameters of the hadronic event structure that affect the analysis of this thesis have been tuned on the values measured by L3. A description of the determination of QCD model parameters is given in reference [93].

5.2.2 Simulation of b hadron decays

The production of hadron flavours within the JETSET Monte Carlo program [79] is monitored by parameters that control the production probability of quark-antiquark pairs $q\overline{q}$ and diquark pairs qq and their respective flavour content $u : d : s : c \sim 1 : 1 : 0.3 : 10^{-11}$. A reliable description for the production of all hadron flavours, and in particular of b hadron flavours, has been obtained with these tuned parameters defined at the quark level. The production of different b hadron spin states (B, B^*) is based on simple spin counting arguments, namely $B : B^* \sim 1 : 3$, which is in agreement with present experimental data [94].

The simulation of b hadron decays is done in two steps. First, the flavour content of the final state is selected and second, the kinematic distribution of the final state particles in the phase space is generated. For the "main" bottom hadrons, B^+ and B^0, several branching ratios are already known. These are the semileptonic branching ratios $\mathcal{B}(B^0 \rightarrow D^- l\, \bar{\nu}) = (1.9 \pm 0.5)$ % and $\mathcal{B}(B^0 \rightarrow D^{*-} l\, \bar{\nu}) = (4.6 \pm 0.3)$ % with $l = e, \mu$ [5], measured at the $\Upsilon(4S)$ resonance. A comparison of these values with the inclusive semileptonic branching ratio (see chapter 8) yields the semileptonic D^{**} production rate $\mathcal{B}(B^0 \rightarrow D^{*-} l\, \bar{\nu}) = (3.9 \pm 0.7)$ %. The L3 experiment has measured the total semileptonic branching ratio $\mathcal{B}(b \rightarrow \nu X) = (23.1 \pm 1.5)$ % [95] from which the branching ratio into τ leptons $\mathcal{B}(b \rightarrow \tau \nu X) = (1.7 \pm 1.2)$ % has been derived.

In addition branching ratios of a few two-body decays have been measured recently. The observed channels, as for instance $B^0 \rightarrow D^-\pi^+, D^-\rho^+, D^{*-}D_s^+$, contribute a total branching ratio of $\sim 13\%$ of all b hadron decays [5].

The rest of the decay modes ($\sim 64\%$) is generated using a simple flavour combination scheme relying on the spectator model. The flavour content of the final state is made up of the quarks coming from the weak decay of the c quark, the spectator quark and the $q\overline{q}$ pairs generated in the same way as in the fragmentation. The final state multiplicity is selected according to a distribution that depends on the hadron mass only. The reliability of this multiplicity distribution has been tested by a L3 measurement [96] of the particle multiplicities of identified semileptonic and hadronic b jets. The observed multiplicity differences between these jets have been attributed to the multiplicity of the W^* hadronic current in b decays. The results have been found to be in agreement with the JETSET hadronization model. In particular the mass dependence of the average W^* hadronic multiplicity has been verified in comparison with τ decays.

In the second step of the simulation, the kinematic distribution of the final state particles in the phase space, the V-A structure of the charged weak current has to be taken into account. In b decays the V-A matrix element is relevant for the leptonic weak current $W^* \to l\,\bar{\nu}$ *and* for the hadronic $b \to c\,W^*$ transition. The polarization of the W^* emitted in the $b \to c$ transition has been observed by the measured momentum spectra of charged leptons and neutrinos [20, 21]. These measurements show that the V-A structure of quark matrix elements is retained in transitions among heavy hadrons. The MC simulation reflects this particular b decay property by a distribution of the charm decay product according to the V-A matrix element.

5.2.3 Determination of model parameters

The allowed range of the model parameters in the simulation of heavy quark decays has been chosen according to the results of the LEP Electroweak Working Group [17, 92], the Particle Data Group [5], and, in some cases, was directly fitted from the L3 data. The number of heavy quark events among all hadronic events was normalized according to the LEP measurements of R_b and R_c [17]. The best estimation of the mean value of the Peterson fragmentation function $\langle x_E \rangle_b$, of the average b decay multiplicity $\langle n_b \rangle$ and of the average fraction of longlived hadrons $\langle n_K \rangle$ has been obtained from fits to the L3 data. The effective charm decay length has been determined according to the values given by the Particle Data Group and the LEP Electroweak Working Group. The charm lifetimes $\tau(D^0), \tau(D^+), \tau(D_s), \tau(\Lambda_c)$ were taken from the Particle Data Group [5]. The production of charm hadron species in $c\overline{c}$ events was described by the values from the LEP Electroweak Working Group [92]. For the composition of charm hadrons produced in b decays the values of the Particle Data Group [5] have been used. A summary of all parameter ranges is given in table 5.1.

The estimation of the average b decay multiplicity $\langle n_b \rangle$ was, to a large extent, independent of the lifetime measurement. The number of tracks at the secondary vertices was a free parameter in the vertex fit within the constraint of a minimum of three tracks. The average multiplicity observed at the secondary vertices followed the original b decay multiplicity $\langle n_b \rangle$. The sensitivity to $\langle n_b \rangle$ was optimized by a fit performed as a function of the decay length. The fit result is shown in fig. 5.1. The peak at zero decay length was due to light quark events. The enhancement at positive decay lengths was caused by b and c events and its magnitude served as a measure of $\langle n_b \rangle$. The fitted value,

$$\langle n_b \rangle = 4.90 \pm 0.04 \;, \tag{5.7}$$

is in agreement with other measurements [97]. The quoted error is the statistical uncertainty. The correlation with the τ_b measurement is negligible within a τ_b variation of less than 50 fs, a value that is large compared to the final uncertainty of the τ_b measurement of 20 fs.

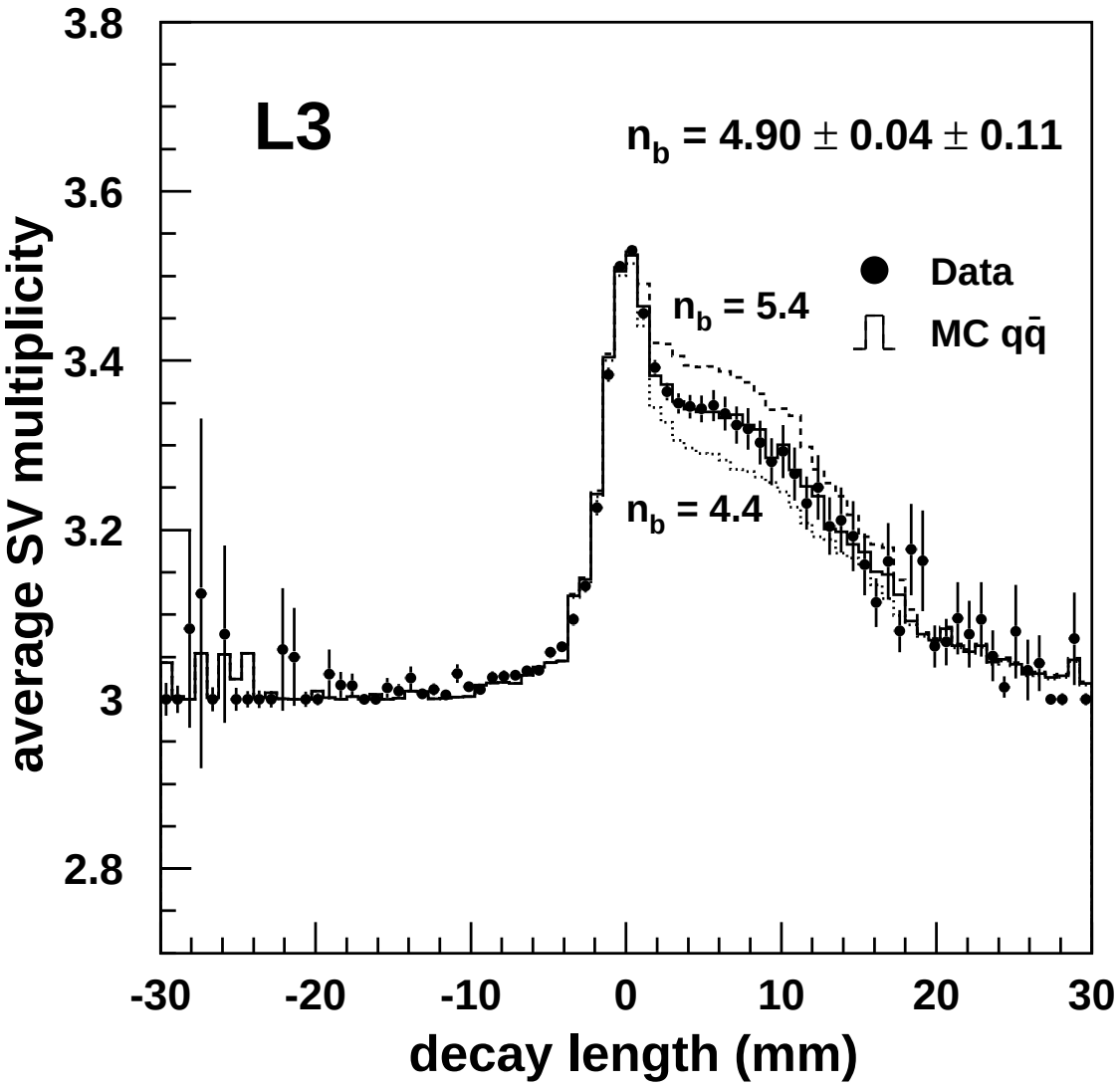

Figure 5.1: Average multiplicity of tracks at the secondary vertices as a function of the decay length. The points represent the 1994 data and the histogram shows the MC distribution for the fitted b decay multiplicity $\langle n_b \rangle = 4.90$.

Parameter	Allowed range	Comment
R_b	0.2179 ± 0.0012	LEP
R_c	0.1715 ± 0.0056	LEP
$\langle x_E \rangle_b$	0.710 ± 0.004	fitted
$\langle x_E \rangle_c$	0.484 ± 0.008	LEP
$\langle n_b \rangle$	4.90 ± 0.12	fitted
$\langle n_K \rangle$	1.29 ± 0.02	fitted
D^0 lifetime	(0.415 ± 0.004) ps	PDG
D^+ lifetime	(1.057 ± 0.015) ps	PDG
D_s lifetime	(0.467 ± 0.017) ps	PDG
Λ_c lifetime	(0.206 ± 0.012) ps	PDG
D^+ fraction in $c\overline{c}$ events	0.233 ± 0.028	LEP
D^0 fraction in $c\overline{c}$ events	0.102 ± 0.037	LEP
c baryon fraction in $c\overline{c}$ events	0.065 ± 0.029	LEP
$\mathcal{B}(B^{0,+} \to D^+ X)$	0.242 ± 0.033	PDG
$\mathcal{B}(B^{0,+} \to D_s X)$	0.086 ± 0.016	PDG
$\mathcal{B}(B_s \to D_s X)$	0.87 ± 0.31	PDG

Table 5.1: Table of allowed ranges of the model parameters. The comments "LEP" and "PDG" stand for the proposed ranges of the LEP Electroweak Working Group [17, 92] and the Particle Data Group [5], respectively. The entries are marked by "fitted" if the parameters were determined by the analysis of this thesis.

5.3 Decay length method

A fit of the decay length distribution was performed using the data sample collected by L3 in the years 1994 and 1995. The fit included 890,506 secondary vertices. The result is:

$$\tau_b = (1582 \pm 10) \text{ fs} . \tag{5.8}$$

The error represents only the statistical uncertainty. The systematic error will be investigated later. The fitted range of the background parameters is summarized in table 5.2. The decay length distribution for the fitted parameters is shown in fig. 5.2. Agreement between data and MC is observed and the positive tail due to b decays is clearly visible.

An improvement of the statistical accuracy was achieved by a better separation of $b\overline{b}$ and background events. The pair-production of b quarks was exploited here. The events were divided into two categories depending upon the value of the decay distance in the opposite jet. The samples were obtained by requiring the decay distance in the opposite jet greater or smaller than a certain value, respectively. The cut value was chosen at a decay distance of 2 mm. This separated the reconstructed decays into a b enriched sample of 164,451 vertices and a background enriched sample of 726,055 vertices. Both distributions were fitted simultaneously.

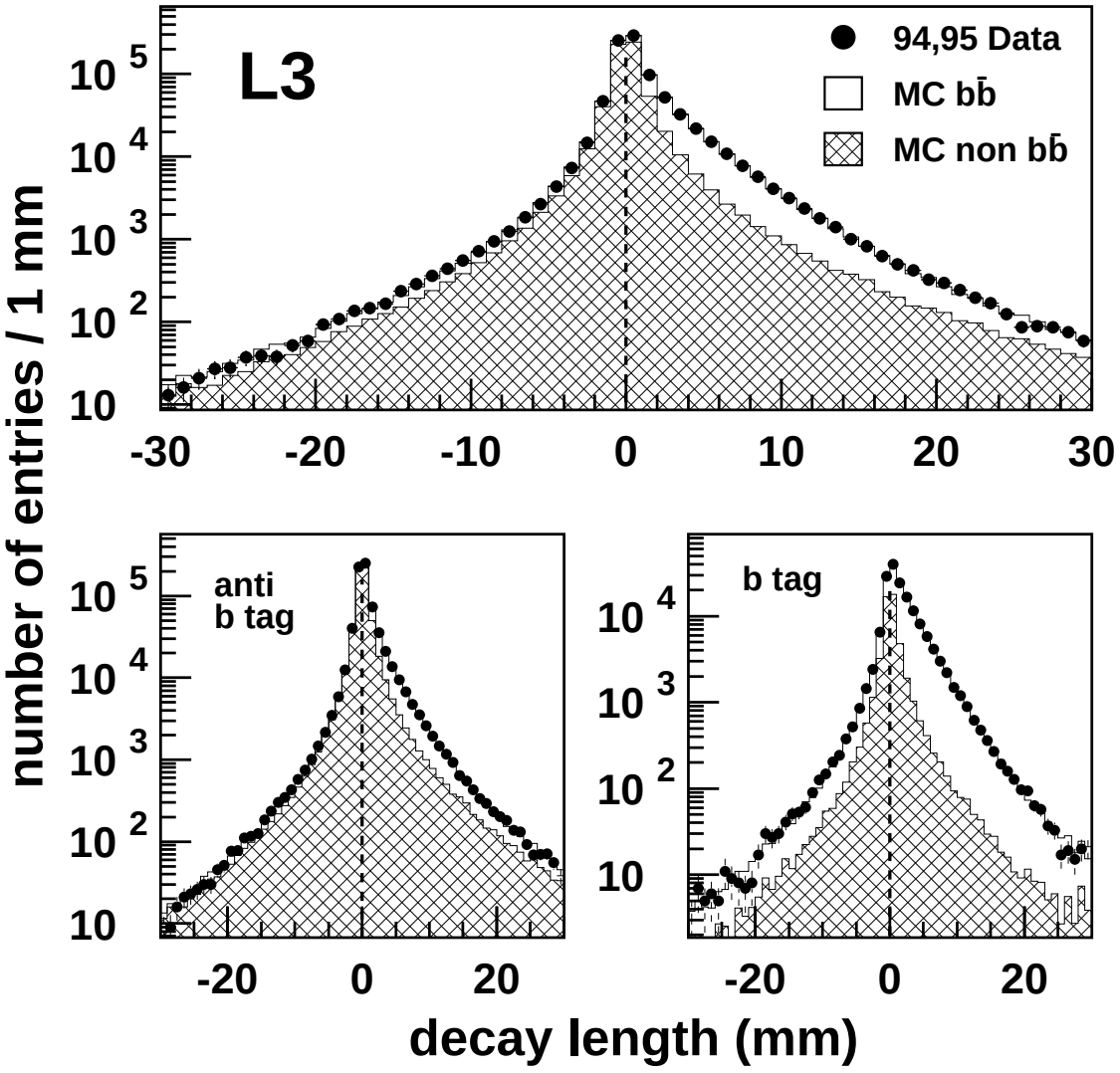

Figure 5.2: Decay length distribution of reconstructed secondary vertices. The points represent the data of the years 1994 and 1995 and the histogram shows the MC distribution for the fitted lifetime. The upper row contains the total data sample. The lower row shows two subsamples that pass an anti-b tag (left) and a b tag (right), respectively.

Background fit parameter	Fit result
f_1	0.93 ± 0.07
s_1	0.27 ± 0.02
f_2	0.0053 ± 0.0008
s_2	28.3 ± 2.6
$\langle n_K \rangle$	1.33 ± 0.05

Table 5.2: Fit results for the background parameters in the decay length fit. The widths s_1, s_2 of the Gaussian smearing are given in units of the estimated errors.

In this way b and non-b events contributing to the same bin of the decay length distribution were accounted for with different statistical weights in the fit.

In order to avoid a systematic uncertainty due to the b normalization in both subsamples an additional fit parameter f_b was introduced. It described the fraction of b events in the b enriched subsample. The total number of b events was constrained to the MC value as in the previous fit to the single distribution.

The combined fit to both subsamples yielded:

$$\begin{aligned} \tau_b &= (1584 \pm 8)\,\text{fs}\,, \\ f_b &= 0.693 \pm 0.003\,. \end{aligned} \tag{5.9}$$

The respective distributions are shown in fig. 5.2. The fitted value for f_b is in agreement with the b fraction in the MC of 0.692 ± 0.001. The results for the background parameters are the same as in table 5.2.

5.4 Impact parameter method

Similar fits as described in the previous section have been performed to the average impact parameter distribution. The average impact parameter was defined as the error-weighted average of the impact parameters of all tracks per secondary vertex. The reference point for the impact parameters was the estimated primary vertex. The τ_b fit result obtained from the single-jet impact parameter distribution in the 1994/95 data sample is:

$$\tau_b = (1562 \pm 8)\,\text{fs}\,. \tag{5.10}$$

The error represents the statistical uncertainty. The background parameters are listed in tab. 5.3. The distribution is visualized in fig. 5.3.

The fit was repeated with the same subsamples as defined in the previous section using a cut on the decay length in the opposite jet. As before for the decay length distribution, the lifetime τ_b, the normalization fraction f_b and the background parameters have been fitted. The values are:

$$\begin{aligned} \tau_b &= (1563 \pm 7)\,\text{fs}\,, \\ f_b &= 0.691 \pm 0.003\,. \end{aligned} \tag{5.11}$$

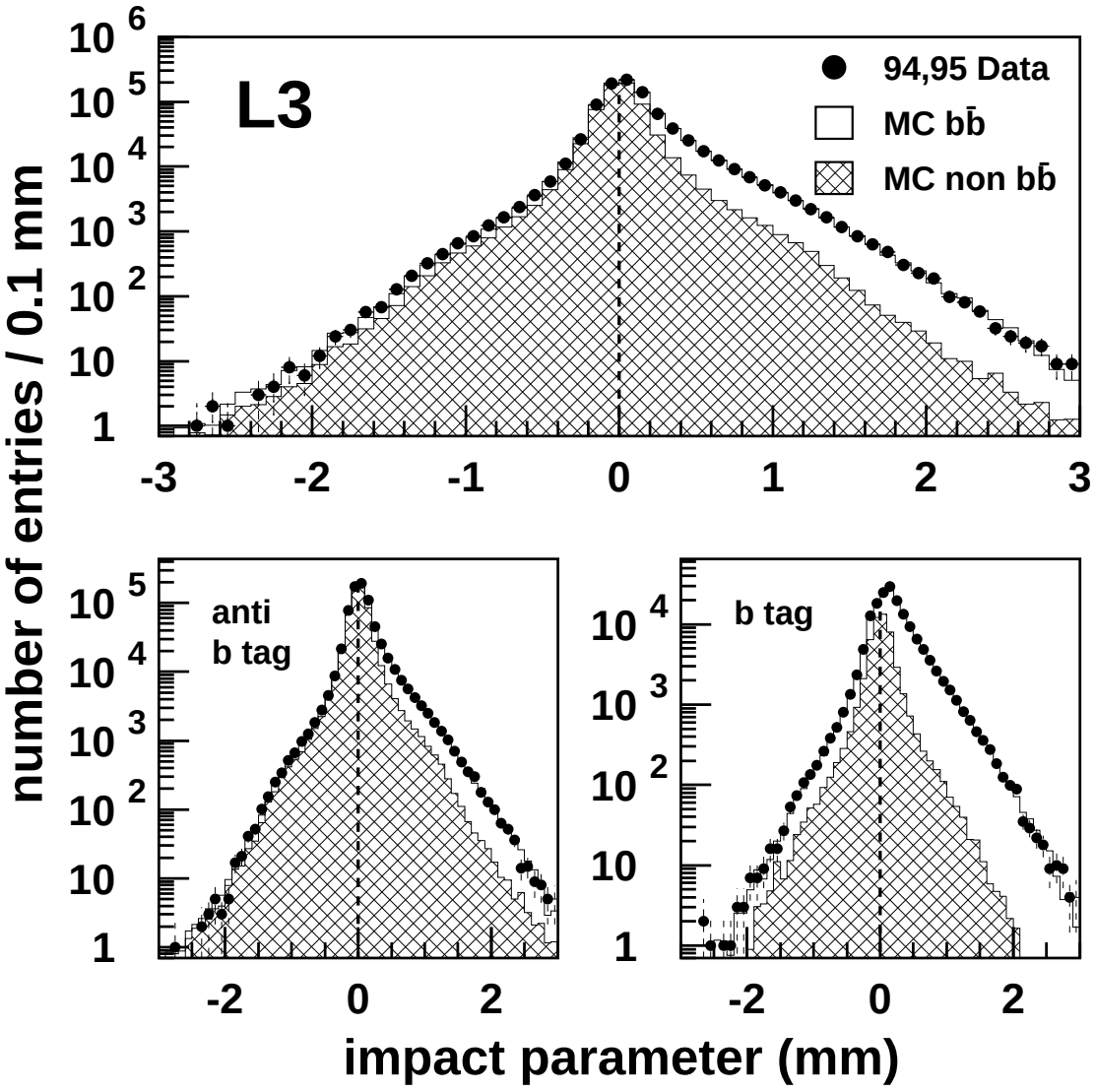

Figure 5.3: Average impact parameter distribution of tracks from secondary vertices. The points represent the data of the years 1994 and 1995 and the histogram shows the MC distribution for the fitted lifetime. The upper row contains the total data sample. The lower row shows two subsamples that pass an anti-b tag (left) and a b tag (right), respectively.

Background fit parameter	Fit result
f_1	0.65 ± 0.15
s_1	0.21 ± 0.04
f_2	0.024 ± 0.003
s_2	7.4 ± 0.6
$\langle n_K \rangle$	1.29 ± 0.02

Table 5.3: Fit results for the background parameters in the impact parameter fit. The widths s_1, s_2 of the Gaussian smearing are given in units of the estimated errors.

The graphical representations are given in fig. 5.3. The values of the background parameters were found unchanged compared to the ones in table 5.3.

5.5 Systematic uncertainties and cross checks

This section explains how the systematic uncertainties of the τ_b value have been determined. It further describes which cross checks have been performed in order to establish the validity of the lifetime fit.

Two classes of systematic uncertainties were considered. The first class treats systematic effects inherent to the measurement method. The important uncertainties of the detector performance were:

1. Uncertainties of the L3 tracking detectors.
2. Uncertainties of the LEP beam position.

The second class is related to physics assumptions and approximations which affect the lifetime measurement:

1. Production of b and c quarks.
2. Heavy quark fragmentation.
3. Decays of b and c hadrons.

These error sources shall now be treated in detail. The general procedure for the error estimation of τ_b was the following. A certain parameter in the MC simulation was changed according to the uncertainty in this parameter. First, the multiplicity fit was repeated and second, the lifetime fit was performed with the MC adjusted to the new $\langle n_b \rangle$ value. The change in the τ_b result was attributed to a systematic uncertainty of the τ_b measurement. The errors on the τ_b value are described in the text, the errors on the $\langle n_b \rangle$ value are not mentioned in the text but are given in table 5.4.

5.5.1 Detector uncertainties

The uncertainties of measurements in the L3 tracking detectors concern the efficiency of the track reconstruction and the resolution.

The agreement between data and Monte Carlo in the average number of quality tracks per event was better than 0.1 tracks. In particular the angular dependence of the average number of quality tracks was compared between data and Monte Carlo. Agreement was observed in the azimuthal angular dependence but small deviations have been seen in the polar angular dependence. Reweighting the MC sample to the observed track multiplicity resulted in a change of τ_b by 2 fs for the decay length method and by 5 fs for the impact parameter method.

The uncertainty in the resolution function has been estimated by varying the resolution correction parameters within the errors taking into account their respective correlations. The error on τ_b was 5 fs for both methods.

Systematic effects of the TEC calibration were estimated by repeating the lifetime fit switching off the local corrections applied to the track impact parameters. The fit results with and without the correction have been compared in a selected subsample. The difference of 3 fs in the τ_b value was counted as the systematic error from the TEC calibration. In addition the error was considered to include the uncertainty from local SMD calibration uncertainties which have been found to be very small [74].

The definition of the sign of the decay length depended on the jet direction. The resolution on the jet direction was estimated from comparisons between data and Monte Carlo on a two jet event sample. The maximum discrepancy found was 2 mrad. Reweighting the MC events according to the jet direction resolution yielded a shift in τ_b of 5 fs.

The uncertainty in the knowledge of the beam spot size and position was determined by varying the size of the beam spot within the accuracy of the 200-event-vertex (15 μm in x and 10 μm in y) and introducing a bias of 10 μm in x and 5 μm in y for the central beam position. The MC decay length and impact parameter distributions were reweighted according to the new beam location and uncertainty, yielding a change in the lifetime of 7, respectively 6 fs.

The uncertainties from the detector performance add up to a total uncertainty in τ_b of 11 fs, for both the decay length and the impact parameter method.

5.5.2 Uncertainties from modeling of heavy quarks

The precision of the lifetime measurement was further limited due to heavy-quark physics modeling. The dominant contributions arise from the uncertainty in the inclusive description of b decays. Theoretical uncertainties have been estimated by a variation of the model parameters as recommended by the LEP Heavy Flavour Electroweak Group in [17, 92].

The uncertainty in the production fraction R_b of b hadrons in hadronic Z decays was conservatively estimated from the difference between the LEP average [17] and the SM value. Its effect on τ_b was found to be small, 4 fs. The uncertainty from R_c, varied within the LEP uncertainty [17] was found to be 1 fs.

Systematic errors due to b and c fragmentation were determined by varying ϵ_b and ϵ_c in the Peterson fragmentation function [91] according to $\langle x_E \rangle_b = 0.702 \pm 0.008$ for b fragmentation and $\langle x_E \rangle_c = 0.484 \pm 0.008$ for c fragmentation [92]. The value of ϵ in the fragmentation function is directly related to the fraction x_E of the beam energy carried by the b or c hadron. Reweighting functions were calculated which parametrize the 1σ difference to the central x_E values according to the Peterson fragmentation function. For the b fragmentation the reweighting functions are shown in fig. 5.4. The uncertainty in τ_b from b fragmentation was estimated at 30 fs and 9 fs for the decay length and impact parameter measurement, respectively. In case of the decay length measurement the uncertainty of 30 fs dominated the total systematic error. The use of the impact parameter measurement enabled an important reduction of the systematic uncertainty.

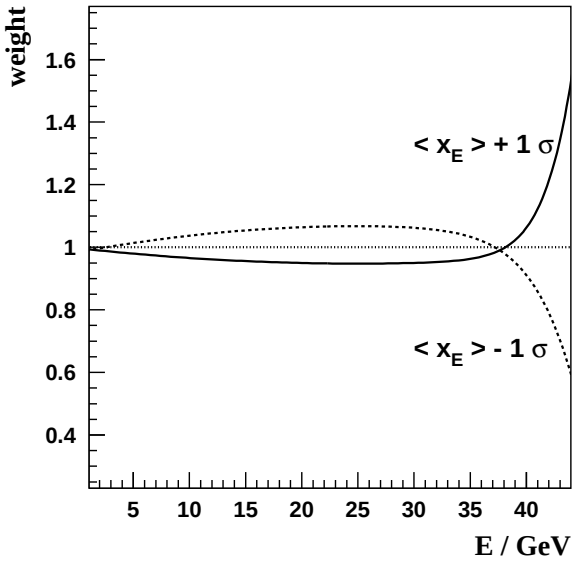

Figure 5.4: Reweighting functions in dependence of the b hadron energy.

The b fragmentation error has also a contribution due to the uncertainty in the shape of the fragmentation function. Several models [98] were tuned on the mean value $\langle x_E \rangle_b = 0.702$ and the maximum shift in the lifetime found was 2 fs. The fragmentation functions of the different models in comparison with the Peterson function are shown in fig. 5.5.

The error from the uncertainty in c fragmentation has been estimated to be 2 fs for the decay length and less than 1 fs for the impact parameter measurement.

An uncertainty in the shape of the b decay multiplicity distribution was taken into account by replacing the Monte Carlo distribution with a binomial distribution of the same mean and variance as in the Monte Carlo. The b decay multiplicity fit was repeated and shifted $\langle n_b \rangle$ by 0.06 and τ_b by 4 fs.

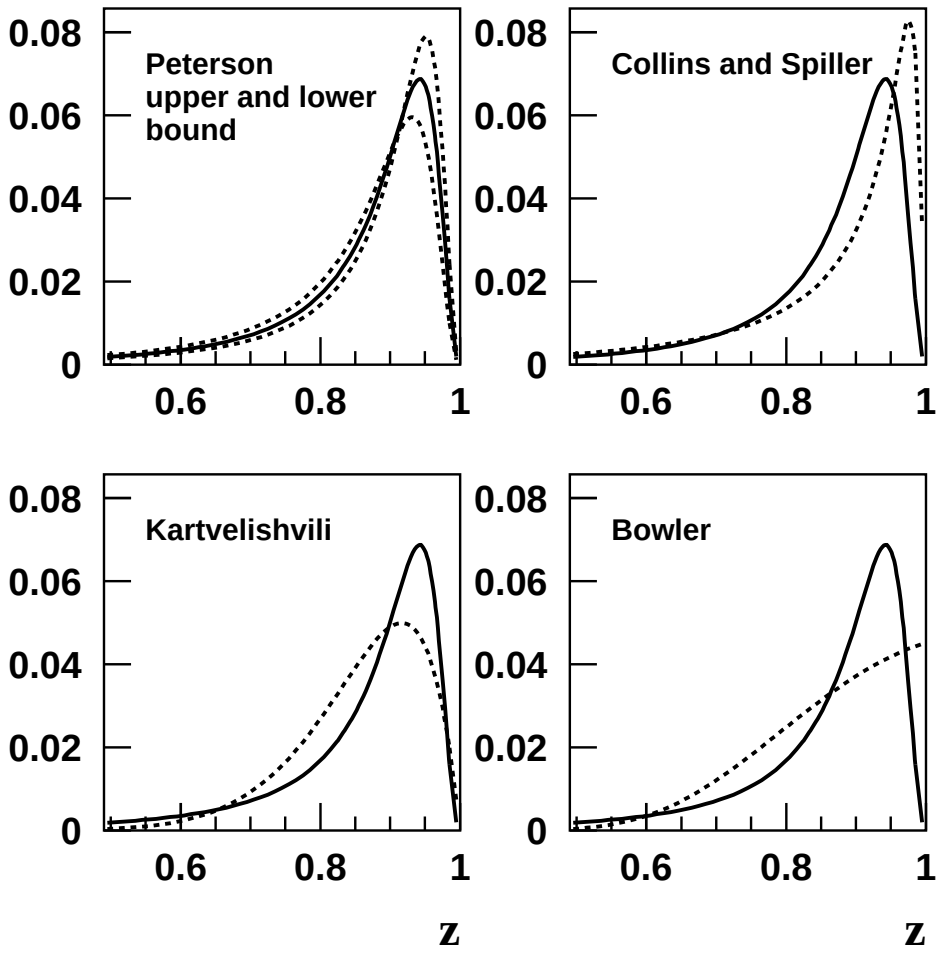

Figure 5.5: Fragmentation functions in different models for the same value of the average b hadron energy of $\langle x_E \rangle_b = 0.702$.

Sensitivity to the modeling of c quarks, occurring as primary $c\overline{c}$ events and as decay products of b hadrons, was estimated by varying the lifetimes of c hadrons and the fraction of c hadrons in $c\overline{c}$ events and b decays. The production of the different D mesons and Λ_c baryons in $c\overline{c}$ events was varied according the LEP averages [92] and the branching fractions $\mathcal{B}(B^{0,+} \to D^+ X)$, $\mathcal{B}(B^{0,+} \to D_s X)$ and $\mathcal{B}(B_s \to D_s X)$ as well as the lifetimes of c hadrons were varied following the world averages [5].

The total error in τ_b due to modeling of b and c events is 32 fs for the decay length and 16 fs for the impact parameter measurement. The contributions to the systematic error in the b lifetime measurement are summarized in table 5.4. The table also shows the corresponding systematic errors in the average b multiplicity $\langle n_b \rangle$. The final result on $\langle n_b \rangle$ is:

$$\langle n_b \rangle = 4.90 \pm 0.04 \pm 0.11\,, \tag{5.12}$$

where the first error describes the statistical uncertainty and the second error the systematic uncertainty.

Error source	$\Delta\tau_b^{DL}$ (fs)	$\Delta\tau_b^{IP}$ (fs)	Δn_b
Detector Uncertainties	11	11	0.08
Quality track multiplicity	2	5	0.04
Resolution function	5	5	0.07
TEC calibration and SMD alignment	3	3	<0.01
Beam spot size and position	7	6	<0.01
Jet direction resolution	5	5	<0.01
Heavy Quark Physics Modeling	32	16	0.08
R_b	4	4	0.02
R_c	2	2	0.01
b fragmentation	30	9	0.02
c fragmentation	2	<1	<0.01
b decay multiplicity distribution	4	4	0.06
D fraction in $c\bar{c}$ events	2	3	<0.01
D content in b decays	10	11	0.04
D lifetimes	2	3	<0.01

Table 5.4: Systematic errors in the measurement of τ_b. The first column shows the errors for the decay length method, the second for the impact parameter method. The corresponding errors in the b decay multiplicity $\langle n_b \rangle$ are given in the third column.

5.5.3 Cross checks

The detector performance has been studied by looking for variations in the measured lifetime between different detector parts. The total data sample was divided into four azimuthal and two polar sections of the detector. No systematic dependence on the azimuthal angle and the forward/backward region could be inferred. In order to check possible influence of the TEC calibration the lifetime has been measured in subsamples of the local angle relative to the TEC wires. The variations

did not exceed the statistical fluctuations. The dependence of the fit results on the b decay multiplicity distribution has been cross checked by changing the weight given to the entries in the fit according to the measured multiplicity at the secondary vertices. The decay length and impact parameter distributions have been reweighted by n_{SV}, where n_{SV} was the secondary vertex multiplicity. The change in τ_b was 5 fs for the decay length and 4 fs for the impact parameter measurement. These changes have been attributed to the different statistical composition of the samples and no additional error was assigned to τ_b. A graphical presentation of the cross checks results is shown in fig. 5.6.

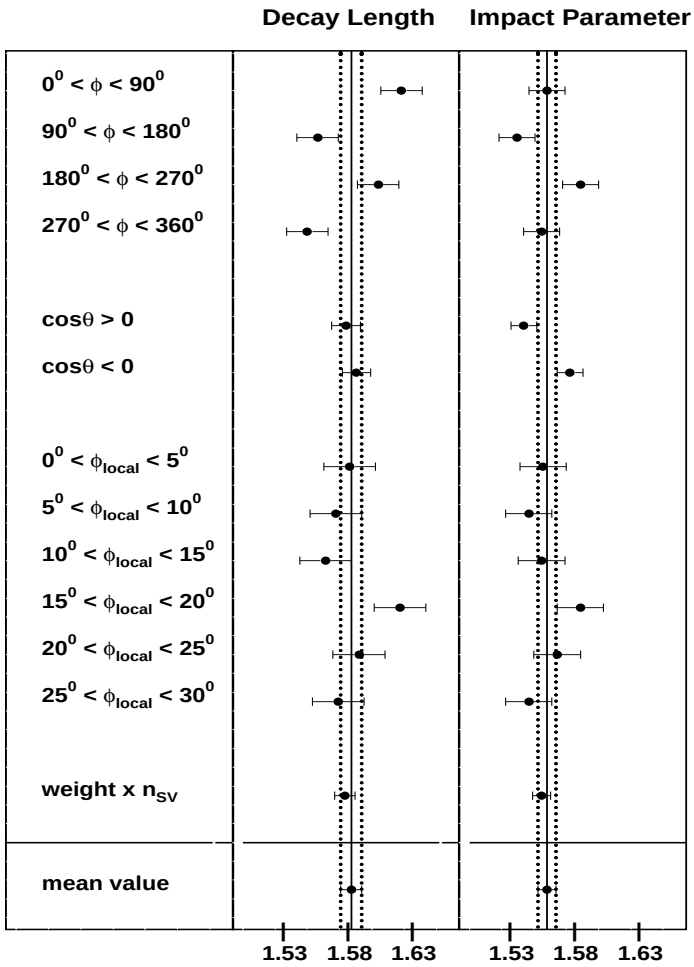

Figure 5.6: Fitted lifetime values and their statistical errors obtained from the cross checks described in the text.

5.6 Combination of decay length and impact parameter results

The decay length and impact parameter measurements are within their different sensitivities to the b fragmentation consistent with each other. Both results were combined by a simultaneous determination of the average lifetime τ_b and the average b hadron energy $\langle x_E \rangle_b$. The combination was performed on the basis that a certain value of $\langle x_E \rangle_b$ exists for which both lifetime measurements deliver identical τ_b values.

A linear dependence of the fit results τ_i (i=1,2) on $\langle x_E \rangle_b$ was assumed: $\tau_i = \tau_i^0 + a_i \, \Delta\langle x_E \rangle_b$. The values τ_i^0 are the fit results obtained at the LEP value for the b hadron energy of $\langle x_E \rangle_b^0 = 0.702$. These are $\tau_1^0 = 1.584$ ps for the decay length measurement and $\tau_2^0 = 1.563$ ps for the impact parameter measurement. The difference between the $\langle x_E \rangle_b$ value obtained from this thesis and the LEP value is denoted by $\Delta\langle x_E \rangle_b = (\langle x_E \rangle_b - \langle x_E \rangle_b^0)$. The coefficients a_i were determined from the MC ($a_1 = -3.750$ ps for the decay length measurement and $a_2 = -1.125$ ps for the impact parameter measurement).

The χ^2 function is given by:

$$\chi^2(\tau_b, \langle x_E \rangle_b) = (\, \tau_1 - \tau_b \, , \, \tau_2 - \tau_b \,) \begin{pmatrix} V_{11} & V_{12} \\ V_{12} & V_{22} \end{pmatrix}^{-1} \begin{pmatrix} \tau_1 - \tau_b \\ \tau_2 - \tau_b \end{pmatrix} . \qquad (5.13)$$

The matrix V in the definition of χ^2 is the covariance matrix of the decay length and impact parameter measurement. The diagonal elements V_{11} and V_{22} have been obtained from the total lifetime error from which the uncertainty from $\langle x_E \rangle_b$ was subtracted in quadrature. The correlation $\rho = [V_{12}/(V_{11}V_{22})]^{1/2}$ between the impact parameter and the decay length measurement in the remaining uncertainties has been estimated to $\rho = 0.87$, where the statistical errors alone were found to be correlated with $\rho = 0.63$ and the systematic errors were fully correlated. The statistical correlation is mainly determined by the spread in the fragmentation function. The narrower the shape of the fragmentation function is the stronger the statistical correlation.

The χ^2 fit result is:

$$\begin{aligned} \tau_b &= (1554 \pm 7 \pm 17) \text{ fs} \, , \\ \langle x_E \rangle_b &= 0.710 \pm 0.004 \, . \end{aligned}$$

The situation is illustrated in fig. 5.7. The first error of τ_b is statistical and the second error is the systematic uncertainty. The error on $\langle x_E \rangle_b$ contains both statistical and systematic uncertainties. The result for $\langle x_E \rangle_b$ is consistent with the LEP estimate [92] derived from lepton energy spectra. This measurement prefers a harder fragmentation with the central value placed at the 1σ upper level of the LEP range in $\langle x_E \rangle_b$. The uncertainty is significantly improved compared to the previous LEP estimate.

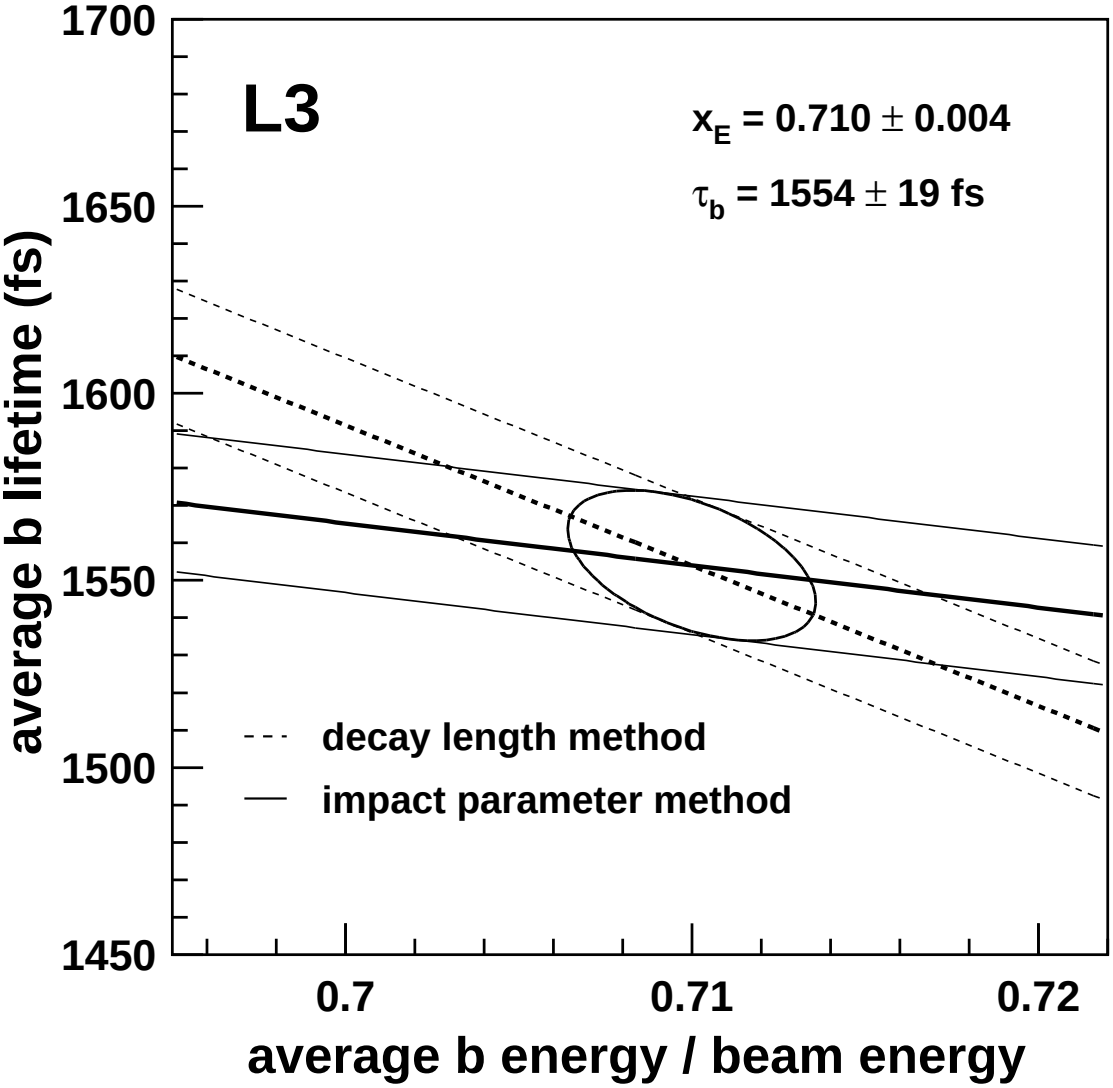

Figure 5.7: Comparison of impact parameter and decay length measurement. Both measurements are compatible with each other at an average b energy of $\langle x_E \rangle_b = 0.710 \pm 0.004$ (scaled to the beam energy) and a b lifetime of $\tau_b = 1554 \pm 19$ fs.

The contributions to the total systematic error of the b lifetime are similar to those in table 5.4, except the uncertainty due to the b fragmentation, which is reduced to 5 fs. By the combination of both methods the uncertainty from fragmentation is no longer the dominant systematic uncertainty. The greatest uncertainty in the value of τ_b arises from the uncertainty in inclusive branching ratios $B \to D\,X$ which affect the effective charm decay length.

I summarize again the value of the average b decay multiplicity:

$$\langle n_b \rangle = 4.90 \pm 0.04 \pm 0.11\,, \tag{5.14}$$

with the statistical and systematic uncertainty.

Chapter 6

Bottom hadron identification

It is the aim of this chapter to explain how a B_s flavour identification at LEP could be exploited in the best way for a measurement of the lifetime difference of a shortlived and a longlived B_s meson.

A certain procedure to enlarge the fraction of B_s mesons in the b sample up to a purity p may have an efficiency ϵ. Which minimum purity p is necessary for a given value of ϵ of this procedure to improve the accuracy of the $\Delta\Gamma/\Gamma$ measurement relative to the case without this procedure? Under the assumption that the uncertainty is dominated by the statistical error the answer is given by fig. 6.1. The line in fig. 6.1 represents the threshold above which the procedure gets efficient.

Which practical tools are known to identify B_s mesons with these required properties? First, a full reconstruction of final states of B_s decays is possible. However these exclusive decay channels have very small branching fractions of the order 10^{-4}. The first observation of the B_s meson and a measurement of its mass were obtained with fully reconstructed decays such as $B_s \to D_s^- \pi^+$ and $B_s \to J/\Psi\,\Phi$ [99]. The total number of reconstructed decays amounts to only a handful with the full LEP statistics on the Z resonance. Although these samples are almost free of background their event numbers are much too small to be used in a measurement of $\Delta\Gamma/\Gamma$.

A partial reconstruction of B_s mesons can be obtained from semileptonic decays $B_s \to D_s^{(*,**)}\, l\, \nu$ in which the D_s meson is fully reconstructed. Samples of typical 100 $D_s\, l$ events are obtained at LEP. However also these event numbers are still not competitive for the aim of a measurement of $\Delta\Gamma/\Gamma$ of B_s mesons.

The limitations of the discussed methods arise from the high value of the b quark mass opening many channels for its decay. Only a small branching ratio is taken by a specific final state configuration. In order to be free of limitations arising from exclusive or semiexclusive reconstructed B_s decays a more inclusive method is favoured in this thesis. This method makes use of the conservation of the electric charge in b decays. In principle, the charge can be measured in each b hadron final state and can be related to the initial b flavour. In this way charged

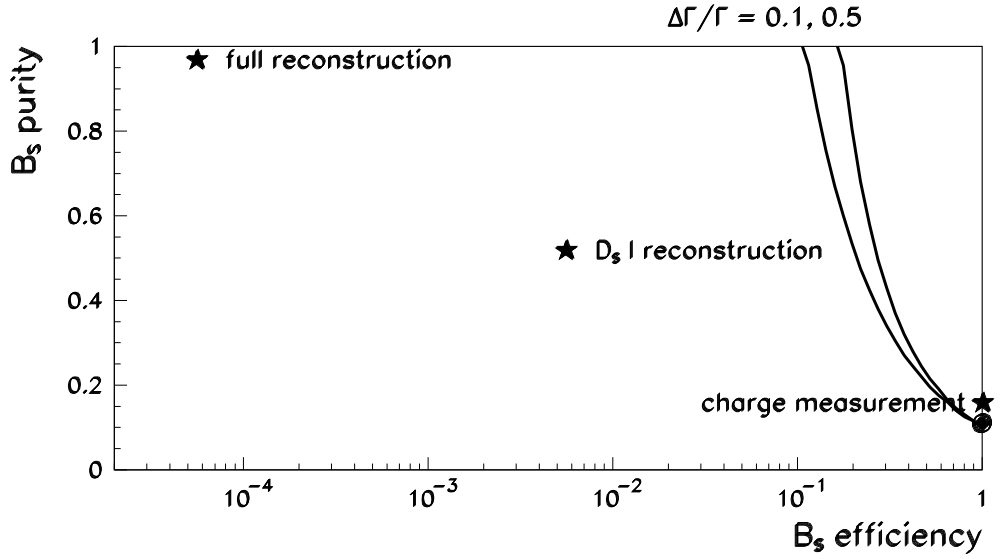

Figure 6.1: Lines of equal statistical accuracy in a measurement of $\Delta\Gamma/\Gamma$ of B_s mesons in the efficiency - purity plane. Two lines of equal accuracy are shown for two values of $\Delta\Gamma/\Gamma = 0.1$ and 0.5. The point of 100% B_s efficiency and 10% B_s purity corresponds to the intrinsic sensitivity without any b flavour recognition. For efficiency - purity values above the curve an improvement in the accuracy of $\Delta\Gamma/\Gamma$ is reached. The crosses indicate the regions that are achieved by a full B_s reconstruction, a partial D_s lepton reconstruction and a charge measurement.

and neutral b hadrons can be separated from each other. However the price of an increase in efficiency is the loss of purity. A maximum B_s purity of 17% can be reached in the limit of a perfect charge measurement.

The technical procedure for the flavour-dependent b lifetime fit is the following. The decay length values (and the impact parameter values, respectively) are sorted into two distinct distributions depending upon the value of the measured charge at the secondary vertices. One histogram contains the decay length values compatible with a unit charge at the secondary vertices and the other one those with zero charge. These distributions are fitted simultaneously using as free parameters the lifetimes of neutral and charged b hadrons and $\Delta\Gamma$ of B_s mesons. No distinction is made between the different types of neutral b hadrons, the neutral mesons B^0, B_s and the neutral baryon Λ_b.

6.1 Charge measurement in inclusive b decays

The conservation of charge implies that the sum of all charges of b decay particles is identical to the charge of the mother b hadron. The measurement of this sum of

charges reduces to a measurement of charge signs because all elementary particles have charges of -1, 0 or +1 in units of the proton charge. The charge sign is determined by the direction of the track curvature relative to the magnetic field. It can be measured with almost no uncertainty for particles with typical momenta of hadronic Z events. The uncertainty in the estimation of the b hadron charge arises from ambiguities in deciding whether a track comes from the primary event vertex or from the secondary decay vertex. A vertex charge Q_{vertex} has been defined as the sum of charges Q_i of all tracks $i = 1, \cdots, N_{SV}$ at a secondary vertex weighted by the probabilities ω_i that the tracks are from the secondary vertex:

$$Q_{vertex} = \sum_{i=1}^{N_{SV}} Q_i \, \omega_i \quad . \tag{6.1}$$

The probability ω_i is defined as

$$\omega_i = \frac{\exp(-\chi^2_{i,SV}/2)}{\exp(-\chi^2_{i,PV}/2) \; + \; \exp(-\chi^2_{i,SV}/2)} \tag{6.2}$$

with the χ^2_i contribution of the i-th track taken from equation (4.11) relative to the primary (PV) or secondary vertex (SV). Similar definitions have been already used by the DELPHI, OPAL and SLD Collaborations [100].

The b hadron charge can only be measured correctly if all charges of the decay particles are included in the sum. For that reason two quality samples of tracks have been distinguished. On the one side there were the tracks obeying the criteria of chapter 4 which were used for the calculation of the primary and secondary vertex positions. These tracks should contain SMD measurements. However for the calculation of the vertex charge Q_{vertex} all tracks have been used that satisfy the TEC chamber selection criteria independent of the presence of SMD hits.

The distribution of the (real) charge values Q_{vertex} is expected to show a peak at zero for B^0 mesons, at $+1$ for B^+ mesons and at -1 for B^- mesons. The uncertainties in the definition of the probabilities ω_i lead to overlapping tails. The distributions are shown in the left column of fig. 6.2.

The sign of the vertex charge distinguishes between B^+ and B^-. But it is not directly related to our purpose of a separation of charged and neutral B mesons. In consideration of the tails in fig. 6.2 a separation of a unit charge difference is rather difficult. Further information from the sign of Q_{vertex} can be derived from an independent knowledge of the flavour of the b quark contained in the b hadron, namely b or $\bar{b}$. A charged B meson containing a b ($\bar{b}$) quark is a B^- (B^+) meson, respectively. A variable to measure the b quark flavour in hadronic b decays is the jet charge [101].

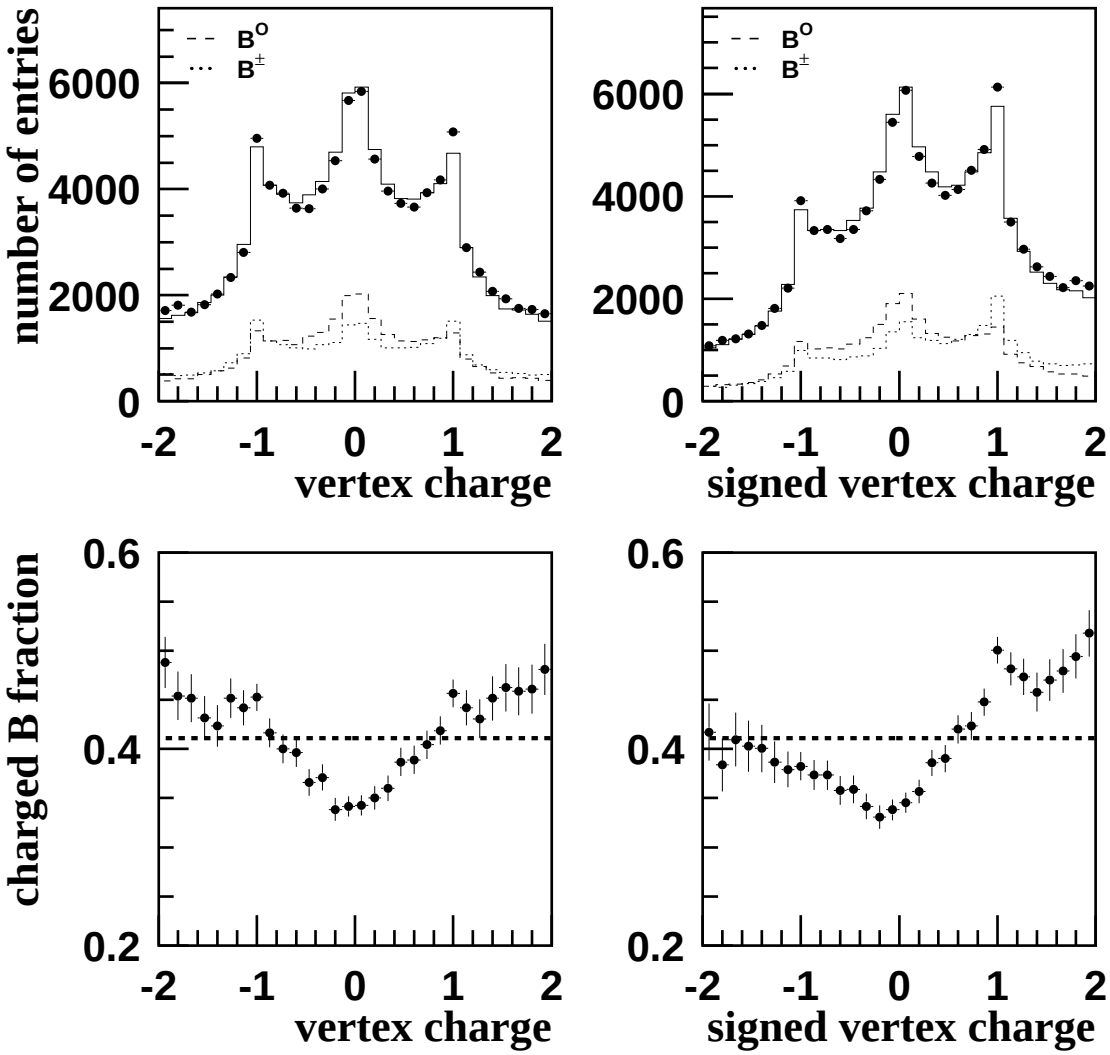

Figure 6.2: Vertex charge distributions in data (points) and MC (histogram). The distributions of the original vertex charge and the sign modified vertex charge are presented in the left and right column, respectively. The first row shows the total distributions in a comparison of data and MC. The B^0 contribution is shown by the dashed histogram and the $B^\pm$ contribution by the dotted histogram. An enrichment of b events was obtained by a cut on the decay length required to be greater than 2 mm. In the second row the fraction of charged B mesons in the b hadron MC sample is shown as a function of the respective vertex charge values. The line indicates the average fraction of charged B mesons.

The jet charge is defined as the sum of charges Q_i from all tracks $i = 1, \cdots, N_{jet}$ contained in a jet weighted by the normalized momentum component $p_{i\,||}$ parallel to the jet axis:

$$Q_{jet} = \frac{\sum_{i=1}^{N_{jet}} Q_i \, p_{i\,||}}{\sum_{i=1}^{N_{jet}} p_{i\,||}} \quad . \tag{6.3}$$

The vertex charge was modified by a sign defined with the jet charge. It is positive if the vertex charge and the jet charge have the same sign and negative if they have opposite signs:

$$Q_{vertex} \rightarrow Q_{vertex}^{signed} = sign(Q_{jet})\, Q_{vertex} \quad . \tag{6.4}$$

The distributions of the Q_{vertex}^{signed} values with the new sign definition are shown in the right column of fig. 6.2. The $B^{\pm}$ contribution shows a peak at $+1$ and the B^0 contribution at zero.

The accuracy of the charge estimation depends on the decay distance. If the decay distance is smaller than the experimental resolution the track origin is not well defined. The uncertainty of the charge measurement is reduced the greater the decay length is. This behaviour is illustrated in fig. 6.3.

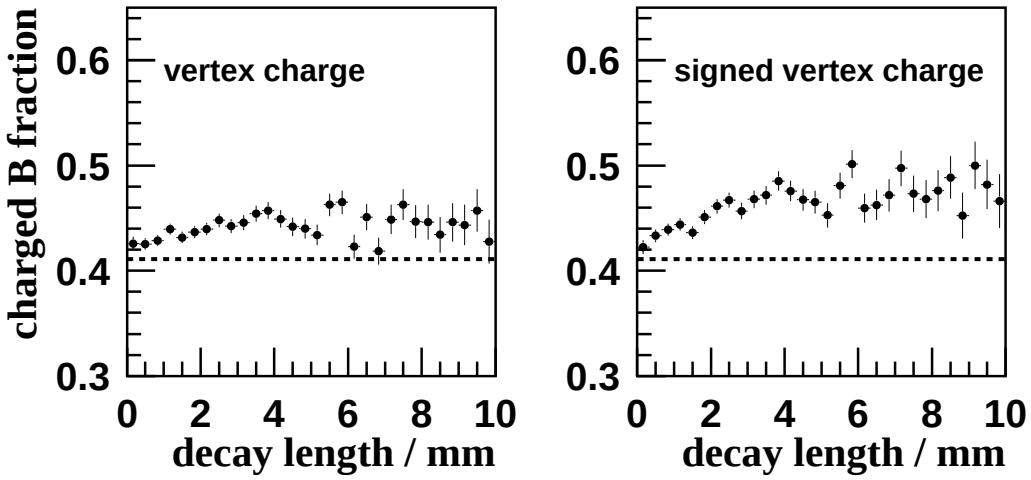

Figure 6.3: Quality dependence of the charge estimation on the decay length. The fraction of charged B mesons in the sample with vertex charge values $|Q_{vertex}| > 0.7$ (left) and signed vertex charge values $Q_{vertex}^{signed} > 0.5$ (right) is shown as a function of the decay distance. The line indicates the average fraction of charged B mesons.

After a decay length of about 3 mm (one average lifetime) the accuracy of the charge measurement reaches its saturation value. The minimum length of 3 mm is small compared to the decay distances where the sensitivity to $\Delta\Gamma$ of B_s mesons is greatest, namely in the region of more than five average lifetimes, as explained in section 2.2.3. The decrease in accuracy below 3 mm is therefore not important for the measurement of $\Delta\Gamma$. In the lifetime fit the decay length dependence of the charge measurement is taken into account by a fit model that relies on a full MC simulation. The correlations between the decay length and the vertex charge measurement are determined from the MC.

Chapter 7

Lifetimes of neutral and charged b hadrons and $\Delta\Gamma$ of B_S mesons

In this chapter the lifetime information contained in the position of the secondary vertices is combined with the b flavour information from the charge measurement. Neutral and charged b hadrons are enriched in two respective decay length (and impact parameter) distributions. The separation into two categories is done by the value of the signed vertex charge, defined in section 6.1. The decay length entries with $Q_{vertex}^{signed} > 0.5$ contribute to the B^+ enriched histogram, those with $Q_{vertex}^{signed} < 0.5$ to the B^0 enriched histogram.

7.1 The free parameters in the fit

The original fit of a single lifetime parameter is extended to a lifetime fit for the specific b hadron types. In general there are four b hadron flavours, B^+, B^0, B_s and Λ_b, produced in Z decays that have six independent lifetimes. Each neutral B meson, B^0 and B_s, consists of two mass eigenstates with two distinct lifetimes. We will follow our previous hypothesis (see chapter 2) that the lifetime difference of the B^0 meson is negligible and consider five lifetime parameters: $\tau(B^+), \tau(B^0), \tau(B_s^1), \tau(B_s^2)$ and $\tau(\Lambda_b)$.

Out of these three parameters can be determined by a charge-sensitive decay time measurement. These are the B^+ lifetime $\tau(B^+)$, the average lifetime of neutral b hadrons $\tau(B^0) = (\tau(B_s^1) + \tau(B_s^2))/2 = \tau(\Lambda_b)$ and the lifetime difference of the B_s meson states $\Delta\tau(B_s) = (\tau(B_s^1) - \tau(B_s^2))/2$. Here it is assumed that the neutral b hadron lifetimes of B^0, Λ_b and the average lifetime of the B_s meson are identical. The fit is done in two steps. At first the three parameters $\tau(B^+), \tau(B^0)$ and $\Delta\tau(B_s)$ are derived from a simultaneous fit to the B^+ and B^0 enriched histograms. In a second step the LEP results on b hadron lifetimes are included in the fit. The L3 fit is constrained to the LEP results for $\tau(B^+), \tau(B^0), \tau(B_s) = (\tau(B_s^1) + \tau(B_s^2))/2$ and $\tau(\Lambda_b)$. In this way all five lifetime parameters can be evaluated. Assumptions about neutral hadron lifetimes are replaced by measurements.

7.2 Fit results

7.2.1 Three-parameter fit

A set of lifetime variables for the three-parameter fit was chosen as:

1. the average lifetime $\tau_b = f_+ \, \tau(B^+) + f_0 \, \tau(B^0)$.

2. the lifetime ratio $r = \tau(B^+)/\tau(B^0)$.

3. the B_s rate difference $\Delta\Gamma/\Gamma$. It is related to the lifetimes $\tau(B_s^1), \tau(B_s^2)$ via: $\tau(B_s^{1,2}) = \tau(B^0)/(1 \pm \Delta\Gamma/2\Gamma)$.

Two normalization parameters are needed to control the fraction of charged to neutral hadrons and the fraction of B_s mesons in the neutral hadron sample for which two lifetimes are fitted. The choice of the normalization parameters was performed according to the suggestions of the Particle Data Group [5]. The composition of the b hadron sample was described by the fraction f_{B_s} of B_s mesons, the fraction f_{Λ_b} of b baryons and assuming equal production of B^0 and B^+ mesons, $f_{B_0} = f_{B^+} = (1 - f_{B_s} - f_{\Lambda_b})/2$. Measurements of branching ratios of other experiments [57] have been used to estimate f_{B_s} and f_{Λ_b} from the number of observed events in flavour-specific decay channels. In addition an alternative method has been applied to determine f_{B_s} with the time integrated mixing parameter $\chi^{LEP} = f_{B^0}\chi_d + f_{B_s}\chi_s$. A value for f_{B_s} can be extracted from the measured value of χ_d at the $\Upsilon(4S)$ resonance and the relation $\chi_s = 0.5$ which follows from the lower limit on ΔM_{B_s} .

The estimates from the LEP oscillation working group [57] were derived from a combination of both methods. The values are:

$$\begin{aligned} f_{B_s} &= 0.105 \, ^{+0.016}_{-0.015} \, , \\ f_{\Lambda_b} &= 0.106 \, ^{+0.037}_{-0.027} \, . \end{aligned} \tag{7.1}$$

The parameters f_{B_s} and f_{Λ_b} were included as fit parameters into the lifetime fit and their values were constrained to the LEP estimates (7.1).

Four distributions, namely the B^+ and B^0 enriched histograms of respective two quality samples, have been fitted simultaneously by the use of the three lifetime parameters $\tau_b, r, \Delta\Gamma/\Gamma$, the normalization parameters $f_b, f_{B_s}, f_{\Lambda_b}$ and the background parameters $f_1, s_1, f_2, s_2, \langle n_K \rangle$. The quality samples were defined in the same way as in chapter 5 by a cut on the decay length in the opposite jet. The numbers of vertices contained in the four samples and the distribution of charged and neutral b hadrons are summarized in table 7.1. The parameter of the b fragmentation was adjusted to the previously measured value of $\langle x_E \rangle_b = 0.710 \pm 0.004$.

Sample	1	2	3	4
Total number	319,374	72,224	406,681	92,227
MC b purity	17%	69%	17%	69%
MC B^+ purity	45%	45%	38%	38%

Table 7.1: Sample composition of the fitted distributions. The numbers stand for: (1) B^+ enriched, anti-b tag; (2) B^+ enriched, b tag; (3) B^0 enriched, anti-b tag and (4) B^0 enriched, b tag.

In the following the fit results are presented. All errors quoted in this section are statistical only. The systematic uncertainty is investigated in section 7.3 of this chapter.

The result of the decay length fit was:

$$\begin{aligned} \tau_b &= (1554 \pm 12)\,\text{fs}\,, \\ r &= 1.11 \pm 0.07\,, \\ \Delta\Gamma/\Gamma &= 0.0\,^{+0.31}_{-0.0}\,, \\ f_b &= 0.691 \pm 0.004\,, \\ f_{B_s} &= 0.098 \pm 0.014\,, \\ f_{\Lambda_b} &= 0.092 \pm 0.023\,. \end{aligned} \tag{7.2}$$

The decay length distributions are shown in fig. 7.1. The 95% confidence level limit on $\Delta\Gamma/\Gamma$ is

$$\Delta\Gamma/\Gamma < 0.47 \qquad (95\%\,\text{C.L.})\,. \tag{7.3}$$

The same fit procedure has been applied to the impact parameter distributions of the respective subsamples. The parameter values found in the impact parameter fit were:

$$\begin{aligned} \tau_b &= (1554 \pm 13)\,\text{fs}\,, \\ r &= 1.11 \pm 0.08\,, \\ \Delta\Gamma/\Gamma &= 0.13\,^{+0.31}_{-0.13}\,, \\ f_b &= 0.693 \pm 0.004\,, \\ f_{B_s} &= 0.102 \pm 0.014\,, \\ f_{\Lambda_b} &= 0.094 \pm 0.022\,. \end{aligned} \tag{7.4}$$

The fit is shown in fig. 7.2. At 95% confidence level the value of $\Delta\Gamma/\Gamma$ is lower than:

$$\Delta\Gamma/\Gamma < 0.59 \qquad (95\%\,\text{C.L.})\,. \tag{7.5}$$

The values of the background parameters are the same as in the previous fits given in table 5.2 and table 5.3.

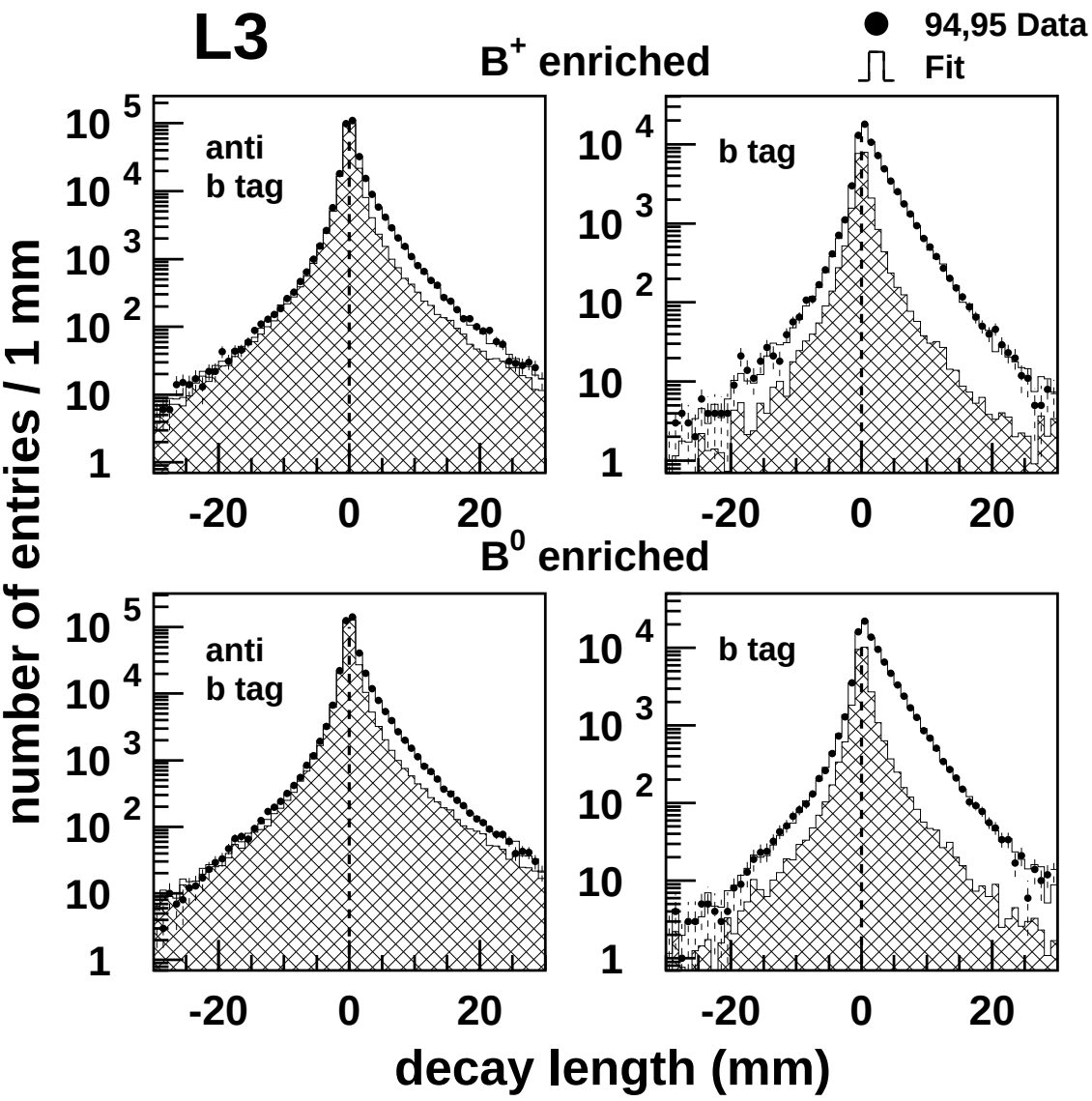

Figure 7.1: Decay length distributions in four subsamples. The upper row contains the B^+ enriched distribution, the lower row the B^0 enriched distribution in respectively a b enriched quality sample (right) and a b reduced sample (left). The points represent the data of the years 1994 and 1995 and the histograms show the MC distributions for the fitted lifetime parameters.

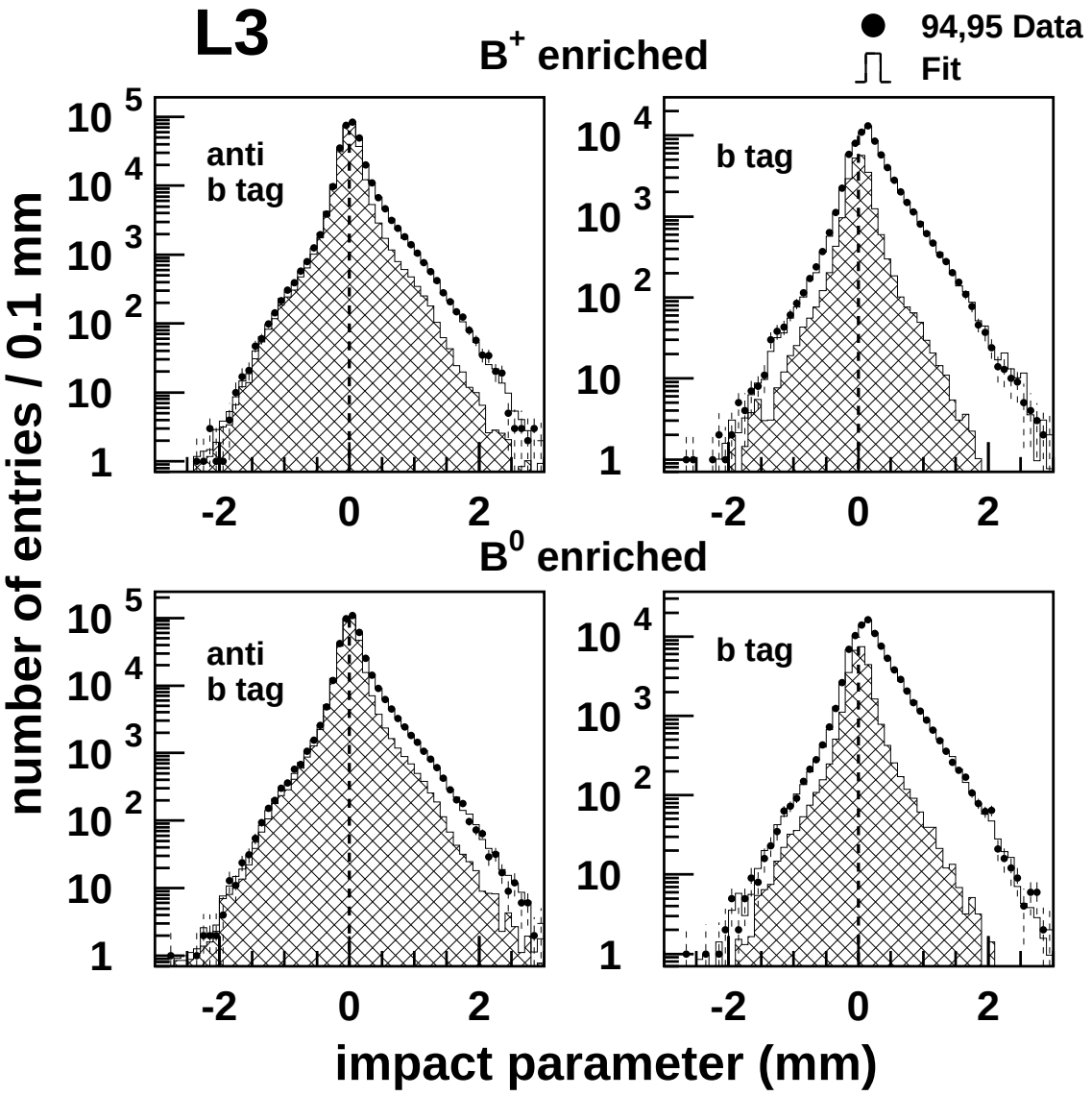

Figure 7.2: Impact parameter distributions in four subsamples. The upper row contains the B^+ enriched distribution, the lower row the B^0 enriched distribution in respectively a b enriched quality sample (right) and a b reduced sample (left). The points represent the data of the years 1994 and 1995 and the histograms show the MC distributions for the fitted lifetime parameters.

Fig. 7.3 and fig. 7.4 show examples of different fit parameters in order to illustrate the sensitivity to the lifetime ratio r and the B_s rate difference $\Delta\Gamma/\Gamma$. The fit results of the decay length fit are shown together with $r = 0.8, 1.4$ and $\Delta\Gamma/\Gamma = 0.8$ in the high b purity samples of the B^+ and B^0 enriched distributions. It is visible that both parameters r and $\Delta\Gamma/\Gamma$ can be determined almost independently from each other. A change of the parameter r causes changes in the B^+ and B^0 enriched distributions of opposite directions. In the case of a change of $\Delta\Gamma/\Gamma$ these changes go into the same direction.

The magnitude of the changes in the B^+ and B^0 enriched distributions caused by changes of r is different. The effects are stronger in the B^+ distribution than in the B^0 distribution. This behaviour has its origin in the different values of the composition of the sample from charged and neutral b hadrons. Under the constraint $\tau_b = f_+ \tau(B^+) + f_0 \tau(B^0)$ the changes for the lifetimes $\tau(B^+)$ and $\tau(B^0)$ under a change of r are larger for that lifetime with the smaller value of f, namely B^+. As a result the B^+ enriched distribution is more sensitive to the value of r than the B^0 enriched distribution. The dependence of the distributions on r is characterized by an other feature: In the limit of large decay length values the number of entries for values of $r \neq 1$ is always greater than for $r = 1$ independent if r is smaller or greater than one. All distributions are superpositions of a B^+ and a B^0 decay length distribution and the behaviour at large values of the decay length is always dominated by the long-lived component independent if this is the B^+ or the B^0 component.

The changes in the distributions introduced by different values of $\Delta\Gamma/\Gamma$ are in agreement with the expectations derived in chapter 2. At small values of the decay length the fit is not sensitive to $\Delta\Gamma/\Gamma$. In this region the superposition of a short- and a longlived B_s component is identical to a distribution of a B_s meson with a single average lifetime. The enrichment of neutral B mesons is visible in fig. 7.4 where the dependence on $\Delta\Gamma/\Gamma$ is more pronounced in the B^0 enriched distribution as compared to the B^+ enriched distribution.

7.2.2 LEP constrained five-parameter fit

The result of the three-parameter fit for τ_b and r can be compared with the LEP result of measurements of individual lifetimes. The lifetimes of B^+, B^0, B_s and Λ_b hadrons have been measured in exclusive decay channels. The results of the experiments have been combined by the LEP B Lifetime Working Group [102]. The average LEP values are [1]:

$$\begin{aligned} \tau(B^+) &= (1670 \pm 40)\,\text{fs}\,, \\ \tau(B^0) &= (1570 \pm 40)\,\text{fs}\,, \end{aligned}$$

[1]Note that different definitions of the parameter $\tau(B^0)$ have been applied. In the three-parameter fit $\tau(B^0)$ was the average lifetime of all neutral b hadrons, i.e. of B^0, B_s and Λ_b. In contrast to that, in the five-parameter fit $\tau(B^0)$ was used as the lifetime of the B^0 meson.

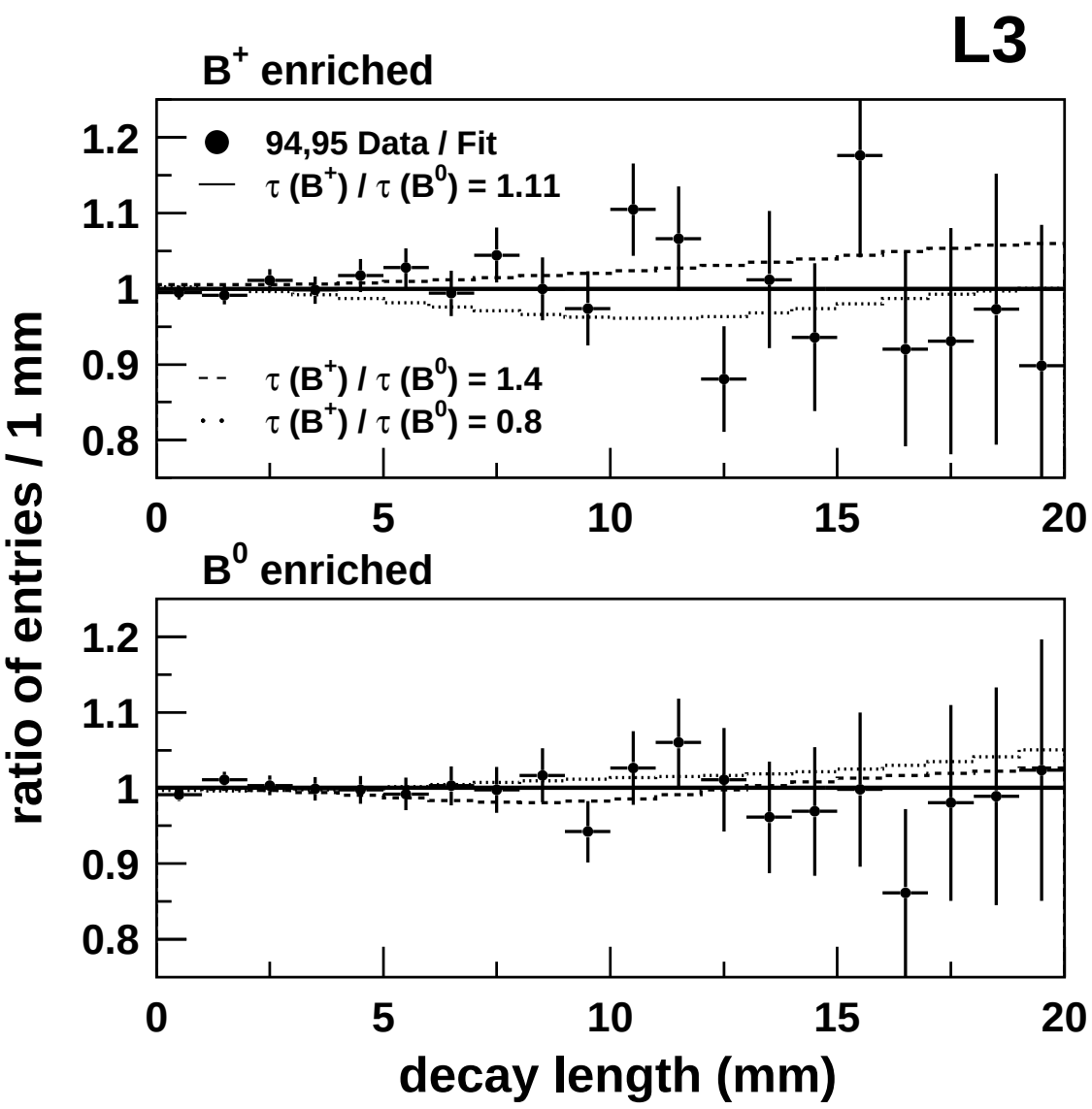

Figure 7.3: Dependence of the decay length fit on the lifetime ratio $r = \tau(B^+)/\tau(B^0)$. The decay length distributions of the b-tagged quality sample are shown in the B^+ enriched part (upper row) and in the B^0 enriched part (lower row). The solid curves represent the MC distributions for the fit parameter $r = 1.11$, the dashed curves for the value $r = 1.4$ and the dotted curves for the value $r = 0.8$.

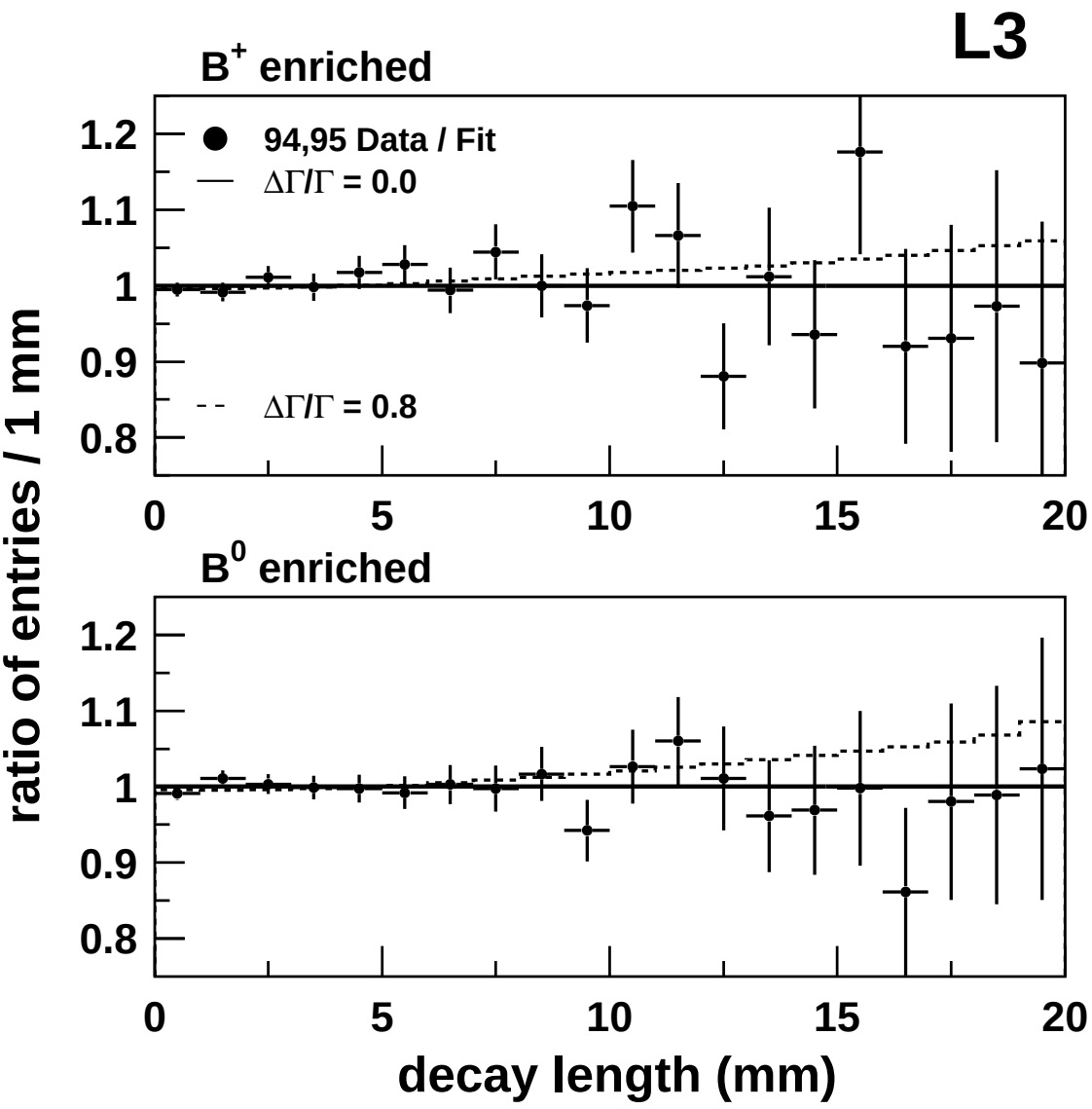

Figure 7.4: Dependence of the decay length fit on the rate difference $\Delta\Gamma_{B_s}$. The decay length distributions of the b-tagged quality sample are shown in the B^+ enriched part (upper row) and in the B^0 enriched part (lower row). The solid curves represent the MC distributions for the fit parameter $\Delta\Gamma/\Gamma = 0.0$, the dashed curves for the value $\Delta\Gamma/\Gamma = 0.8$.

$$\begin{aligned} \tau(B_s) &= (1490 \pm 60)\ \text{fs}\,, \\ \tau(\Lambda_b) &= (1220 \pm 50)\ \text{fs}\,. \end{aligned} \tag{7.6}$$

The fit parameters τ_b and r are related to the LEP measurements via:

$$\begin{aligned} \tau_b &= (1 - f_{B_s} - f_{\Lambda_b})\,\frac{\tau(B^+) + \tau(B^0)}{2} + f_{B_s}\,\tau(B_s) + f_{\Lambda_b}\,\tau(\Lambda_b)\,, \\ r &= \frac{\frac{1}{2}(1 + f_{B_s} + f_{\Lambda_b})\,\tau(B^+)}{\frac{1}{2}(1 - f_{B_s} - f_{\Lambda_b})\,\tau(B^0) + f_{B_s}\,\tau(B_s) + f_{\Lambda_b}\,\tau(\Lambda_b)}\,. \end{aligned} \tag{7.7}$$

The LEP values for τ_b and r according to eq. (7.1) and (7.6),

$$\begin{aligned} \tau_b &= (1564 \pm 28)\ \text{fs}\,, \\ r &= 1.12 \pm 0.07\,, \end{aligned} \tag{7.8}$$

are in agreement with the values of the three-parameter fit (7.2) and (7.4).

It is thus possible to combine the result of the three-parameter fit with the statistical independent LEP result for $\tau(B^+), \tau(B^0), \tau(B_s)$ and $\tau(\Lambda_b)$. The number of fit parameters is enlarged by including $\tau(B_s)$ and $\tau(\Lambda_b)$ as new free parameters into the fit. In this way the systematic uncertainty coming from differences in the values of neutral b hadron lifetimes is eliminated. In the five-parameter fit, this uncertainty is included in the statistical error.

The lifetime variables estimated in the five-parameter fit were:

1. the B^+ lifetime $\tau(B^+)$
2. the B^0 lifetime $\tau(B^0)$.
3. the average B_s lifetime $\tau(B_s)$.
4. the B_s rate difference $\Delta\Gamma/\Gamma$.
5. the average b baryon lifetime $\tau(\Lambda_b)$.

Superimposing the constraints (7.1) and (7.6) to the decay length fit the values of the lifetimes and normalization fractions were determined as:

$$\begin{aligned} \tau(B^+) &= (1652 \pm 30)\ \text{fs}\,, \\ \tau(B^0) &= (1548 \pm 30)\ \text{fs}\,, \\ \tau(B_s) &= (1481 \pm 55)\ \text{fs}\,, \\ \Delta\Gamma/\Gamma &= 0.0\ {}^{+0.26}_{-0.0}\,, \\ \tau(\Lambda_b) &= (1233 \pm 47)\ \text{fs}\,, \\ f_b &= 0.692 \pm 0.004\,, \\ f_{B_s} &= 0.100 \pm 0.014\,, \\ f_{\Lambda_b} &= 0.090 \pm 0.020\,. \end{aligned} \tag{7.9}$$

The upper limit value on $\Delta\Gamma/\Gamma$ at 95% confidence level is:

$$\Delta\Gamma/\Gamma < 0.45 \qquad (95\%\,\text{C.L.})\,. \tag{7.10}$$

In case of the impact parameter fit the values were measured as:

$$\begin{aligned}
\tau(B^+) &= (1654 \pm 32)\,\text{fs}\,, \\
\tau(B^0) &= (1552 \pm 32)\,\text{fs}\,, \\
\tau(B_s) &= (1485 \pm 56)\,\text{fs}\,, \\
\Delta\Gamma/\Gamma &= 0.04\,{}^{+0.36}_{-0.04}\,, \\
\tau(\Lambda_b) &= (1219 \pm 49)\,\text{fs}\,, \\
f_b &= 0.694 \pm 0.004\,, \\
f_{B_s} &= 0.103 \pm 0.014\,, \\
f_{\Lambda_b} &= 0.094 \pm 0.022\,.
\end{aligned} \tag{7.11}$$

The limit value on $\Delta\Gamma/\Gamma$ at 95% confidence level is:

$$\Delta\Gamma/\Gamma < 0.56 \qquad (95\%\,\text{C.L.})\,. \tag{7.12}$$

The correlations between the fit variables of the four fits (7.2), (7.4), (7.9) and (7.11) are listed in the appendix A.

7.3 Systematic uncertainties

Some of the systematic uncertainties are already contained in the statistical error. These are the uncertainties from the fraction of B_s and Λ_b hadrons and from the lifetimes of individual b hadrons. In particular, the five-parameter fit is free of any systematic limitations from these error sources.

There are further uncertainties from detector effects and heavy quark model assumptions. These error sources have been already discussed in their effect on the average b lifetime τ_b in chapter 5. The error analysis has been repeated here in order to estimate the systematic uncertainty of

1. $\tau_b, r = \tau(B^+)/\tau(B^0)$ and $\Delta\Gamma/\Gamma$ in case of the three-parameter fit.
2. $\Delta\Gamma/\Gamma$ in case of the five-parameter fit.

The result of this error analysis for the parameters τ_b and $r = \tau(B^+)/\tau(B^0)$ is summarized in table 7.2. The detector and model parameters have been varied by the same amount as in chapter 5 except for the fragmentation parameter. The table below shows the uncertainty for $\langle x_E \rangle_b = 0.710 \pm 0.004$ as determined in section 5.6 of this thesis. It has been found that the corresponding errors on $\Delta\Gamma/\Gamma$ to that of table 7.2 are completely negligible. The total error on $\Delta\Gamma/\Gamma$ from all

Error source	$\Delta\tau_b^{DL}$ (fs)	Δr^{DL}	$\Delta\tau_b^{IP}$ (fs)	Δr^{IP}
Detector Uncertainties	10	0.016	11	0.017
Quality track multiplicity	3	0.007	5	0.010
Resolution function	5	0.003	5	0.002
TEC calibration and SMD alignment	3	0.012	3	0.011
Beam spot size and position	6	0.005	6	0.005
Jet direction resolution	4	0.004	5	0.005
Heavy Quark Physics Modeling	19	0.026	14	0.026
R_b	4	0.001	5	0.002
R_c	2	<0.001	2	<0.001
b fragmentation	15	0.015	5	0.007
c fragmentation	2	0.001	<1	<0.001
b decay multiplicity distribution	4	0.006	4	0.006
D fraction in $c\bar{c}$ events	1	0.004	3	0.004
D content in b decays	10	0.019	11	0.022
D lifetimes	2	0.002	3	0.002
B^+/B^0 separation	2	0.006	3	0.010

Table 7.2: Systematic errors in the measurement of τ_b and $r = \tau(B^+)/\tau(B^0)$. The first two columns show the errors for the decay length method, the last two for the impact parameter method.

these error sources is smaller than 0.05 for both the decay length and the impact parameter measurement. It has therefore no impact on the final result for $\Delta\Gamma/\Gamma$.

The analysis of this chapter is affected by an additional systematic uncertainty arising from the charge measurement. Systematic uncertainties in the measurement of the secondary vertex charge influence the number of B^+ and B^0 hadrons in the B^+ and B^0 enriched samples. A scale uncertainty in the b hadron composition of 5% of the changes introduced by the cut on the vertex charge has been considered. This scale uncertainty concerns the distribution of charged and neutral b hadrons among the B^+ and B^0 enriched samples; the total number of charged and neutral b hadrons is controled by the fit parameters f_{B_s} and f_{Λ_b}. The errors on the lifetime variables due to this uncertainty are given in the last line of table 7.2.

A cross check on the charge measurement has been performed for the charged B sample exploiting the forward-backward asymmetry of b quark production in Z decays. The vertex charge of $B^{\pm}$ mesons measures the flavour of the b quark constituent. The distribution of the cosine of the polar angle of the event thrust axis with respect to the e^- direction signed by the reconstructed vertex charge is sensitive to unexpected mis-assignments of the vertex charge. The observed asymmetry in the signed $\cos\theta_T$ distribution would be flattened the less the reliability of the vertex charge measurement. The distribution was found to be in agreement with the expected asymmetry from the lepton measurement [13] and the reliability

of the vertex charge measurement as estimated from the MC [103].

The final results for τ_b and r are:

$$\begin{aligned} \tau_b &= (1554 \pm 12 \pm 22)\ \text{fs}\,, \\ r &= 1.11 \pm 0.07 \pm 0.03\,, \end{aligned} \tag{7.13}$$

as determined in the decay length measurement and

$$\begin{aligned} \tau_b &= (1554 \pm 13 \pm 18)\ \text{fs}\,, \\ r &= 1.11 \pm 0.08 \pm 0.03\,, \end{aligned} \tag{7.14}$$

as determined in the impact parameter measurement. The first errors represent the statistical the second the systematic uncertainties.

I repeat the results for $\Delta\Gamma/\Gamma$. They include all sources of systematic uncertainty. In the decay length measurement the value of the 95% C.L. upper limit is:

$$\Delta\Gamma/\Gamma < 0.45 \qquad (95\%\,\text{C.L.})\,, \tag{7.15}$$

and in the impact parameter measurement it is:

$$\Delta\Gamma/\Gamma < 0.56 \qquad (95\%\,\text{C.L.})\,. \tag{7.16}$$

I consider it as sufficient to give one digit for the final 95% confidence limit on $\Delta\Gamma/\Gamma$. Then both results from the decay length and the impact parameter measurements are equal. The final value for the upper limit on $\Delta\Gamma/\Gamma$ including statistical and systematic uncertainties is:

$$\Delta\Gamma/\Gamma < 0.5 \qquad (95\%\,\text{C.L.})\,. \tag{7.17}$$

7.4 Discussion of the fit results

7.4.1 The lifetime ratio $\tau(B^+)/\tau(B^0)$

There exist quantitative predictions for the ratios of individual b hadron lifetimes based on the Operator Product Expansion formalism [104]. As already mentioned in chapter 2 the quantities of interest are expanded in powers of Λ_{QCD}/m_b in this formalism. The results show that $1/m_b$ terms do not contribute to bottom lifetime differences. Differences of baryon-meson lifetimes start with $1/m_b^2$ terms and those of meson-meson lifetimes start only with $1/m_b^3$ terms. The theoretical predictions are [104]:

$$\begin{aligned} \tau(B^+)/\tau(B^0) &= 1 + 0.05 \left(\frac{f_B}{200\ \text{MeV}} \right)^2\,, \\ \tau(B_s)/\tau(B^0) &= 1 \pm \mathcal{O}(0.01)\,, \\ \tau(\Lambda_b)/\tau(B^0) &= 0.9 - 0.95\,. \end{aligned} \tag{7.18}$$

The measured ratio of $r = 1.11 \pm 0.08$ is consistent with this theoretical predictions and, as already mentioned, is also in agreement with the other LEP measurements (7.6).

At present, a deviation between experimental result and theoretical prediction is observed for the b baryon lifetime. The measured value of $\tau(\Lambda_b)/\tau(B^0) = 0.78 \pm 0.04$ [102] is not compatible with the theoretical estimate of eq. (7.18). This discrepancy is still an unsolved problem [104]. The measurement of r of this thesis cannot contribute to this discussion since there is no direct sensitivity to the lifetime of b baryons. The value of $\tau(\Lambda_b)$ is only visible in its effect on the average lifetime of neutral b hadrons. However within the uncertainty on r it is not possible to observe effects of the order of the discrepancies as seen in the other LEP experiments.

7.4.2 The upper limit on $\Delta\Gamma/\Gamma$

The upper limit on $\Delta\Gamma/\Gamma$ of 0.5 at 95% confidence level is compatible with the SM expectation. The theoretical upper limit of 95% confidence level for values compatible with the SM is $\Delta\Gamma/\Gamma < 0.4$ [62]. The theoretical uncertainty arises from uncertainties in the values of hadronic matrix elements.

The result for $\Delta\Gamma/\Gamma$ of this thesis can be compared with a preliminary result of the CDF Collaboration [105] of $\Delta\Gamma/\Gamma < 1.0$ at 95% confidence level. This result was obtained from a D_s lepton sample. It has not yet been published. Both results agree with each other. The upper limit value that was derived in this thesis is a factor of two better than the CDF value.

Chapter 8

Determination of the $|V_{cb}|$ value

8.1 The $|V_{cb}|$ value

The value of the $|V_{cb}|$ element of the Cabibbo-Kobayashi-Maskawa matrix can be determined from the semileptonic width of b hadrons, as calculated in [34]. The experimental value of the semileptonic width is provided by measurements of the average b hadron lifetime τ_b and the semileptonic branching ratio $\mathcal{B}(B \to X_c\, l\, \nu)$, $\Gamma(B \to X_c\, l\, \nu) = \mathcal{B}(B \to X_c\, l\, \nu) \;/ \tau_b$. The simple expression (2.8) of chapter 2 is repeated to relate these measurements to the $|V_{cb}|$ value [34]:

$$|V_{cb}| = 0.0408 \left(\frac{\mathcal{B}(B \to X_c\, l\, \nu)}{0.105} \right)^{1/2} \left(\frac{1.6 \text{ ps}}{\tau_b} \right)^{1/2} . \tag{8.1}$$

In this chapter the $|V_{cb}|$ value will be calculated with the world average values of the b lifetime τ_b and the semileptonic branching ratio $\mathcal{B}(B \to X_c\, l\, \nu)$.

Typically the semileptonic branching ratio $\mathcal{B}(B \to X_c\, l\, \nu)$ with c quarks in the final state is not measured directly, but rather the total branching ratio $\mathcal{B}(B \to X\, l\, \nu)$ with $X = X_c + X_u$. In order to separate the contributions from $b \to c$ and $b \to u$ transitions it is necessary to have a measurement of $|V_{ub}\,/\,V_{cb}|$. The measurement of $|V_{ub}\,/\,V_{cb}|$ [41] described in chapter 2 will be used to obtain the semileptonic branching ratio $\mathcal{B}(B \to X_c\, l\, \nu)$. This is a small correction because $|V_{ub}|$ was measured to be much smaller than $|V_{cb}|$.

8.1.1 Measurement of τ_b

The measurement of τ_b described in this thesis is included in the world average result that combines measurements of LEP, SLD and CDF as shown in fig. 8.1 [102]. The majority of the measurements has been performed on e^+e^- colliders [85–87] whereas recently a first measurement of τ_b at a proton collider has been reported by the CDF Collaboration [88] at the Tevatron.

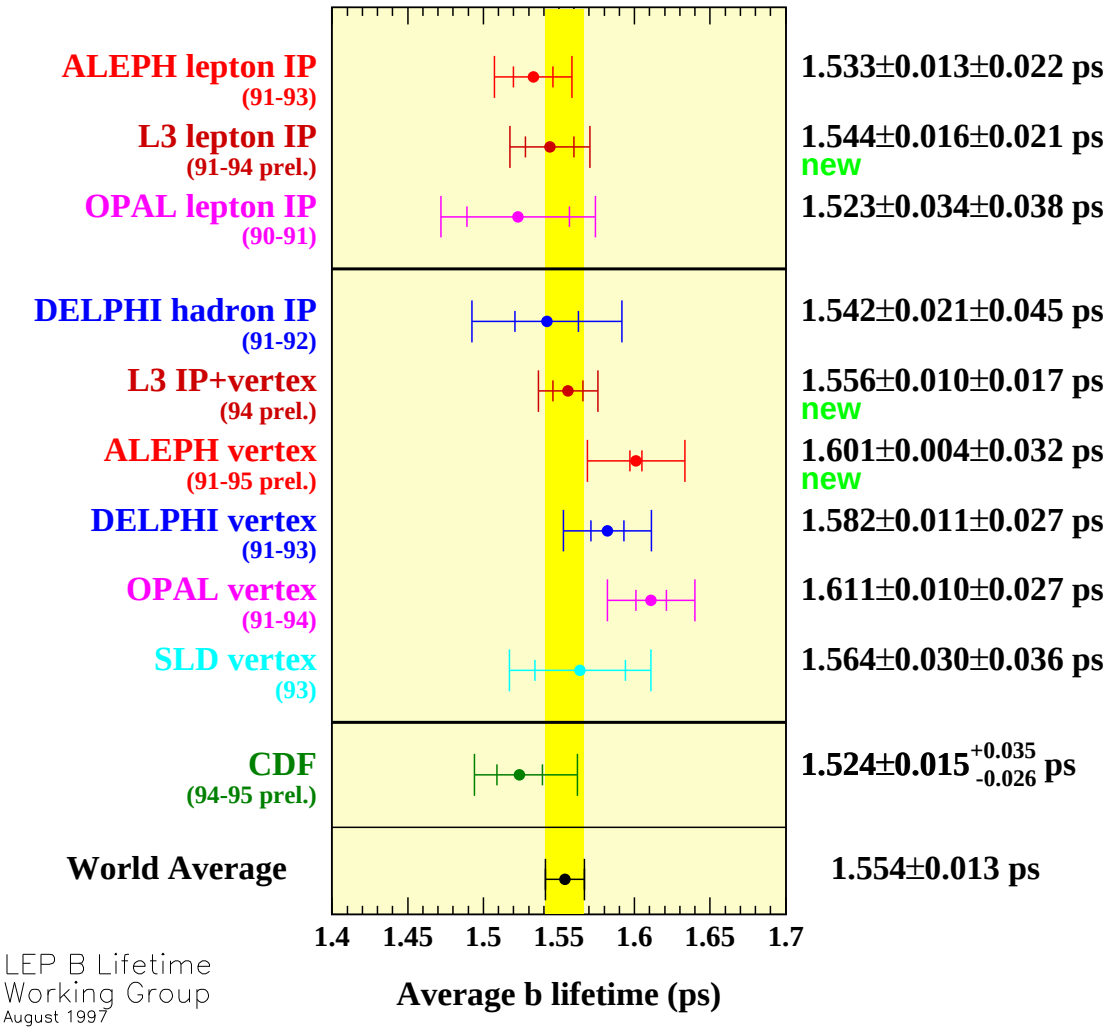

Figure 8.1: Combination of the τ_b measurements of LEP, SLD and CDF. The average value was calculated by the LEP B Lifetime Working Group [102].

Three methods are commonly used to measure τ_b. The first block in fig. 8.1 combines measurements that are based on the impact parameter distribution of leptons with high momentum and high transverse momentum [85]. The dominant systematic errors come from uncertainties in the detector performance, as for instance uncertainties in the lepton identification. The model dependence concerning the b production and the semileptonic decay is small. The statistical accuarcy is determined by the semileptonic branching ratio of $\sim 10\%$.

The results of τ_b measurements with a vertex algorithm [87] similar to the one of this thesis [86] are presented in the second block of fig. 8.1. The b lifetime is derived from the impact parameter or from the decay length distribution. The main systematic errors come from the b fragmentation (in case of decay length methods) and from the modeling of hadronic b decays. Currently these measurements of block two in fig. 8.1 constitute the most accurate measurements of τ_b, both from the statistical and the systematic accuracy.

The third block in fig. 8.1 shows the result of the CDF Collaboration [88] using J/Ψ decays that offer a competitive way at proton colliders when compared to the e^+e^- accelerators LEP and SLC. The distribution of production vertices of $\mu^+\mu^-$ pairs from J/Ψ decays is fitted with two free parameters, the b lifetime and the fraction of J/Ψ's that result from the decay of b hadrons. The statistical and systematic accuracy is of comparable order to that of a single LEP experiment.

The combination of all τ_b measurements has been performed by the LEP B Lifetime Working Group [102]. Uncertainties on fragmentation, decay modeling, branching fractions and charm lifetimes are considered as fully correlated among the experiments. The world average is:

$$\tau_b = (1.554 \pm 0.013)\ \text{ps}\ . \tag{8.2}$$

The final uncertainty is dominated by fragmentation and decay model effects.

8.1.2 Measurement of $\mathcal{B}(B \to X_c\, l\, \nu)$

Measurements of the semileptonic branching ratio $\mathcal{B}(B \to X\, l\, \nu)$ have been performed at the $\Upsilon(4S)$ [106] and at LEP [107]. The experimental situation at LEP and at the $\Upsilon(4S)$ is different with respect to the b hadron sample composition. At the $\Upsilon(4S)$ only B^+ and B^0 mesons are produced.

Using a double-tagging technique at the $\Upsilon(4S)$ it is possible to measure the semileptonic branching ratio over essentially the full lepton momentum range. The $b\overline{b}$ event is tagged by requiring a very energetic lepton. The second lepton in the event is used to analyze the momentum spectrum of the decay. The signal of prompt $b \to l$ leptons has to be distinguished from cascade leptons of secondary charm decays $b \to c \to l$. Kinematic and charge correlations are used to disentangle the different contributions. At the $\Upsilon(4S)$ there is no angular correlation among prompt $b \to l$ leptons from different B decays whereas leptons from the same B decay tend to have back-to-back directions. Leptons of prompt $b \to l$ decays have

opposite signs of electric charge. However if one of the decays proceeds via $b \to c \to l$ the signs of the lepton charges are equal. Applying this technique the uncertainties from the shape of the lepton spectrum are extremely small because almost the full semileptonic branching fraction is measured. The results of the original ARGUS and the recent CLEO measurements [106] are shown in fig. 8.2. The average of the ARGUS and CLEO results is $\mathcal{B}(B \to X\,l\,\nu) = (10.40 \pm 0.16\,(\text{stat}) \pm 0.30\,(\text{syst}))\%$. The largest systematic uncertainties are the errors on the tracking and lepton identification efficiency.

At LEP the kinematic situation is different and other sources of systematic uncertainties are relevant. The LEP measurements [107] are based on studies of the momentum and transverse momentum distributions of leptons with respect to the closest jet. Leptons from b hadron decays are characterized by large momenta due to the hard b fragmentation and by large transverse momenta due to the large b mass. Events with two leptons are also used to reduce systematic uncertainties. The LEP average, $\mathcal{B}(B \to X\,l\,\nu) = (11.15 \pm 0.05\,(\text{stat}) \pm 0.19\,(\text{syst}))\%$, was derived from a simultaneous fit to all heavy flavour parameters at LEP. The $\mathcal{B}(B \to X\,l\,\nu)$ value depends on $R_b = \Gamma_{b\bar{b}}/\Gamma_{\text{had}}$, the average energy fraction $\langle x_E \rangle_b$ carried by the b hadron, the b flavour mixing parameter χ and the branching ratio $\mathcal{B}(b \to c \to l)$. The dependence on R_b is introduced by the normalization of the number of selected events to the total number of hadronic events. The value of $\langle x_E \rangle_b$ determines the shape of the lepton spectra. The latter two parameters are relevant for the separation of prompt $b \to l$ and secondary $b \to c \to l$ leptons.

Fig. 8.2 shows all $\mathcal{B}(B \to X\,l\,\nu)$ measurements. A 2σ inconsistency between the $\Upsilon(4S)$ and the LEP value is observed. The discrepancy can be hardly attributed to the different hadron composition. By means of theoretical expectations [108] the measured values can be corrected for the different b hadron composition. The correction is small and of opposite sign as to explain the discrepancy [108]. At present there is no explanation for the discrepancy. This might be a hint for possible problems in the understanding of the semileptonic decay process. For that reason, half of the difference between the $\Upsilon(4S)$ and the LEP value is assigned as a systematic uncertainty that is added to the final error used for the evaluation of $|V_{cb}|$. I will continue with a world average of $\mathcal{B}(B \to X\,l\,\nu) = (10.96 \pm 0.41)$ %.

The branching ratio with c quarks in the final state is related to $\mathcal{B}(B \to X\,l\,\nu)$ via:

$$\mathcal{B}(B \to X_c\,l\,\nu) = \left[1 + \frac{f_u}{f_c}\left|\frac{V_{ub}}{V_{cb}}\right|^2\right]^{-1} \mathcal{B}(B \to X\,l\,\nu)\;, \tag{8.3}$$

where f_c and f_u are the phase-space factors defined in eq. (2.6) for c and u quarks, respectively. Using the values $m_c = 1.3 \pm 0.2$ GeV, $m_u = 0.1 \pm 0.1$ GeV and $|V_{ub}\,/\,V_{cb}| = 0.08 \pm 0.015$ [41] the branching ratio $\mathcal{B}(B \to X_c\,l\,\nu)$ was determined to be:

$$\mathcal{B}(B \to X_c\,l\,\nu) = (10.84 \pm 0.41)\%\;. \tag{8.4}$$

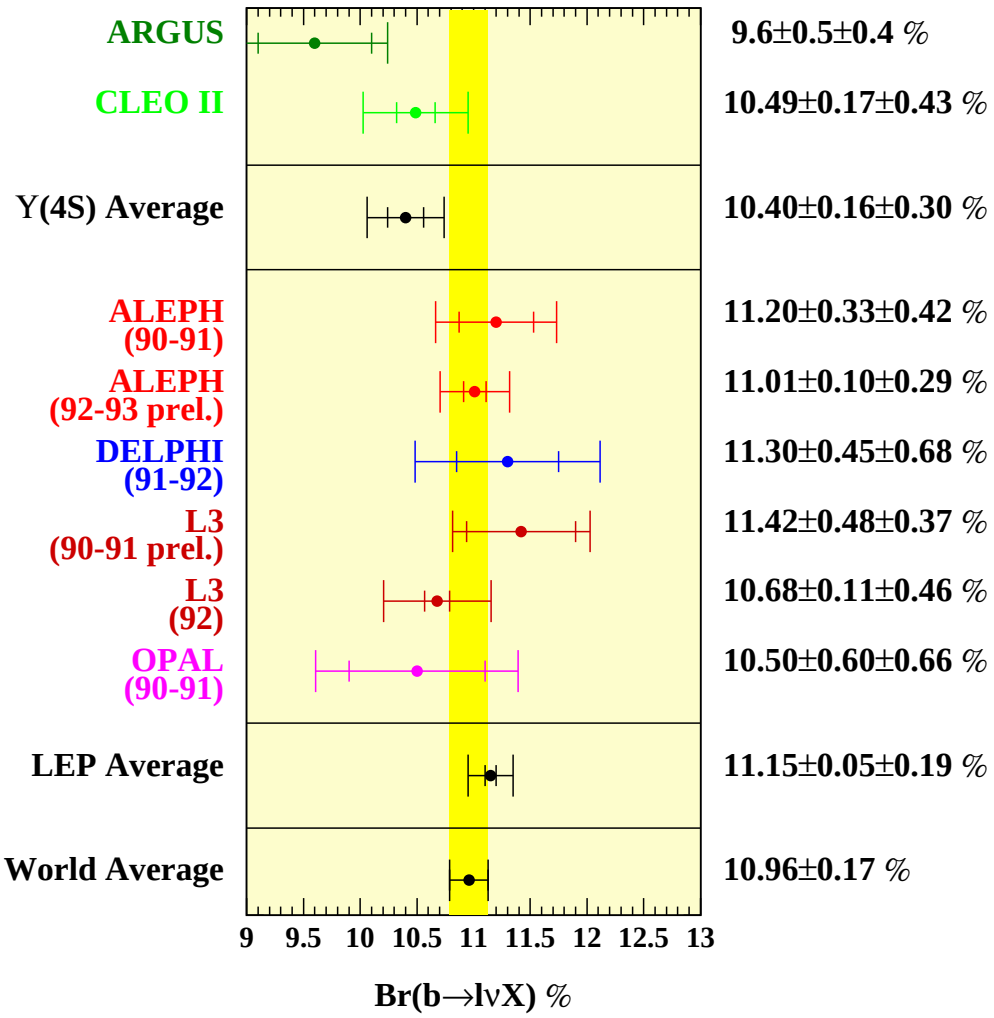

Figure 8.2: Combination of the $\mathcal{B}(B \to X\,l\,\nu)$ measurements at the $\Upsilon(4S)$ and at LEP. The average of the LEP results takes into account the correlation with other b parameters.

8.1.3 Result

The application of formula (8.1) yields a value for $|V_{cb}|$ of:

$$|V_{cb}| = (42.06 \pm 0.18\,(\Delta\tau_b) \pm 0.80\,(\Delta\mathcal{B}(B \to X_c\, l\, \nu))) \times 10^{-3}\,, \qquad (8.5)$$

where the first error summarizes the uncertainty from the τ_b measurement and the second that of the $\mathcal{B}(B \to X_c\, l\, \nu)$ measurement.

The dominant error is that of the uncertainty in the semileptonic branching ratio. The accuracy of the lifetime measurement is at the 1% level whereas the relative discrepancy between the values of the semileptonic branching ratio at the Υ(4S) and at LEP is much larger than 1%.

The size of the theoretical uncertainties in the previous formula has been estimated by 5% as suggested in reference [34]. The final result is:

$$|V_{cb}| = (42.1 \pm 0.8\,(\mathrm{exp}) \pm 2.1\,(\mathrm{theo})) \times 10^{-3}\,, \qquad (8.6)$$

where the first quoted error is due to the measured results for τ_b and $\mathcal{B}(B \to X_c\, l\, \nu)$ and the second error comes from theoretical uncertainties in the estimation of the semileptonic width. The measurement uncertainties in the $|V_{cb}|$ determination are already small compared to the theoretical limitations. The theoretical uncertainties are dominated from the uncertainties in the quark masses. Improvements in the knowledge of the heavy quark masses can be expected from future studies of the lepton spectra near the kinematic endpoint. However the accuracy on m_b and $m_b - m_c$ is principally limited. The $|V_{cb}|$ determination from the inclusive width comes already close to its intrinsic limitations.

Comparing the impact of the three sources of uncertainty, namely $\Delta\tau_b$, $\Delta\mathcal{B}(B \to X_c\, l\, \nu)$ and $\Delta m_b, \Delta(m_b - m_c)$, the error from the b lifetime is the smallest one.

8.2 Comparison with the $|V_{cb}|$ determination from the decay $B \to D^*\, l\, \bar{\nu}$

The principle of the measurement has been described in detail in section 2.1.2. From a study of the q^2 distribution in the decay $B \to D^*\, l\, \bar{\nu}$ many experimental groups [37, 38] have derived values of $|V_{cb}|\mathcal{F}(q^2_{max})$. Following the procedure in reference [36] a value of

$$|V_{cb}| = (39.2 \pm 2.3\,(\mathrm{exp}) \pm 1.6\,(\mathrm{theo})) \times 10^{-3} \qquad (8.7)$$

has been obtained. The result of [36] was updated by the recent LEP measurements [38]. The average value of the experimental results, $|V_{cb}|\mathcal{F}(q^2_{max}) = (35.7 \pm 2.1) \times 10^{-3}$, has been calculated assuming that the systematic errors are independent among the experiments except the error from the b lifetime that is common to all measurements. The rest of the systematic error is dominated by

uncertainties in detector efficiencies. The $|V_{cb}|$ value (8.7) was determined using the theoretical prediction $\mathcal{F}(q^2_{max}) = 0.91 \pm 0.04$ [36].

The agreement of both results (8.6) and (8.7) from the inclusive and exclusive approach confirms in a quantitative way the validity of the quark mixing hypothesis in $b \to c$ transitions. The final value when combing them is:

$$|V_{cb}| = (41.0 \pm 1.0\,(\mathrm{exp}) \pm 1.4\,(\mathrm{theo})) \times 10^{-3}\ . \tag{8.8}$$

Here it has been assumed that the experimental and the theoretical errors are independent. The reasons for that assumption were given in chapter 2. The accuracy of the $|V_{cb}|$ value has improved by almost a factor of two as compared to the Particle Data Group value [5].

The determination of $|V_{cb}|$ corresponds to a value of the CKM parameter A in the Wolfenstein parametrization (2.3) of:

$$A = 0.85 \pm 0.04\ . \tag{8.9}$$

Chapter 9

Lower bound on the value of $|V_{td}\,/\,V_{ts}|$

9.1 Determination of the value of $|V_{td}\,/\,V_{ts}|$

Measurements of the $B^0 - \overline{B}^0$ oscillation frequency ΔM_{B^0} and of the decay rate difference $\Delta\Gamma_{B_s}$ of B_s mesons constrain the ratio of top quark couplings to down and strange quarks, $|V_{td}\,/\,V_{ts}|$. A relation between $|V_{td}\,/\,V_{ts}|$ and the measured values can be derived from the mass splitting ratio $\Delta M_{B^0}\,/\,\Delta M_{B_s}$ given in reference [60] and the ratio of the B_s mass to width difference $\Delta\Gamma_{B_s}\,/\,\Delta M_{B_s}$ calculated in [62]:

$$\left|\frac{V_{td}}{V_{ts}}\right| = \sqrt{\frac{\Delta\Gamma_{B_s}}{\Delta M_{B_s}}\,\frac{m_{B_s}}{m_{B^0}}}\,\left(\frac{f_{B_s}}{f_{B^0}}\right)\,\sqrt{\frac{\Delta M_{B^0}}{\Delta\Gamma_{B_s}}}\,. \tag{9.1}$$

In this equation the ratio $\Delta\Gamma_{B_s}\,/\,\Delta M_{B_s}$, the mass ratio m_{B_s}/m_{B^0} and the ratio of decay constants f_{B_s}/f_{B^0} are numerical factors. The ratio $\Delta\Gamma_{B_s}\,/\,\Delta M_{B_s} = (5.6 \pm 2.6) \times 10^{-3}$ has been calculated within the heavy quark expansion including next-to-leading order terms in the $1/m_b$ expansion and leading-logarithmic terms of QCD [62]. A precise error analysis on $\Delta\Gamma_{B_s}\,/\,\Delta M_{B_s}$ has not been investigated yet but an accuracy of $\sim 10\%$ should be within the reach of the near future [62]. The value of the B_s/B^0 mass ratio has been measured to be $m_{B_s}/m_{B^0} = 1.018 \pm 0.001$ [5]. The ratio of decay constants $f_{B_s}/f_{B^0} = 1.16 \pm 0.1$ has been derived from lattice-QCD and QCD sum rules calculations [60].

Taking these values a relation,

$$\left|\frac{V_{td}}{V_{ts}}\right| = 8.8 \times 10^{-2}\,\sqrt{\frac{\Delta M_{B^0}}{\Delta\Gamma_{B_s}}}\,, \tag{9.2}$$

was obtained. The uncertainty on this relation is not known at present because the error on the value of $\Delta\Gamma_{B_s}\,/\,\Delta M_{B_s}$ has not been calculated yet. At any rate the present experimental uncertainty on $\Delta M_{B^0}\,/\,\Delta\Gamma_{B_s}$ is much larger than the theoretical uncertainty on the factor in eq. (9.2). In the following I will neglect any theoretical uncertainty in eq. (9.2). The results derived from eq. (9.2)

should be understood as an example to illustrate the impact of a measurement of $\Delta M_{B^0} \,/\, \Delta\Gamma_{B_s}$.

9.1.1 Result

A lower limit on the ratio $\Delta M_{B^0} \,/\, \Delta\Gamma_{B_s}$ has been obtained from the LEP result on the B^0 mass difference $\Delta M_{B^0} = 0.466 \pm 0.019$ ps^{-1} [57] and the upper limit on $(\Delta\Gamma/\Gamma)_{B_s} < 0.5$ from this thesis. Using the value of the average B_s lifetime, $\tau(B_s) = (1.49 \pm 0.06)$ ps, from the LEP B Lifetime Group [102] the upper limit on $\Delta\Gamma_{B_s}$ is:

$$\Delta\Gamma_{B_s} < 0.3 \text{ ps}^{-1} \qquad (95\% \text{ C.L.}) \,. \tag{9.3}$$

These values are equivalent to a lower limit on $\Delta M_{B^0} \,/\, \Delta\Gamma_{B_s}$ of:

$$\frac{\Delta M_{B^0}}{\Delta\Gamma_{B_s}} > 1.4 \qquad (95\% \text{ C.L.}) \,. \tag{9.4}$$

By application of formula (9.2) a lower bound on the value of $|V_{td} \,/\, V_{ts}|$ was determined as:

$$\left|\frac{V_{td}}{V_{ts}}\right| > 0.1 \qquad (95\% \text{ C.L.}) \,. \tag{9.5}$$

9.1.2 Upper bound on the value of ΔM_{B_s}

The constant ratio of $\Delta\Gamma_{B_s} \,/\, \Delta M_{B_s}$ [62],

$$\frac{\Delta\Gamma_{B_s}}{\Delta M_{B_s}} = 5.6 \times 10^{-3} \,, \tag{9.6}$$

allows the translation of an upper limit on $\Delta\Gamma_{B_s}$ into an upper limit on ΔM_{B_s} . An upper limit value for the oscillation frequency ΔM_{B_s} of B_s mesons was found to be:

$$\Delta M_{B_s} < 60 \text{ ps}^{-1} \qquad (95\% \text{ C.L.}) \,. \tag{9.7}$$

It is equivalent to an upper limit value for the often used dimensionless variable x_s:

$$x_s = \frac{\Delta M_{B_s}}{\Gamma_{B_s}} < 90 \qquad (95\% \text{ C.L.}) \,. \tag{9.8}$$

Chapter 10

Summary and conclusions

At first the results of this thesis are fitted into the more general context of the determination of the Cabibbo-Kobayashi-Maskawa (CKM) matrix elements. The discussion is followed by a second part in which the particular outcome of this thesis is presented in more detail.

10.1 Status of the CKM matrix elements

In this section it is summarized what is known about the magnitudes of CKM matrix elements. The results of the measurements are discussed with respect to their consistency with the CKM quark mixing scheme and the conclusions that can drawn within this approach.

10.1.1 What can we learn from magnitudes?

Tests of unitarity

The measurements of magnitudes of CKM matrix elements can be used to check the unitarity of the CKM matrix. The sums of absolute squares of rows or columns should equal one. The values of the elements of the 2×2 Cabibbo matrix are taken from the Particle Data Group [5]:

$$\begin{array}{ll} |V_{ud}| = 0.9736 \pm 0.0010 \ , & |V_{us}| = 0.2205 \pm 0.0018 \\ |V_{cd}| = 0.224 \pm 0.016 \ , & |V_{cs}| = 1.01 \pm 0.18 \ . \end{array} \tag{10.1}$$

The values of elements involving quarks of the third family are given in chapter 2 and the value of $|V_{cb}|$ was calculated in this thesis (chapter 8). The test yields:

$$\begin{array}{c} \sum_u = |V_{ud}|^2 + |V_{us}|^2 + |V_{ub}|^2 = \\ (0.9479 \pm 0.0019) + (0.0486 \pm 0.0008) + (0.000011 \pm 0.000004) = 0.9965 \pm 0.0021 \end{array}$$

$$\begin{array}{c} \sum_c = |V_{cd}|^2 + |V_{cs}|^2 + |V_{cb}|^2 = \\ (0.050 \pm 0.007) + (1.02 \pm 0.36) + (0.0017 \pm 0.0001) = 1.07 \pm 0.36 \ . \end{array} \tag{10.2}$$

For the third row, the quantity $\sum_t = |V_{td}|^2 + |V_{ts}|^2 + |V_{tb}|^2$, the test is so far not possible, since no measurement of $|V_{tb}|$ exists which does not rely already on the assumption of unitarity.

The best measured value, $\sum_u = |V_{ud}|^2 + |V_{us}|^2 + |V_{ub}|^2$, shows a deviation from one by almost two standard deviations whereas $\sum_c = |V_{cd}|^2 + |V_{cs}|^2 + |V_{cb}|^2$ is consistent with one within the (much greater) estimated uncertainty. In both cases the dominant errors come from the diagonal terms $|V_{ud}|$ and $|V_{cs}|$. The value of $|V_{ud}|$ is still under discussion. It is derived from superallowed Fermi transitions in nuclei. The experiments already reach a relative accuracy of 2×10^{-4}. However the estimation of the radiative corrections still has a larger uncertainty and the numerical results have changed in the last two years (see discussion in [5]). The value of $\sum_u = |V_{ud}|^2 + |V_{us}|^2 + |V_{ub}|^2$ might be a hint for new particles, but it is not yet significant at present. Unfortunately the element $|V_{cs}|$ is the Cabibbo element with the smallest relative accuracy and the conclusions from the estimation of $\sum_c = |V_{cd}|^2 + |V_{cs}|^2 + |V_{cb}|^2$ are limited.

The allowed range of values of the CKM matrix elements at 68% confidence level can be summarized as follows:

$$\begin{pmatrix} 0.9726 \text{ to } 0.9746 & 0.219 \text{ to } 0.222 & 0.0027 \text{ to } 0.0039 \\ 0.208 \text{ to } 0.240 & 0.83 \text{ to } 1.19 & 0.039 \text{ to } 0.043 \\ 0.007 \text{ to } 0.011 & 0.029 \text{ to } 0.041 & 0 \text{ to } 1 \end{pmatrix} . \qquad (10.3)$$

The accuracy in the estimation of the CKM elements decreases the heavier the respective quark. Only very little information exists on CKM elements involving the top quark. However the constraints of unitarity connect different elements. A certain range for one element restricts the range of others. What can we conclude for the top quark elements from the measurements of up and charm quark elements under the assumption of unitarity? Using the measurements of the first and second row in equation (10.3) together with unitarity, and assuming only three families, the 1σ ranges on the values of CKM elements are:

$$\begin{pmatrix} 0.9747 \text{ to } 0.9755 & 0.220 \text{ to } 0.223 & 0.0027 \text{ to } 0.0039 \\ 0.220 \text{ to } 0.223 & 0.9739 \text{ to } 0.9747 & 0.039 \text{ to } 0.043 \\ 0.006 \text{ to } 0.012 & 0.038 \text{ to } 0.042 & 0.99908 \text{ to } 0.99922 \end{pmatrix} . \qquad (10.4)$$

The ranges given here are different from those in equation (10.3) because of the inclusion of unitarity. Six measurements (of $|V_{ud}|, |V_{us}|, |V_{ub}|, |V_{cd}|, |V_{cs}|, |V_{cb}|$) were used to determine three real parameters, the number of independent rotations. The fact that $\sum_u < 1$ has pushed the central values for $|V_{ud}|$ and $|V_{us}|$ about one standard deviation higher than the original input values given in eq. (10.3). It is remarkable that the range for $|V_{td}|$ in eq. (10.4) obtained from unitarity is in agreement with the one from the measurement of the $B^0 - \overline{B}^0$ oscillation frequency in eq. (10.3) [58]. However the precision in $|V_{td}|$ is not yet sufficient to get stringent constraints on the complex phase in the CKM matrix. Note that only a direct measurement of $|V_{td}|$ can be used for an estimation of this phase. Its value cannot

be derived from the unitarity constraint. The determination of the complex phase in the CKM matrix is the topic of the next section.

Constraints for CP violation

How do the measurements of magnitudes of CKM elements constrain the allowed range in the plane of the Wolfenstein parameters ρ and η? The parameters ρ and η are determined by measurements of the values of $|V_{ub}|$ and $|V_{td}|$. The 1σ region in the (ρ, η) plane as estimated from the values of eq. (10.3) is shown in fig. 10.1. A considerable improvement in the knowledge of ρ and η could be obtained from an improved measurement of the matrix element $|V_{td}|$.

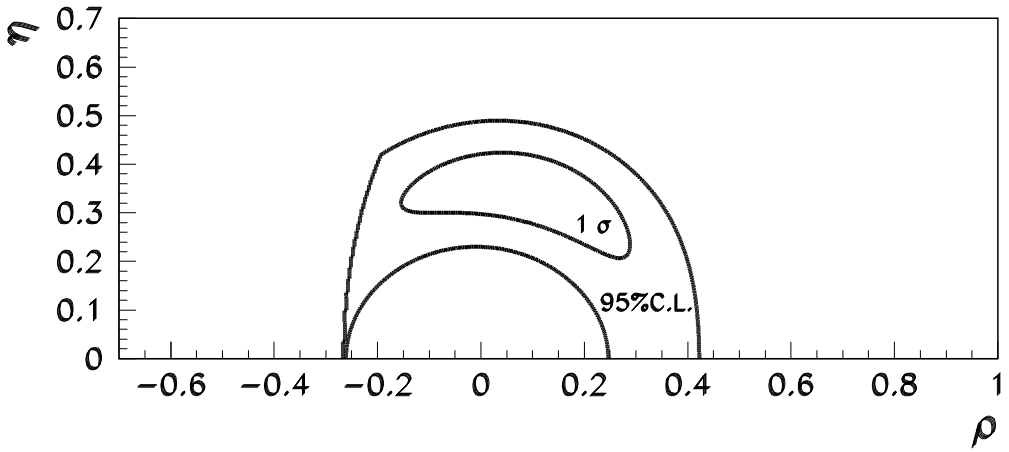

Figure 10.1: Contours of 1σ (inner curve) and 95% (outer curve) confidence level for regions in the (ρ, η) plane.

The present knowledge about the value of $|V_{td}|$ is provided by measurements of the $B^0 - \overline{B}^0$ oscillation frequency ΔM_{B^0} and is limited by intrinsic theoretical uncertainties. Several experimental proposals have been investigated to overcome these uncertainties. These proposals favour a measurement of $|V_{td} \,/\, V_{ts}|$ rather than of $|V_{td}|$ because many uncertainties cancel in the ratio. The value of $|V_{td}|$ can be directly obtained from the value of $|V_{td} \,/\, V_{ts}|$ due to the equalness of $|V_{ts}|$ with the precisely known element $|V_{cb}|$. The upper edge of the range in values of $|V_{td} \,/\, V_{ts}|$ is explored by lower limits on the mass difference ΔM_{B_s} of B_s mesons and by upper limits on the branching ratio $\mathcal{B}(b \to d\gamma)$. In contrast, the lower edge of the range in values of $|V_{td} \,/\, V_{ts}|$ is examined by upper limits on the rate difference $\Delta\Gamma_{B_s}$ of B_s mesons. The situation is illustrated in fig. 10.2. Among these results the limit on ΔM_{B_s} is already stringent enough to improve the 95% C.L. region in the (ρ, η)

plane. The contour of 95% C.L. including the ΔM_{B_s} limit [61] is superimposed on the 1σ contour in fig. 10.1.

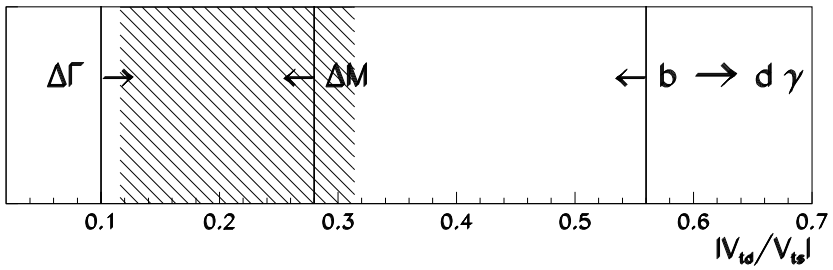

Figure 10.2: Limits of 95% confidence level on the value of $|V_{td}\,/\,V_{ts}|$. The hatched region shows the range of 95% confidence level as estimated from the $B^0 - \overline{B}^0$ oscillation frequency ΔM_{B^0} [58]. The upper limits are derived from a limit on the $B_s - \overline{B}_s$ oscillation frequency ΔM_{B_s} [61] and from a limit on the branching ratio of Cabibbo suppressed penguin decays $b \to d\gamma$ [46]. The lower limit on the value of $|V_{td}\,/\,V_{ts}|$ is that one of this thesis.

There are also constraints for ρ and η from CP violation in the neutral kaon system. For example, the measured value of the CP violating parameter ϵ constrains the point (ρ, η) to lie on a hyperbola for fixed values of the hadronic matrix elements. However the values of these hadronic matrix elements are not precisely known. A discussion of the constraints from the CP violating parameters in the $K^0 - \overline{K}^0$ system would go beyond the realm of this thesis. It can be found in reference [60]. The constraints obtained therein are in agreement with the ones from the measurement of $|V_{ub}|$ and $|V_{td}|$ and lead to small improvements in the knowledge about ρ and η.

10.2 The issue of this thesis

The results of this thesis are twofold. On one side a precision measurement of the average b hadron lifetime in Z decays was performed:

$$\tau_b = (1554 \pm 7 \pm 17)\ \text{fs}\ . \tag{10.5}$$

Together with other measurements [85,87,88,106,107] a value of the CKM matrix element $|V_{cb}|$ of

$$|V_{cb}| = (41.0 \pm 1.0\,(\text{exp}) \pm 1.4\,(\text{theo})) \times 10^{-3} \tag{10.6}$$

has been obtained from it.

On the other side differences in the lifetimes of various b hadron species have been measured. The ratio of lifetimes of charged to neutral b hadrons in Z decays was determined as:

$$\tau(B^+)/\tau(B^0) = 1.11 \pm 0.07 \pm 0.03 \; . \tag{10.7}$$

An upper limit for the rate difference among the short- and longlived B_s meson state was found as:

$$(\Delta\Gamma/\Gamma)_{B_s} < 0.5 \qquad (95\%\,\text{C.L.}) \; . \tag{10.8}$$

From this upper limit on $\Delta\Gamma_{B_s}$ a lower limit on the ratio of CKM elements $|V_{td}\,/\,V_{ts}|$ was derived as:

$$\left|\frac{V_{td}}{V_{ts}}\right| > 0.1 \qquad (95\%\,\text{C.L.}) \; . \tag{10.9}$$

This limit on the value of $|V_{td}\,/\,V_{ts}|$ comes close to the frontiers of knowledge in the value of the strongly suppressed coupling strength $|V_{td}|$, as shown in fig. 10.2.

The prime motivation for a precise knowledge of the value of $|V_{td}|$ lies in its relation to the magnitude of CP violation effects. The value of $|V_{td}|$ is one important ingredient for the test of the CKM mechanism of CP violation. Less is known about this mechanism although it is a fundamental constituent of the SM and was formulated 25 years ago. It is for the first time that a lower limit on the value of $|V_{td}|$ has been obtained that is independent of the theoretical estimate of the B^0 meson decay constant.

The result of this thesis could be a starting point for a series of attempts to measure $\Delta\Gamma_{B_s}$ in other experiments. The sensitivity to $\Delta\Gamma_{B_s}$ could be improved by an increase in size of the analyzed data sample. Large data samples of B_s mesons exist at present and others will be produced in the near future. A similar analysis as in this thesis could be applied to the other LEP experiments and to future b factories. The following section gives an introduction into the possibilities at LEP, HERA-B and BABAR.

10.2.1 A brief look into the future

The main purpose of the future b factories like HERA-B and BABAR is a measurement of CP violating asymmetries in decays of B^0 mesons to CP eigenstates. These measurements can be complemented by measurements of the magnitudes of $|V_{ub}|$ and $|V_{td}|$. The combination of measurements of the phases and of the magnitudes of CKM matrix elements probes the CKM mechanism of CP violation. A possible scenario of hypothetical measurements with a resolution as it could be achieved in the year 2000 [109, 110] is shown in fig. 10.3. In particular measurements of $|V_{ub}|$ and $|V_{td}|$ can resolve ambiguities in the determination of the Wolfenstein parameters ρ and η.

LEP

It would be interesting to continue the program of this thesis by the foundation of a LEP working group with the aim of an estimation of a combined LEP result on $\Delta\Gamma_{B_s}$. The necessary experimental apparatus and analysis techniques exist in all the four LEP experiments. The inclusive measurements of the average b lifetime would have to be extended by $\Delta\Gamma_{B_s}$ as a new fit parameter. The statistics could be enlarged by a factor of seven as compared to this thesis when the full LEP statistics of the years 1991 to 1995 will be used. The total number of B_s mesons is of the order 10^5.

HERA-B

The HERA-B experiment at DESY Hamburg [109] will accumulate a large number of b hadrons from 1999 onwards. In particular, 10^5 B_s mesons will be collected by the dilepton-trigger each year of data taking. A precise lifetime information will be available for the lepton tracks. The value of $\Delta\Gamma_{B_s}$ could be inferred from the lepton impact parameter distribution. Precise measurements of the B_s fraction in the analyzed sample and careful studies of the background distribution have to be performed. The analysis could be supplemented with a lifetime measurement in the decay channel $B_s \to J/\Psi\,\Phi$ which is foreseen in the program of HERA-B [109]. The final state is a CP eigenstate of dominantly even CP parity [63] and the lifetime measured here is the lifetime of the shortlived B_s state. The number of expected events in this channel amounts to 10^3 per year.

BABAR

The BABAR experiment at Stanford [110] is designed to study CP violation of B^0 mesons at the $\Upsilon(4S)$ resonance. The e^+e^- collider is also capable to run at the $\Upsilon(5S)$ resonance in which decays B_s mesons are produced. Per year of data taking at the $\Upsilon(5S)$ a similar number of B_s mesons as the total number at LEP could be obtained, namely 10^5. The $\Delta\Gamma_{B_s}$ analysis could be performed by an inclusive reconstruction of the b decay positions in all the events at the $\Upsilon(5S)$. The background from non-b events and from b events other than B_s mesons could be determined by reference measurements at the $\Upsilon(4S)$ and in the continuum. The advantage of a $\Delta\Gamma_{B_s}$ measurement at BABAR lies in the possibility of a discrimination between $\Delta\Gamma$ effects of B^0 and B_s mesons by a comparison of the measurements at the $\Upsilon(4S)$ and at the $\Upsilon(5S)$ resonance. As in the other experiments a measurement of the B_s fraction contained in the analyzed data sample is of major importance for the quantitative result on $\Delta\Gamma_{B_s}$.

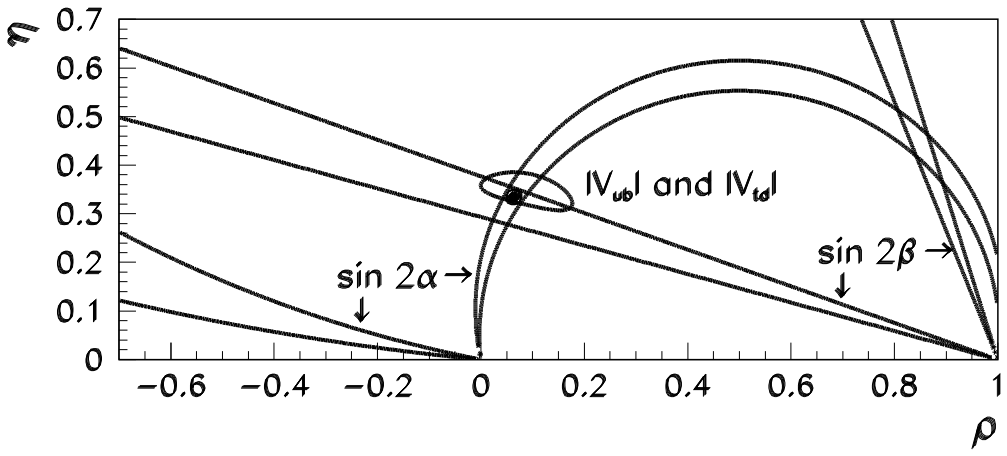

Figure 10.3: Contours of hypothetical measurements of CKM magnitudes ($|V_{ub}\,/\,V_{cb}| = 0.080 \pm 0.007$, $|V_{td}\,/\,V_{ts}| = 0.215 \pm 0.020$) and CKM angles ($\sin 2\alpha = 0.3 \pm 0.1, \sin 2\beta = 0.60 \pm 0.06$). The point shows the region consistent with all "measurements".

Appendix A

Correlation of fit variables

The following matrices contain the correlation parameters between the fit variables of the three- and five-parameter fit described in chapter 7.

Three-parameter fit

	τ_b	r	$\Delta\Gamma/\Gamma$	f_b	f_{B_s}	f_{Λ_b}
τ_b	1	0.01	-0.03	-0.22	0.03	0.35
r		1	0.04	0.16	0.18	0.08
$\Delta\Gamma/\Gamma$			1	0.07	0.05	0.04
f_b				1	0.15	0.13
f_{B_s}					1	0.02
f_{Λ_b}						1

Table A.1: Correlation coefficients between the fit variables $\tau_b, r = \tau(B^+)/\tau(B^0), \Delta\Gamma/\Gamma, f_b, f_{B_s}$ and f_{Λ_b} in the decay length fit.

	τ_b	r	$\Delta\Gamma/\Gamma$	f_b	f_{B_s}	f_{Λ_b}
τ_b	1	-0.08	-0.65	-0.20	0.01	0.27
r		1	0.05	0.19	0.22	0.14
$\Delta\Gamma/\Gamma$			1	0.27	-0.13	0.07
f_b				1	0.08	0.10
f_{B_s}					1	0.0
f_{Λ_b}						1

Table A.2: Correlation coefficients between the fit variables $\tau_b, r = \tau(B^+)/\tau(B^0), \Delta\Gamma/\Gamma, f_b, f_{B_s}$ and f_{Λ_b} in the impact parameter fit.

It can be seen that in the decay length measurement all correlation coefficients are small. However in the impact parameter measurement, where a non-zero value of $\Delta\Gamma/\Gamma$ has been fitted, the correlation between $\Delta\Gamma/\Gamma$ and the other fit variables is important. Both fits, the three- and the five-parameter fit show this property.

Five-parameter fit

	$\tau(B^+)$	$\tau(B^0)$	$\tau(B_s)$	$\Delta\Gamma/\Gamma$	$\tau(\Lambda_b)$	f_b	f_{B_s}	f_{Λ_b}
$\tau(B^+)$	1	-0.38	-0.09	0.03	-0.05	0.06	0.06	0.34
$\tau(B^0)$		1	-0.21	0.04	-0.07	0.0	0.07	0.28
$\tau(B_s)$			1	-0.02	-0.06	-0.05	-0.04	0.07
$\Delta\Gamma/\Gamma$				1	0.02	0.10	0.04	0.10
$\tau(\Lambda_b)$					1	-0.07	0.02	0.14
f_b						1	0.09	0.11
f_{B_s}							1	-0.03
f_{Λ_b}								1

Table A.3: Correlation coefficients between the fit variables $\tau(B^+), \tau(B^0), \tau(B_s), \Delta\Gamma/\Gamma, \tau(\Lambda_b), f_b, f_{B_s}$ and f_{Λ_b} in the decay length fit.

	$\tau(B^+)$	$\tau(B^0)$	$\tau(B_s)$	$\Delta\Gamma/\Gamma$	$\tau(\Lambda_b)$	f_b	f_{B_s}	f_{Λ_b}
$\tau(B^+)$	1	-0.16	-0.02	-0.41	-0.07	0.06	0.12	0.21
$\tau(B^0)$		1	-0.01	-0.34	-0.07	0.04	0.0	0.33
$\tau(B_s)$			1	-0.19	-0.05	0.0	-0.05	0.16
$\Delta\Gamma/\Gamma$				1	0.02	0.23	-0.06	0.11
$\tau(\Lambda_b)$					1	-0.11	-0.02	0.07
f_b						1	-0.02	0.11
f_{B_s}							1	-0.12
f_{Λ_b}								1

Table A.4: Correlation coefficients between the fit variables $\tau(B^+), \tau(B^0), \tau(B_s), \Delta\Gamma/\Gamma, \tau(\Lambda_b), f_b, f_{B_s}$ and f_{Λ_b} in the impact parameter fit.

Bibliography

[1] S. Weinberg, Phys. Rev. Lett. **19** (1967) 1264;
A. Salam, Elementary Particle Theory, ed. N. Svartholm, (Almquist and Wiksells, Stockholm 1969) 367;
S. L. Glashow, J. Iliopoulos and L. Maiani, Phys. Rev. **D2** (1970) 1285.

[2] UA1 Collab., G. Arnison *et al.*, Phys. Lett. **B122** (1983) 103;
UA2 Collab., M. Banner *et al.*, Phys. Lett. **B122** (1983) 476;
C. Rubbia, Nobel Lecture, Rev. Mod. Phys. **57** (1985) 699.

[3] N. Cabibbo, Phys. Rev. Lett. **10** (1963) 531;
M. Kobayashi and T. Maskawa, Prog. Theor. Phys. **49** (1973) 652.

[4] ARGUS Collab., H. Albrecht *et al.*, Phys. Lett. **B192** (1987) 245.

[5] Particle Data Group, R. M. Barnett *et al.*, Phys. Rev. **D54** (1996), Part I.

[6] R. P. Feynman and M. Gell-Mann, Phys. Rev. **109** (1958) 193.

[7] N. Isgur and M. B. Wise, *Heavy Quark Symmetry*, B decays, ed. S. Stone, (World Scientific, 2nd edition, Singapore 1994) 231.

[8] CFS Collab., S. W. Herb *et al.*, Phys. Rev. Lett. **39** (1977) 252.

[9] J. J. Aubert *et al.*, Phys. Rev. Lett. **33** (1974) 1404;
J. E. Augustin *et al.*, Phys. Rev. Lett. **33** (1974) 1406.

[10] MARK I Collab., M. L. Perl *et al.*, Phys. Rev. Lett. **35** (1975) 1489.

[11] PLUTO Collab., Ch. Berger *et al.*, Phys. Lett. **B76** (1978) 243;
DASP II Collab., C. W. Darden *et al.*, Phys. Lett. **B76** (1978) 246.

[12] CLEO Collab., D. Andrews *et al.*, Phys. Rev. Lett. **44** (1980) 1108 and Phys. Rev. Lett. **45** (1980) 219.

[13] L3 Collab., M. Acciarri *et al.*, Phys. Lett. **B335** (1994) 542;
B. Bertucci, contributed paper to the ICHEP 96 (Warsaw) Conf., PA05-049.

[14] L3 Collab., M. Acciarri *et al.*, Z. Phys. **C62** (1994) 551.

[15] R. Marshall, Z. Phys. **C43** (1989) 607.

[16] CDF Collab., F. Abe *et al.*, Phys. Rev. Lett. **74** (1995) 2626;
D0 Collab., S. Abachi *et al.*, Phys. Rev. Lett. **74** (1995) 2632.

[17] LEP Collab. and Electrow. Work. Group, D. Abbaneo *et al.*, CERN-PPE/96-183.

[18] J. Lys, S. Protopopescu, P. Tipton, talks presented at ICHEP 96 (Warsaw) Conf.

[19] M. Dittmar and Z. Was, CERN-TH.7186/94.

[20] CLEO Collab., B. Barish *et al.*, Phys. Rev. Lett. **76** (1996) 1570.

[21] L3 Collab., M. Acciarri *et al.*, Phys. Lett. **B351** (1995) 375.

[22] see discussion by A. Pais, Inward Bound, (Oxford Univ. Press, N.Y. 1986) 563.

[23] B. J. Bjorken and S. L. Glashow, Phys. Lett. **11** (1964) 255;
Y. Hara, Phys. Rev. **134** (1964) B701;
Z. Maki and Y. Ohnuki, Prog. Theor. Phys. **32** (1964) 144.

[24] C. D. Bouchiat, J. Iliopoulos and P. Meyer, Phys. Lett. **B38** (1972) 519.

[25] J. L. Rosner, *The Cabibbo-Kobayashi-Maskawa Matrix*, B decays, ed. S. Stone, (World Scientific, 2nd edition, Singapore 1994) 470.

[26] K. Winter, Nucl. Phys. (Proc. Suppl.) **B38** (1995) 211; W. L. Louis, *ibid.* 229; G. Drexlin, *ibid.* 235.

[27] C. S. Wu *et al.*, Phys. Rev. **105** (1957) 1413.

[28] J. H. Christenson, J. W. Cronin, V. L. Fitch and R. Turlay, Phys. Rev. Lett. **13** (1964) 138;
R. N. Cahn and G. Goldhaber, The experimental foundations of particle physics, (Cambridge Univ. Press, Cambridge 1995) 193.

[29] L. Wolfenstein, Phys. Rev. Lett. **13** (1964) 562.

[30] MAC Collaboration, E. Fernandez *et al.*, Phys. Rev. Lett. **51** (1983) 1022;
MARK-II Collaboration, N. S. Lockyer *et al.*, Phys. Rev. Lett. **51** (1983) 1316.

[31] L. Wolfenstein, Phys. Rev. Lett. **51** (1983) 1945.

[32] Y. Nir and H. R. Quinn, *Theory of CP Violation in B Decays*, B decays, ed. S. Stone, (World Scientific, 2nd edition, Singapore 1994) 520.

[33] C. S. Kim and A. D. Martin, Phys. Lett. **B225** (1989) 186.

[34] M. Shifman, N. G. Uraltsev and A. Vainshtein, Phys. Rev. **D51** (1995) 2217;
N. G. Uraltsev, Int. J. Mod. Phys. **A11** (1996) 515;
N. G. Uraltsev, *Theoretical aspects of the heavy quark expansion*, Beauty 96, ed. F. Ferroni, P. Schlein, Nucl. Inst. and Meth. in Phys. Res. **A384** (1996) 17.

[35] M. Neubert and C. T. Sachrajda, CERN-TH/96-19 (hep-ph/9603202).

[36] M. Neubert, CERN-TH/95-107 (hep-ph/9505238).

[37] CLEO Collab., B. Barish *et al.*, Phys. Rev. **D51** (1995) 1014;
CLEO Collab., D. Bortoletto *al.*, Phys. Rev. Lett. **16** (1989) 1667;
ARGUS Collab., H. Albrecht *al.*, Z. Phys. **C57** (1993) 533.

[38] ALEPH Collab., D. Buskulic *et al.*, Phys. Lett. **B359** (1995) 236;
DELPHI Collab., P. Abreu *al.*, Z. Phys. **C71** (1996) 539.

[39] CLEO Collab., R. Ammar *et al.*, Phys. Rev. Lett. **71** (1993) 674.

[40] CLEO Collab., R. Fulton *et al.*, Phys. Rev. Lett. **64** (1990) 16.

[41] M. Artuso, *B decay studies at CLEO*, Beauty 96, ed. F. Ferroni, P. Schlein, Nucl. Inst. and Meth. in Phys. Res. **A384** (1996) 39.

[42] L3 Collab., M. Acciarri *et al.*, CERN-PPE/96-198, Subm. to Phys. Lett., (1996).

[43] CLEO Collab., M. Artuso, *et al.*, Phys. Rev. Lett. **75** (1995) 785.

[44] T. Browder, K. HonScheid and S. Playfer, *A Review of Hadronic and Rare B Decays*, B decays, ed. S. Stone, (World Scientific, 2nd edition, Singapore 1994) 158.

[45] CLEO Collab., M. S. Alam *et al.*, Phys. Rev. Lett. **74** (1995) 2885.

[46] CLEO Collab., R. Ammar *et al.*, contributed paper to the ICHEP 96 (Warsaw) Conf., PA05-093.

[47] A. Ali, *Rare B decays in the Standard Model*, Beauty 96, ed. F. Ferroni, P. Schlein, Nucl. Inst. and Meth. in Phys. Res. **A384** (1996) 8.

[48] CDF Collab., T. J. LeCompte *et al.*, FERMILAB-CONF-96/021-E (1996).

[49] M. Gell-Mann and A. Pais, Phys. Rev. **97** (1955) 1387.

[50] R. P. Feynman *et al.*, The Feynman Lectures on Physics, (Addison-Weslay Company, Massachusetts 1966) volume III.

[51] K. Lande, L. M. Ledermann *et al.*, Phys. Rev. **103** (1956) 1901.

[52] K. Lande, L. M. Ledermann and W. Chinowsky, Phys. Rev. **104** (1957) 1925.

[53] S. Gjesdal *et al.*, Phys. Lett. **52B** (1974) 113.

[54] UA1 Collab., C. Albajar *et al.*, Phys. Lett. **B186** (1987) 247.

[55] J. S. Hagelin, Nucl. Phys. **B193** (1981) 123.

[56] H. Schröder, $B^0 - \overline{B}^0$ *Mixing*, B decays, ed. S. Stone, (World Scientific, 2nd edition, Singapore 1994) 449.

[57] LEP Collab. and LEP B Oscill. Work. Group., V. Andreev *et al.*, LEPBOSC/97-01 and references therein.

[58] A. J. Buras, Nucl. Inst. and Meth. **A368**, (1995) 1.

[59] CLEO Collab., D. Bartelt *et al.*, Phys. Rev. Lett. **71** (1993) 1680.

[60] A. Ali, DESY/96-106.

[61] T. Bowcock, R. Hawkings, G. Passaleva, C. Zeitnitz, *B-physics results from LEP*, Beauty 96, ed. F. Ferroni, P. Schlein, Nucl. Inst. and Meth. in Phys. Res. **A384** (1996) 48.

[62] I. Dunietz, Phys. Rev. **D52** (1995) 3048;
M. Beneke, G. Buchalla and I. Dunietz, Phys. Rev. **D54** (1996) 4419.

[63] R. Aleksan *et al.*, Phys. Lett. **B316**, (1993) 567.

[64] M. Gronau, *CP violation in B decays: the Standard Model and beyond*, Beauty 96, ed. F. Ferroni, P. Schlein, Nucl. Inst. and Meth. in Phys. Res. **A384** (1996) 1.

[65] ALEPH Collab., D. Decamp *et al.*, Nucl. Inst. and Meth. **A294** (1990) 127.

[66] DELPHI Collab., P. Aarnio *et al.*, Nucl. Inst. and Meth. **A303** (1991) 233.

[67] L3 Collab., B. Adeva *et al.*, Nucl. Inst. and Meth. **A289** (1990) 35.

[68] OPAL Collab., K. Ahmet *et al.*, Nucl. Inst. and Meth. **A305** (1991) 275.

[69] LEP Design Report,
Part I *The LEP injector chain*, LEP/TH 29 vol. I, CERN, 1983;
Part II *The LEP main ring*, LEP/TH 02 vol. II, CERN, 1984.

[70] LEP Polarization Team, Z. Phys. **C66** (1995) 45.

[71] A. A. Sokolov and I. M. Ternov, Sov. Phys. Dokl. **8** (1964) 1203.

[72] L3 Collab., O. Adriani *et al.*, Phys. Rep. **236** (1993) 1.

[73] A. S. Schwarz, Phys. Rep. **238** (1994) 1.

[74] L3 Collab., M. Acciarri *et al.*, Nucl. Instr. and Meth. **A351** (1994) 300.

[75] S. Petrak, L3 internal note # 1998 (1996).

[76] L3 Collab., F. Beissel *et al.*, Nucl. Instr. and Meth. **A332** (1993) 33.

[77] E. Lieb and R. Völkert, L3 internal note # 2028 (1996).

[78] I. C. Brock *et al.*, Nucl. Instr. and Meth. **A381** (1996) 236.

[79] T. Sjöstrand, Comput. Phys. Commun. **39** (1986) 347;
T. Sjöstrand and M. Bengtsson, Comput. Phys. Commun. **43** (1987) 367.

[80] The L3 detector simulation is based on GEANT Version 3.15.
R. Brun *et al.*, *GEANT 3*, CERN-DD/EE/84-1 (Revised), 1987.
The GHEISHA program (H. Fesefeldt, RWTH Aachen Report PITHA 85/02 (1985)) is used to simulate hadronic interactions.

[81] L3 Collab., M. Acciarri *et al.*, Z. Phys. **C62** (1994) 551.

[82] L3 Collab., M. Acciarri *et al.*, Phys. Lett. **B328** (1994) 223.

[83] JADE Collab., W. Bartel *et al.*, Z. Phys. **C33** (1986) 23.

[84] DELPHI Collab., P. Abreu *et al.*, Z. Phys. **C68** (1995) 353.

[85] ALEPH Collab., D. Buskulic *et al.*, Phys. Lett. **B314** (1993) 459.
L3 Collab., O. Adriani *et al.*, Phys. Lett. **B317** (1993) 474.
OPAL Collab., P. D. Acton *et al.*, Z. Phys. **C60** (1993) 217.

[86] L3 Collab., M. Acciarri *et al.*, Subm. to Phys. Lett., (1997).

[87] ALEPH Collab., D. Buskulic *et al.*, Phys. Lett. **B369** (1996) 151.
DELPHI Collab., P. Abreu *et al.*, Z. Phys. **C63** (1994) 3.
DELPHI Collab., P. Abreu *et al.*, Phys. Lett. **B377** (1996) 195.
OPAL Collab., P. D. Acton *et al.*, Z. Phys. **C73** (1997) 397.
SLD Collab., K. Abe *et al.*, Phys. Rev. Lett. **75** (1997) 3624.

[88] CDF Collab., F. Abe *et al.*, Phys. Rev. Lett. **71** (1993) 3421.

[89] G. Altarelli, G. Parisi, Nucl. Phys. **B126** (1977) 298.

[90] R. D. Field and R. P. Feynman, Nucl. Phys. **136** (1978) 1.

[91] C. Peterson, D. Schlatter, I. Schmitt and P. M. Zerwas, Phys. Rev. **D27** (1983) 105.

[92] LEP Collab. and Electrow. Work. Group., D. Abbaneo *et al.*, LEPHF/96-01.

[93] L3 Collab., B. Adeva *et al.*, Z. Phys. **C55** (1992) 39.

[94] L3 Collab., M. Acciarri *et al.*, Phys. Lett. **B345** (1995) 589.

[95] L3 Collab., M. Acciarri *et al.*, Z. Phys. **C71** (1996) 379.

[96] L3 Collab., M. Acciarri *et al.*, Phys. Lett. **B393** (1997) 477.

[97] CLEO Collab., P. Avery *et al.*, CLEO CONF 96-28;
ARGUS Collab., H. Albrecht *et al.*, Z. Phys. **C 54** (1992) 20;
OPAL Collab., R. Akers *et al.*, Z. Phys. **C 61** (1994) 209;
DELPHI Collab., P. Abreu *et al.*, Phys. Lett. **B 347** (1995) 447.

[98] M. G. Bowler, Z. Phys. **C11** (1981) 169.

P. Collins and T. Spiller, J. Phys. **G11** (1985) 1289.

V. G. Kartvelishvili, A. K. Likhoded and V. A. Petrov, Phys. Lett. **B78** (1978) 615.

[99] CDF Collab., F. Abe *et al.*, Phys. Rev. **D53** (1996) 3496;
CDF Collab., F. Abe *et al.*, Phys. Rev. Lett. **71** (1993) 1685;
ALEPH Collab., D. Buskulic *et al.*, Phys. Lett. **B311** (1993) 425.

[100] OPAL Collab., R. Akers *et al.*, Z. Phys. **C66** (1995) 19;
DELPHI Collab., W. Adam *et al.*, Z. Phys. **C68** (1995) 363;
SLD Collab., K. Abe *et al.*, Phys. Rev. Lett. **79** (1997) 808.

[101] OPAL Collab., R. Akers *et al.*, Z. Phys. **C67** (1995) 365.

[102] LEP B Lifetime Work. Group., L. Di Ciaccio *et al.*, CERN-OPEN/96-007;
http://wwwcn.cern.ch/ claires/lepblife.html.

[103] S. Duensing, L3 internal note (1998).

[104] G. Bellini, I. I. Bigi and P. J. Dornan *et al.*, *"Lifetimes of charm and beauty hadrons"*, Phys. Rep. **289** (1997) 1.

[105] O. Schneider, talk presented at Lepton-Photon 97 (Hamburg) Conf.

[106] ARGUS Collab., H. Albrecht *et al.*, Phys. Lett. **B318** (1993) 397.

CLEO Collab., B. Barish *et al.*, Phys. Rev. Lett. **76** (1996) 1570.

[107] ALEPH Collab., D. Buskulic *et al.*, Z. Phys. **C62** (1994) 179.

DELPHI Collab., P. Abreu *et al.*, Z. Phys. **C66** (1995) 323.

L3 Collab., M. Acciarri *et al.*, Z. Phys. **C71** (1996) 379.

OPAL Collab., R. Akers *et al.*, Z. Phys. **C60** (1993) 199.

[108] M. Neubert, CERN-TH/96-55 (hep-ph/9604412).

[109] Letter of intent for the HERA-B detector, DESY-PRC 94/02.

[110] Letter of intent for the BABAR detector, SLAC-443 (1994).

Acknowledgments

A thesis done in a large collaboration, such as L3, is always the combined effort of many people. It is my pleasure to acknowledge the assistance I received from all members of the L3 Collaboration.

I am grateful to my advisor Thomas Hebbeker who greatly supported my work as his PhD student. He has given time and attention to read and comment my manuscript as it has developed. I owe to him many helpful suggestions.

The idea for this thesis was born in a discussion with Klaus Winter on a journey to CERN, Geneva. It was he who always encouraged me, tried to clarify my thinking and gave me invaluable assistance.

I am indebted to Juan Alcaraz, Alex Nippe, Franz Muheim, Bruna Bertucci, Gerhard Raven, Sajan Easo, Ghita Rahal-Callot, Dimitri Bourilkov, Vuko Brigljevic, Martin Grünewald, Botjo Betev and Ingrid Clare who introduced me as a non-permanent visitor of CERN into the L3 experiment and the Heavy Flavour Analysis Group. If I have got an idea what the L3 experiment is then it was due to their help and willingness to answer my questions.

I thank Hanna Nowak who always offered me a place in her office at CERN and who did the thesis reading of the detector chapters for me. Also she had a lot of humor at hand.

I would like to thank Thomas Lohse from Berlin for the common seminar of L3 and HERA-B students which opened my mind to the topics of future experiments. My thanks go to Olf Epler for solving the mysteries of UNIX whenever they troubled the Berlin computer station.

I would like to thank Walter Downing from Boston, U.S.A., who as a non-specialist has read through all this strange stuff and has considerably improved my English.

Last but not least I would like to thank my parents. Their support was very important for this thesis.